

SCHOOL OF  
CIVIL ENGINEERING

INDIANA

DEPARTMENT OF HIGHWAYS

JOINT HIGHWAY RESEARCH PROJECT

JHRP-87-5

Informational Report

CRACK GROWTH GAGES  
FOR MONITORING FATIGUE DAMAGE

Charles K. Nmai  
Mark D. Bowman



PURDUE UNIVERSITY



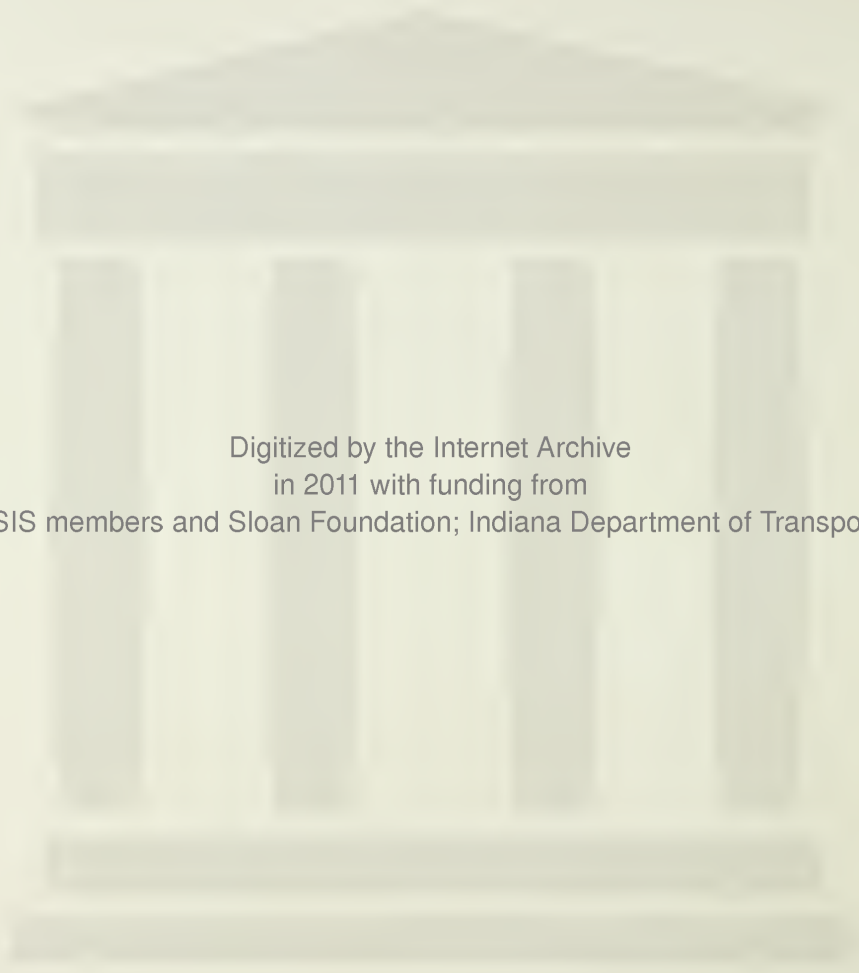
JOINT HIGHWAY RESEARCH PROJECT

JHRP-87-5

Informational Report

CRACK GROWTH GAGES  
FOR MONITORING FATIGUE DAMAGE

Charles K. Nmai  
Mark D. Bowman



Digitized by the Internet Archive  
in 2011 with funding from  
LYRASIS members and Sloan Foundation; Indiana Department of Transportation

Informational Report

CRACK GAGES FOR MONITORING  
FATIGUE DAMAGE

by

Charles K. Nmai  
Graduate Instructor in Research

Mark D. Bowman  
Research Engineer

School of Civil Engineering  
Purdue University  
West Lafayette, Indiana 47907

for the

Joint Highway Research Project  
Purdue University  
West Lafayette, Indiana 47907

File: 7-4-22

September 9, 1987

Information Report

CRACK GROWTH GAGES FOR MONITORING  
FATIGUE DAMAGE

To: H. L. Michael, Director  
Joint Highway Research Project

September 9, 1987

From: M. D. Bowman  
Research Engineer  
School of Civil Engineering

File: 7-4-22

The attached report contains information on a feasibility study of crack gages for use in monitoring fatigue-critical steel details to detect the onset of fatigue crack growth. The crack gage procedure can be used to monitor any detail, provided a reasonable estimate of the stress concentration factor can be obtained. Consequently, the crack gage procedure may be attractive for use in monitoring critical or troublesome details in steel highway bridges.

The study was conducted under the sponsorship of the National Science Foundation. An experimental laboratory study was conducted to assess the reliability of the crack gage procedure in predicting the onset of fatigue crack growth. A discussion of the crack gage design procedure is provided. Also, two examples are given to illustrate different crack gage design philosophies.

Respectfully submitted,

*Mark D. Bowman*

Mark D. Bowman  
Research Engineer

MDB:ms

cc: A. G. Altschaeffl	J. D. Fricker	P. L. Owens
J. M. Bell	D. E. Hancher	B. K. Partridge
M. E. Cantrall	R. A. Howden	G. T. Satterly
W. F. Chen	M. K. Hunter	C. F. Scholer
W. L. Dolch	J. P. Isenbarger	K. C. Sinha
R. L. Eskew	J. F. McLaughlin	C. A. Venable
A. Fendrick	K. M. Mellinger	T. D. White
	R. D. Miles	L. E. Wood

Final Report

CRACK GROWTH GAGES FOR  
MONITORING FATIGUE DAMAGE

by

Charles K. Nmai  
Mark D. Bowman

A Report of an Investigation Conducted  
by  
The School of Civil Engineering  
Purdue University

Supported by  
Structural Mechanics Program  
Division of Civil and Environmental Engineering  
National Science Foundation  
Grant No. CEE - 8404428

PURDUE UNIVERSITY  
WEST LAFAYETTE, INDIANA

June 1987

PLEASE READ INSTRUCTIONS ON REVERSE BEFORE COMPLETING

PART I-PROJECT IDENTIFICATION INFORMATION

1. Institution and Address Purdue University School of Civil Engineering West Lafayette, IN 47907	2. NSF Program Structural Mechanics	3. NSF Award Number CEE-8404428
	4. Award Period From 5/1/84 To 10/30/87	5. Cumulative Award Amount \$53,000

6. Project Title  
Research Initiation: Crack Growth Gages for Monitoring Fatigue Damage

PART II-SUMMARY OF COMPLETED PROJECT (FOR PUBLIC USE)

The study reported herein examines the use of notched crack gages to provide a clear indication of the onset of fatigue crack growth in structural steel details. The crack gage consists of a thin steel coupon which can be bonded to a structural member in the vicinity of a known stress raiser, such as at the end of a cover plate or near a welded stiffener. The crack gage concept has traditionally been used in the aerospace industry to correlate fatigue crack growth in the gage to crack growth in the structure. The present emphasis, however, is to use the crack gage to detect the onset of fatigue crack growth. The geometry of the crack gage is designed such that either initiation or significant crack propagation in the gage provides a direct indication that the structural element has developed a detectable fatigue crack.

In this study the structural element selected for study is a transverse welded butt joint member containing a full-length lack of penetration (LOP) discontinuity. The effect of the LOP discontinuity on the fatigue behavior of transverse welded butt joints is examined, with particular emphasis on the fraction of the cyclic life spent in fatigue crack initiation.

The crack gage fatigue test results are compared with analytical predictions of the fraction of cyclic life spent in crack initiation and crack propagation. Based on these comparisons, the suitability of the crack gage concept for field use is discussed. Also, the fatigue test results of the LOP specimens and the sound weld specimens from this study are compared with those from other studies. Finally, a procedure which may be used to design fatigue crack gages to monitor typical structural details is recommended, and two examples that illustrate the design procedure are presented.

PART III-TECHNICAL INFORMATION (FOR PROGRAM MANAGEMENT USES)

1. ITEM (Check appropriate blocks)	NONE	ATTACHED	PREVIOUSLY FURNISHED	TO BE FURNISHED SEPARATELY TO PROGRAM	
				Check (✓)	Approx. Date
a. Abstracts of Theses		X			
b. Publication Citations		X			
c. Data on Scientific Collaborators	X				
d. Information on Inventions	X				
e. Technical Description of Project and Results		X			
f. Other (specify)					

2. Principal Investigator/Project Director Name (Typed) Mark D. Bowman	3. Principal Investigator/Project Director Signature <i>Mark D. Bowman</i>	4. Date 6/30/87
---	---	--------------------



## TABLE OF CONTENTS

	Page
LIST OF TABLES . . . . .	vi
LIST OF FIGURES. . . . .	vii
CHAPTER 1 - INTRODUCTION . . . . .	1
1.1 General. . . . .	1
1.2 Object and Scope . . . . .	2
1.3 Background . . . . .	3
1.3.1 AASHTO Inspection Procedures . . . . .	3
1.3.2 Crack Gage Concept. . . . .	4
1.3.3 Previous Work on LOP Discontinuities . . . . .	7
CHAPTER 2 - ANALYTICAL MODELS. . . . .	12
2.1 General. . . . .	12
2.2 Fatigue Crack Initiation Models. . . . .	13
2.2.1 Mechanics Analysis. . . . .	15
2.2.2 Cyclic Stress-Strain Behavior . . . . .	17
2.2.3 Fatigue Properties. . . . .	18
2.2.4 Cumulative Fatigue Damage Analysis. . . . .	20
2.2.5 Combination of Requirements . . . . .	22
2.3 Crack Gage Models. . . . .	24
2.3.1 Crack Gage Stresses . . . . .	24
2.3.2 Crack Gage Stress Intensity Factor. . . . .	28
2.3.3 Crack Gage Selection Procedure. . . . .	30
CHAPTER 3 - EXPERIMENTAL INVESTIGATION . . . . .	33
3.1 General. . . . .	33
3.2 Specimen Fabrication . . . . .	34
3.2.1 Structural Component Fabrication. . . . .	34
3.2.1.1 Plain Plate Member . . . . .	35
3.2.1.2 Welded Butt-Joint Member . . . . .	35
3.2.2 Crack Gage Fabrication. . . . .	37
3.3 Load Transfer Tests. . . . .	39

## TABLE OF CONTENTS (continued)

	Page
3.3.1 Test Specimen . . . . .	39
3.3.2 Test Procedure. . . . .	41
3.4 Basic Control Tests. . . . .	42
3.4.1 Test Specimen . . . . .	42
3.4.2 Test Procedure. . . . .	42
3.5 Crack Gage/LOP Fatigue Tests . . . . .	43
3.5.1 Test Specimen . . . . .	43
3.5.2 Instrumentation . . . . .	44
3.5.3 Test Procedure. . . . .	46
 CHAPTER 4 - DISCUSSION AND EVALUATION OF TEST RESULTS. . . . .	  49
4.1 General. . . . .	49
4.2 Load Transfer Test Results . . . . .	50
4.3 Plain Plate, Sound Weld and LOP Fatigue Test Results . . . . .	 54
4.3.1 Results of the Fatigue Tests. . . . .	54
4.3.2 Discussion and Analysis of Test Results. . . . .	 55
4.3.2.1 Plain Plate Specimens. . . . .	55
4.3.2.2 Sound Weld Specimens . . . . .	56
4.3.2.3 LOP Specimens. . . . .	58
4.3.3 Comparison of Test Results with Other Studies . . . . .	 63
4.4 Crack Gage Test Results. . . . .	65
4.5 Comparison of Crack Gages with LOP Specimens. . . . .	 71
 CHAPTER 5 - PRACTICAL APPLICATION OF CRACK GAGE CONCEPT . . . . .	  73
5.1 General. . . . .	73
5.2 Crack Gage Design. . . . .	74
5.3 Numerical Examples . . . . .	76
5.3.1 Example I . . . . .	77
5.3.2 Example II. . . . .	78
5.3.3 Sensitivity Analysis. . . . .	80
5.4 Recommendations for Design . . . . .	82
 CHAPTER 6 - SUMMARY AND CONCLUSIONS. . . . .	 84
6.1 Summary. . . . .	84
6.2 Conclusions. . . . .	85
6.3 Recommendations for Future Work. . . . .	88

## TABLE OF CONTENTS (continued)

	Page
<b>TABLES</b> . . . . .	91
<b>FIGURES</b> . . . . .	107
<b>LIST OF REFERENCES</b> . . . . .	167
<b>APPENDICES</b>	
Appendix A Measured LOP Depths . . . . .	175
Appendix B Photographs of Fracture Surfaces. .	178

## LIST OF TABLES

Table		Page
2.1	Shape Function Values for Stress-Intensity Factor of Edge-Cracked Gage Subjected to Displacement Constraints [63] . . . . .	91
3.1	Physical Properties of ASTM A36 Steel and AWS ER70S-6 Solid Electrode Wire. . . . .	92
3.2	Chemical Properties of ASTM A36 Steel and AWS ER70S-6 Solid Electrode Wire. . . . .	93
3.3	Welding Parameters. . . . .	94
3.4	Structural Component Details. . . . .	95
3.5	Adhesive Properties . . . . .	97
3.6	Crack Gage Details. . . . .	98
4.1	Average Strain Transfer Ratios and Factors. . .	99
4.2	Control Test Results - Plain Plate Specimens. .	99
4.3	Control Test Results - Sound Weld Specimens . .	100
4.4	LOP Fatigue Test Results. . . . .	101
4.5	Summary of Fatigue Strengths (Stress Range) . .	102
4.6	Predicted and Estimated LOP Initiation Lives. .	103
4.7	Predicted and Observed Crack Gage Lives . . . .	104
4.8	Computed Stress Intensity Factors Based on Average Measured Crack Growth Rates. . . . .	106
<b>Appendix</b>		
<b>Table</b>		
A.1	Measured Lack of Penetration (LOP) Depths . . .	176

## LIST OF FIGURES

Figure	Page
2.1	Set-Up Cycle for Compressive Residual Stress. . . . . 107
2.2	Fatigue Notch Factor versus Initiation Life for Different Residual Stress Values. . . . . 108
2.3	General Crack Gage Dimensions . . . . . 109
2.4	Fatigue Notch Factor versus Initiation Life for Different Stress Ranges (E60 weld metal). . . . . 110
2.5	Fatigue Notch Factor versus Initiation Life for Different Stress Ranges (A36 steel) . . . . . 111
2.6	Fatigue Notch Factor versus Notch Root Radius for Different Notch Depths (A36 steel). . . . . 112
3.1	220,000 lb. (979 kN) Fatigue Testing Machine. . . . . 113
3.2	Structural Component Dimensions . . . . . 114
3.3	Cutting of Steel Plate for Specimen Preparation . . . . . 115
3.4	Weld Groove for Sound and Lack of Penetration Welds . . . . . 116
3.5	Meta-Lax Vibration Inducer. . . . . 117
3.6	Blank Crack Gage Dimensions . . . . . 118
3.7	Set-Up Guide used in Bonding Process. . . . . 119
3.8	Load Transfer Specimen showing Strain Gage Locations. . . . . 120
3.9	LOP Test Specimen with Bonded Crack Gages . . . . . 121
3.10	Types of Notched Crack Gages. . . . . 122

## LIST OF FIGURES (continued)

Figure	Page
3.11 Ultrasonic Transducer, Signal Conditioner, and Oscilloscope used in Scanning the LOP Welds . .	123
3.12 Crack Growth Measurement Instrumentation. . . .	124
4.1 Crack Gage Strain versus Remote Stress for Loctite Depend Adhesive (Side 1). . . . .	125
4.2 Crack Gage Strain versus Remote Stress for Loctite Depend Adhesive (Side 2). . . . .	126
4.3 Crack Gage Strain versus Remote Stress for Dymax Adhesive 845 (Side 1) . . . . .	127
4.4 Crack Gage Strain versus Remote Stress for Dymax Adhesive 845 (Side 2) . . . . .	128
4.5 Crack Gage and Component Strain at Zero Load versus Number of Loading Cycles (Loctite Depend Adhesive) . . . . .	129
4.6 Crack Gage and Component Strain at Zero Load versus Number of Loading Cycles (Dymax Adhesive 845). . . . .	130
4.7 Crack Gage and Component Strain at Peak Load versus Number of Loading Cycles (Loctite Depend Adhesive) . . . . .	131
4.8 Crack Gage and Component Strain at Peak Load versus Number of Loading Cycles (Dymax Adhesive 845). . . . .	132
4.9 Relation between Strain Transfer Ratio and Number of Loading Cycles (Loctite Depend Adhesive) . . . . .	133
4.10 Relation between Strain Transfer Ratio and Number of Loading Cycles (Dymax Adhesive 845). . . . .	134
4.11 Strain Transfer Ratio Comparison for Dymax 845 and Loctite Depend Adhesive . . . . .	135
4.12 S-N Curve for Plain Plate Specimens . . . . .	136

LIST OF FIGURES (continued)

Figure	Page
4.13 S-N Curve for Sound Weld Specimens. . . . .	137
4.14 S-N Curve for LOPl-8 Specimens. . . . .	138
4.15 S-N Curve for LOPl-4 Specimens. . . . .	139
4.16 Comparison of Mean Fatigue Strength for Plain Plate, Sound Weld and LOP Tests . . . . .	140
4.17 Ultrasonic Pulse Reflections from Lack of Penetration Discontinuity (LOPl-4-3). . . . .	141
4.18 Ultrasonic Pulse Reflections from Lack of Penetration Discontinuity (LOPl-4-14) . . . . .	142
4.19 Idealized Residual Stress Distribution. . . . .	143
4.20 Comparison between Analytically Predicted and Ultrasonic Estimate of Initiation Life. . . . .	144
4.21 Comparison of Mean Fatigue Strength for Plain Plate Tests . . . . .	145
4.22 Comparison of Mean Fatigue Strength for Sound Weld Tests. . . . .	146
4.23 Comparison of Mean Fatigue Strength for Lack of Penetration Tests . . . . .	147
4.24 Comparison between Analytically Predicted and Experimentally Estimated Initiation Life of Gages. . . . .	148
4.25 Observed and Predicted Crack Growth for Gages CG1-8-4, CG1-8-5 and CG1-8-8. . . . .	149
4.26 Observed and Predicted Crack Growth for Gages CG1-8-6, CG1-8-7, CG1-8-9, and CG1-8-13 . . . . .	150
4.27 Observed and Predicted Crack Growth for Gages CG1-8-10, CG1-8-11 and CG1-8-12 . . . . .	151
4.28 Observed and Predicted Crack Growth for Gages CG1-4-3, CG1-4-7 and CG1-4-8. . . . .	152

## LIST OF FIGURES (continued)

Figure	Page
4.29 Observed and Predicted Crack Growth for Gages CG1-4-4, CG1-4-5 and CG1-4-6. . . . .	153
4.30 Observed and Predicted Crack Growth for Gages CG1-4-9, CG1-4-10, CG1-4-11, and CG1-4-12 . . . .	154
4.31 Observed and Predicted Crack Growth for Gages CG1-4-13, CG1-4-14, CG1-4-15, and CG1-4-16. . . .	155
4.32 Typical Linear Crack Growth Relationship. . . . .	156
4.33 Comparison between Analytically Predicted and Experimentally Observed Propagation Life. . . . .	157
4.34 Comparison between Analytically Predicted and Experimentally Observed Total Fatigue Life. . . . .	158
4.35 Comparison between Experimentally Estimated Gage Initiation Life and Ultrasonic Estimate of LOP Initiation Life. . . . .	159
4.36 Comparison between Experimentally Estimated Gage Initiation Life and Analytically Predicted LOP Initiation Life . . . . .	160
4.37 Comparison between Experimentally Observed Total Gage Life and Total LOP Fatigue Life. . . . .	161
5.1 Crack Gage Selection Procedure. . . . .	162
5.2 Relation between Fatigue Notch Factor and Crack Initiation Life for A36 Steel . . . . .	163
5.3 General Dimensions of a Crack Gage Notch. . . . .	164
5.4 Relation between Fatigue Notch Factor and Notch Dimensions. . . . .	165
5.5 Crack Gage Placement on Fillet Welded Tee Joint . . . . .	166



## LIST OF FIGURES (continued)

Figure	Page
Appendix Figure	
A.1 LOP Depth Measurement Locations . . . . .	177
B.1 Photographs of LOPl-8 Weld Specimen Fracture Surfaces. . . . .	179
B.2 Photographs of LOPl-4 Weld Specimen Fracture Surfaces. . . . .	183

## CHAPTER 1

## INTRODUCTION

1.1 General

The advent of welding has facilitated the process whereby two pieces of metal can be joined together economically. However, sufficient care must be exercised in the design and fabrication of welded joints to minimize the introduction of discontinuities such as porosity, slag inclusions, shrinkage cracks, lack of fusion, and lack of penetration. The presence of such discontinuities in a weldment, if of sufficient magnitude, can significantly reduce the fatigue strength. Fatigue cracks in highway bridges that initiated from weld discontinuities have been reported [10,11], and in some instances have led to brittle fracture [19].

Current specifications for the design of cyclically loaded structures such as highway bridges, railway bridges, offshore structures, and crane girders not only limit or prohibit the presence of weld discontinuities, but they also require the use of sufficiently low design stresses that reduce the likelihood of the initiation and propagation of cracks that can lead to failure. Thus, it is

highly desirable that inspection procedures utilize techniques that will enable the early detection of fatigue crack growth in structures that are fabricated with acceptable levels of quality. Regulations for fatigue crack detection are currently deployed by the U.S. Air Force for the maintenance of aircraft [1].

Depending on the desired quality level and importance of the structure, the inspection procedures may need to be very elaborate. However, due to the expense and time involved in checking all of the details in a structure, a simple and yet effective procedure would be very beneficial. It is believed that the placement of crack gages at a number of critical points in a structure is one method that can be used to provide an early indication of fatigue crack initiation or sub-critical crack growth. Fatigue crack gages, which are small notched coupons that can be bonded to the surface of a structure, have been studied extensively for use in the aircraft industry [2,8,13,15,16,25,48,56]. The periodic inspection of strategically positioned gages will help determine the necessity for a more elaborate inspection in critical areas of the structure.

## 1.2 Object and Scope

The primary objective of the present study is to

experimentally investigate the feasibility of using a crack gage to detect the onset of fatigue crack initiation and early crack growth in fatigue-critical steel details. In particular, the effect of lack of penetration (LOP) discontinuities on the fatigue behavior of transverse butt-welded joints will be examined. Butt joint groove welded specimens containing internal LOP weld discontinuities were tested with crack gages bonded to the specimen surface. Fatigue test results are compared with analytical predictions of the fraction of cyclic life spent in crack initiation and crack propagation.

### 1.3 Background

#### 1.3.1 AASHTO Inspection Procedures

The guidelines for inspection provided in the current Manual for Maintenance Inspection of Bridges by the American Association of State Highway and Transportation Officials (AASHTO) [35] are stated in very general terms. For steel stringers and girders, the manual requires that the members be examined for cracking and corrosion, especially along the upper or top flange, around rivet or bolt heads, and at contact surfaces of flange plates, connections and bearings. The provisions for checking welds is stated as follows:

"Inspect weld areas for cracks, especially at unusual type connections, on curved sections, re-entrant corners, copes, and at all areas where there is an abrupt change in size of metal or configuration which might produce an area of concentrated stress or in areas where vibration and movement could produce fatigue stress."

No specific methods of inspection are outlined in the manual. Current techniques range from visual observation of the welds to the use of ultrasonics, radiography, or acoustic emission monitoring to check for the presence of cracks. The microscopic nature of fatigue cracks, especially in the early stages of development, make their detection by such inspection techniques fairly remote. This is especially true of sub-surface weld discontinuities, such as lack of penetration (LOP).

### 1.3.2 Crack Gage Concept

Many structural parts suffer fatigue damage as a result of carrying fluctuating loads. The useful life of the part, or the structure as a whole, is limited by the amount of fatigue damage that can be tolerated without a significant decrease in the design factor of safety. Design procedures involve the identification of structural sections that may be fatigue critical and the application of conservative design techniques to minimize fatigue damage.

Where possible, the structural sections should be tested in the laboratory under simulated operating conditions to estimate their actual fatigue life and to pinpoint potential fatigue problem areas using thorough inspection procedures. The use of laboratory test results in the design of the structure is generally quite successful in preventing fatigue failures in actual service. However, most testing methods are not helpful in estimating the accumulated fatigue damage or the remaining fatigue life of a particular structural part or the structure itself. This is mainly due to the randomness in actual service loading and the vastly different environmental conditions under which structures operate.

The need to estimate fatigue damage accumulation led to the development of fatigue damage indicators, which consisted of a gage or indicator that could be placed directly on a structural part in actual service. Thus, the accumulated fatigue damage suffered by the structural part and the remaining fatigue life after a given period of service could be estimated. Several devices were designed in the aircraft industry to estimate fatigue damage and the remaining fatigue life [21,57,68]. The initial techniques were aimed at recording the stresses or strains experienced at critical structural control points on individual aircraft through the use of flight load recorders, acoustic emission, mechanical strain gages, and electronically recorded strain gages. However, considerable effort and

analyses, as well as expense, were required to obtain a fair representation of the measured stress history experienced at the control point during a given service period, and to correlate the stress history with crack growth damage. Hence, it was necessary to develop alternate and more straightforward methods to monitor fatigue damage.

Smith [56] developed the Fatigue Damage Indicator (FDI) to monitor fatigue crack initiation damage in aircraft structures. The FDI was an edge-cracked coupon which could be adhesively bonded to a structural piece subjected to repeated loadings. One of the main objectives in the development of the FDI was to provide an indicator which exhibited a fatigue crack independently of and in advance of the occurrence of a fatigue crack in the structural part to which it was bonded. This was achieved by pre-cracking the coupon and by varying the unbonded length of the coupon [56]. The crack length in the FDI was then correlated with accumulated fatigue damage in the test piece. Monitoring of the FDI at various points in the aircraft structure made it possible to monitor cumulative fatigue damage in the aircraft.

Johnson and Paquette [25] also developed a pre-cracked Service Life Monitoring Coupon (SLMC). The dimensions and placement of the SLMC were selected such that the coupon experienced essentially the same loading and environment as the critical structural control point. Thus, the crack length measured by the coupon could be directly related to

potential crack growth at other locations.

Based on the FDI crack growth results [56], Gallagher et al. [13] concluded that the FDI did possess stress intensity factor characteristics which would make the rate of crack growth independent of the FDI crack length. Thus, the FDI could be used as a crack gage to relate its crack growth behavior with crack growth damage accumulation in the structure to which it is bonded. Grandt et al. [2,15] also suggested various analytical expressions which relate stress in the structural member to stress induced in the crack gage, and crack length in the structure to crack length in the crack gage. Subsequent experimental tests [2,16,48] demonstrated good agreement between the test and the predicted crack lengths.

### 1.3.3 Previous Work on LOP Discontinuities

One of the first investigations that examined the effect of lack of penetration (LOP) discontinuities on the fatigue behavior of welded joints was conducted by Warren [65]. Cyclic tests of transverse welded butt joints containing slag inclusions, fine longitudinal cracks, and LOP were conducted under an alternating axial load. Although scatter of the test results made it difficult to draw firm conclusions with regard to the relative severity of the various discontinuities, LOP appeared to be one of the most serious of the discontinuities investigated.



Newman and Dawes [45] tested 4-in. (100-mm) wide by 1/2-in. (12.7-mm) thick transverse butt welded specimens that contained LOP discontinuities. Specimens containing one of two types of LOP discontinuities were tested: 0.063-in. (1.6-mm) deep by 0.75-in. (19-mm) long LOP in one series, and 0.063-in. deep by 1.25-in. (32-mm) long LOP in the second. The LOP severities examined correspond to 2.3 and 3.9% of the gross cross-sectional area of the specimens, respectively. The specimens were tested under zero-to-tension loading. The test results initially indicated that fracture initiated at the weld toe when the specimens were tested with the weld reinforcement intact - i.e., in the as-welded condition. To encourage failure from the LOP, the weld toe was dressed in subsequent tests to reduce the stress concentration at the toe.

Nucleation of propagating fatigue cracks occurred at either the LOP discontinuity or the edge of the weld reinforcement, whichever acted as the greater stress raiser. Contouring of the weld toe resulted in failure from the LOP discontinuity alone. The test results demonstrated that fatigue strength decreases with increased LOP length. Newman and Dawes [45] also demonstrated that an approximate relation exists between fatigue strength and percentage reduction in cross-sectional area as a result of the LOP discontinuity. The fatigue strength of the 1.25-in. LOP-series at 100,000 and 2 million cycles was, respectively, 91% and 74% of the fatigue strength of the 0.75-in. LOP-

series.

The decrease in fatigue strength with decreased cross-sectional area was also reported by Guyot et al. [18], who tested 5.6-in. (140-mm) wide by 0.8-in. (20-mm) thick transverse butt welded specimens. The butt welds contained LOP discontinuities with several length and depth combinations. The LOP lengths varied from 0.2-in. (5-mm) up to the full specimen width. The LOP depths ranged from 0.04-0.20 in. (1-5 mm), and were located at various levels in the plate thickness. The fatigue strength at two million cycles was found to decrease when either the length or the depth of the LOP increased.

Ekstrom and Munse [9] examined the effect of porosity and LOP weld discontinuities on the fatigue behavior of butt-welded connections. The LOP discontinuities were approximately 3/16-in. (4.76-mm) deep and extended along the entire specimen width. To ensure that all failures initiated at the LOP, the weld reinforcement was removed and the surfaces polished. Lack of penetration discontinuities were found to significantly reduce the fatigue strength of the connections. Although the LOP was more severe than those that had been studied by previous researchers [45], Ekstrom and Munse observed that the fatigue behavior of the weldments followed the same general pattern as that obtained from welds with smaller LOP discontinuities. The reduction in fatigue strength increased with an increase in the severity of the stress

raisers.

In an attempt to determine the fraction of life spent in crack propagation, Lawrence and Munse [31] tested low carbon steel specimens containing partial-penetration double-U butt welds. The growth of internal cracks was monitored by radiography and the crack growth data were compared with theoretical fatigue crack growth expressions. The point at which macroscopic crack propagation began was determined from radiographs taken periodically during the tests. Thus, the total fatigue life could be approximately separated into periods of early crack growth and crack propagation. The test results indicated that the fraction of the fatigue life spent in crack initiation constituted approximately one-half the total fatigue life of the specimens. The measured crack growth rate data for the weld metal were found to be considerably different from values reported for A36 steel.

Later tests by Tobe and Lawrence [60] were carried out on partial-penetration butt joint weldments. The specimens were fabricated using double-V groove welds to attach 1/2-in. (12.7-mm) thick ASTM A514 alloy steel plates. The objectives of the investigation were to determine the influence of LOP on the fatigue life of high-strength steel butt welds and to determine, both experimentally and theoretically, the fraction of fatigue life spent in crack initiation and crack propagation. An experimental indication of the crack initiation life was achieved by using

strain gages mounted approximately 0.08-in. (2-mm) from the tip of the LOP. The results of the study demonstrated that fatigue crack initiation life occupied less than 10% of the total life in the range 1,000 to 1 million cycles, and could be predicted using low-cycle fatigue data for weld metal and fatigue crack initiation concepts. The results suggested also that the mean stresses at the LOP tip decay rapidly and that the fatigue notch factor,  $K_f$ , associated with the LOP is very close to the maximum possible  $K_f$  calculated using Peterson's equation [51,52]. Also, the presence of LOP was found to have a detrimental effect on the fatigue resistance of A514 steel weldments. Fatigue life was influenced by LOP size, with LOP discontinuities as small as 0.02-in. (0.5-mm) wide reducing the fatigue life below the normal expectancy for sound welds.

The findings of the above investigations strongly indicate the detrimental effect of LOP discontinuities on fatigue life. These findings have been shown to apply to partial penetration welds as well [31,69].

## CHAPTER 2

## ANALYTICAL MODELS

2.1 General

Phenomenologically, the process that leads to fatigue failure can be divided into the following three stages [12]: (a) crack nucleation, (b) crystallographic (Stage I) crack growth normally in the plane of maximum shear stress, and (c) stable (Stage II) crack growth on planes perpendicular to the maximum tensile stress. However, for engineering applications, it is more convenient to divide fatigue life into two portions: crack initiation life,  $N_I$ , and crack propagation life,  $N_p$ . The fatigue crack initiation life is defined as the number of loading cycles required to initiate a macroscopic, noncritical fatigue crack. The additional number of loading cycles required to propagate such a crack to a critical size is termed the fatigue crack propagation life. The final "critical" crack size must be adequately defined to suit a particular application, as it can be taken to be associated with either a particular detectable crack size or complete fracture of a structural member.

Traditionally, the fatigue analysis of notched members

has been based on the use of the empirical stress-life (or S-N) curve. Recent developments, however, have led to the use of low-cycle fatigue concepts and linear-elastic fracture mechanics (LEFM) principles in the formulation of models for more rational and accurate analyses of fatigue behavior.

The procedures used in calculating the fatigue crack initiation lives of the crack gages and the lack of penetration (LOP) specimens tested in this study are presented in Section 2.2. The mathematical models used in the calculation of crack gage stresses and stress-intensity factors are presented in Section 2.3.

## 2.2 Fatigue Crack Initiation Models

The most highly strained regions of a structural member, such as fillets and notches, are often the initiation sites for fatigue cracks. Hence, in the prediction of the crack initiation life, it is necessary that the most severe stress raisers (or critical locations) in a structure be identified. As a result of the high stress concentrations that normally exist at the critical locations, localized yielding may be possible even though the structure in general behaves elastically. Thus, the application of elastic principles to determine the notch root stresses and strains is often inappropriate.

The "critical location approach" may be used to predict the fatigue crack initiation life of notched members. This approach is based on the following assumptions:

1. The critical locations (the most severe stress raisers) in a structure, such as sharp notches, fillets, or abrupt changes in geometry, can be properly identified.
2. The cyclic behavior of a structural member at a notch root is identical to the cyclic behavior of smooth laboratory specimens tested under appropriate control.

The critical location approach has been used in several analyses [5,6,23,33,52,61,62] to predict the fatigue crack initiation life of notched members. The necessary requirements for such an analysis have been summarized by Topper and Morrow [61] as follows:

1. A mechanics analysis that relates the stresses and strains at the critical location to the nominal stresses and strains.
2. Knowledge of the cyclic stress-strain properties such that the material response at the notch can be determined.

3. Knowledge of the fatigue properties of the material of which the structure is made.
4. A cumulative fatigue damage method to predict the initiation life, taking into account damage accrued from all previous load histories.
5. A method that combines Steps 1-4.

Each of these requirements are briefly discussed below.

### 2.2.1 Mechanics Analysis

The use of elastic stress-strain relationships to determine the stresses and strains at a notch root may be inappropriate due to the existence of high stress concentrations and the possibility of localized yielding at the notch. Neuber [46] and Stowell [58] developed expressions that relate the nominal stress-strain history to the local stress-strain history that occurs at the root of a notch. Both relationships have been shown to give the same degree of accuracy [44]. However, Neuber's equation has been shown experimentally [66] to accurately predict the local strain histories of notched plates subjected to a zero-to-tension cyclic loading. Although Neuber's equation [46] loses accuracy for nominal strains in excess of two percent [14], which seldom occur under normal service conditions, it is more widely used because of its simplicity.

Neuber's equation for both linear and nonlinear



elastic material behavior can be written as:

$$K_t = (K_\sigma K_\epsilon)^{0.5} \quad (2.1)$$

where  $K_t$  = theoretical elastic stress concentration factor;  $K_\sigma = \sigma/S$ , stress concentration factor;  $K_\epsilon = \epsilon/e$ , strain concentration factor;  $\sigma, \epsilon$  = local stress and strain at the notch root; and  $S, e$  = remotely applied nominal stress and strain.

Topper et al. [62] have shown that Neuber's equation is applicable to the notch fatigue problem if the fatigue notch factor,  $K_f$ , is substituted for  $K_t$  and the stress and strain ranges are used.

$$K_f = \left| \frac{\Delta\sigma}{\Delta S} \cdot \frac{\Delta\epsilon}{\Delta e} \right|^{0.5} \quad (2.2)$$

where  $\Delta\sigma, \Delta\epsilon$  = local stress and strain ranges at the notch root;  $\Delta S, \Delta e$  = remote nominal stress and strain ranges. Since the nominal stresses and strains are elastic in most engineering problems, the elastic modulus,  $E$ , may be used to revise Eq. 2.2:

$$\Delta\sigma\Delta\epsilon = \frac{(K_f \Delta S)^2}{E} \quad (2.3)$$

Several empirical relationships have been developed to

determine  $K_f$  [27,47,52]. However, Peterson's equation [52] is the expression most widely used because of its accuracy and simplicity:

$$K_f = 1 + \frac{K_t - 1}{1 + a^*/r_N} \quad (2.4)$$

where  $a^*$  = material constant and  $r_N$  = notch root radius.

### 2.2.2 Cyclic Stress-Strain Behavior

The monotonic and cyclic stress-strain curves for most metals are significantly different. Typically, when the cyclic stress-strain curve falls below the monotonic curve, cyclic softening occurs; cyclic hardening occurs when the cyclic curve lies above the monotonic curve.

Landgraf et al. [28,30] define the cyclic stress-strain curve as the locus of tips of the stable hysteresis loops from companion specimens tested at different, completely reversed, constant strain amplitudes. Morrow [42] suggested an expression, given by Eq. 2.5, which can be used to describe the cyclic stress-strain curve.

$$\frac{\Delta \epsilon}{2} = \frac{\Delta \sigma}{2E} + \left| \frac{\Delta \sigma}{2K'} \right|^{\frac{1}{n'}} \quad (2.5)$$

where  $K'$  = cyclic strength coefficient and  $n'$  = cyclic strain hardening exponent.

The first term on the right hand side of Eq. 2.5 represents the elastic strain amplitude, while the second term represents the plastic strain amplitude. The monotonic stress-strain curve may be written in a similar manner if  $\Delta\sigma$ ,  $\Delta\epsilon$ ,  $K'$  and  $n'$  are replaced by  $\sigma$ ,  $\epsilon$ ,  $K$  and  $n$ , respectively, where  $K$  is the monotonic strength coefficient,  $n$  is the monotonic strain hardening exponent and  $\sigma$  and  $\epsilon$  represent the total stress and strain, respectively.

For most metals subjected to cyclic loading, a stable hysteresis loop is obtained after a relatively few number of load repetitions. Halford and Morrow [20] and Morrow [42] have observed that for most metals the cyclic stress-strain curve, magnified by a factor of two, can be used to approximate the stable hysteresis loop shape. This is consistent with Massing's Hypothesis [39] which states that the hysteresis curve is geometrically similar to the cyclic stress-strain curve magnified by a factor of two. Thus, for materials which obey Massing's hypothesis [39], the hysteresis loop shape can be generated from the cyclic stress-strain curve by doubling the ordinates [20,42].

### 2.2.3 Fatigue Properties

The total strain amplitude can be taken as the sum of

the elastic strain amplitude and the plastic strain amplitude [28]. The elastic strain amplitude,  $\Delta\epsilon_e/2$ , is given by:

$$\frac{\Delta\epsilon_e}{2} = \frac{\sigma_a}{E} \quad (2.6)$$

where  $\sigma_a$  = stress amplitude.

Basquin's equation [3] relates the stress amplitude to the number of reversals to failure:

$$\sigma_a = \sigma_f'(2N_f)^b \quad (2.7)$$

where  $\sigma_f'$  = fatigue strength coefficient,  $b$  = fatigue strength exponent, and  $2N_f$  = number of reversals to failure. Thus, the elastic strain amplitude may be written as:

$$\frac{\Delta\epsilon_e}{2} = \frac{\sigma_f'}{E}(2N_f)^b \quad (2.8)$$

Morrow [43] recommended a modification of Eq. 2.8 to account for the influence of a mean stress,  $\sigma_o$ , as follows:

$$\sigma_a = (\sigma_f' - \sigma_o)(2N_f)^b \quad (2.9)$$

The value of  $\sigma_0$  in Eq. 2.9 is considered positive for a tensile mean stress and negative for a compressive mean stress.

The plastic strain amplitude,  $\Delta\epsilon_p/2$ , is given by

$$\frac{\Delta\epsilon_p}{2} = \epsilon_f' (2N_f)^c \quad (2.10)$$

where  $\epsilon_f'$  = fatigue ductility coefficient, and  $c$  = fatigue ductility exponent.

The total strain amplitude,  $\Delta\epsilon/2$ , is given by summing the elastic and plastic portions:

$$\frac{\Delta\epsilon}{2} = \frac{\Delta\epsilon_e}{2} + \frac{\Delta\epsilon_p}{2} \quad (2.11)$$

Substituting for  $\Delta\epsilon_e/2$  and  $\Delta\epsilon_p/2$  from Eqs. 2.8 and 2.10, respectively, yields an expression relating the total strain amplitude and the number of reversals to failure.

$$\frac{\Delta\epsilon}{2} = \frac{\sigma_f'}{E} (2N_f)^b + \epsilon_f' (2N_f)^c \quad (2.12)$$

#### 2.2.4 Cumulative Fatigue Damage Analysis

Several cumulative damage procedures have been developed to compute the fatigue crack initiation life

[7,26,29,32,34,37,59]. For an accurate analysis, it is necessary to compute and sum the fatigue damage on a reversal by reversal basis until a limiting criterion is satisfied. This requires knowledge of the elastic and plastic strains, and the mean stress for each reversal. For a given reversal, the damage may be computed as the sum of the damage due to the elastic strain, plastic strain, and the mean stress [37]. The damage for the  $i$ -th reversal due to the elastic strain amplitude,  $D_{i,e}$ , is obtained from Eqs. 2.6 and 2.8 and is given by:

$$D_{i,e} = \left| \frac{1}{2N_f} \right|_e = \left| \frac{\Delta\sigma/2}{\sigma_f} \right|^{-1/b} \quad (2.14)$$

The damage for the  $i$ -th reversal due to the plastic strain amplitude,  $D_{i,p}$ , is obtained from Eqs. 2.5 and 2.10 as:

$$D_{i,p} = \left| \frac{1}{2N_f} \right|_p = \left| \frac{(\frac{\Delta\sigma}{K})^{1/n}}{\epsilon_f} \right|^{-1/c} \quad (2.15)$$

Martin [37] developed the following expression to calculate the damage due to the mean stress alone:

$$D_{i,m} = (\epsilon_f')^{\frac{1}{c}} \left| \left| \frac{\Delta\sigma/2}{K'} \right|^{-\frac{1}{n'c}} \right| \left| 1 - \frac{\sigma_o}{\sigma_f'} \right|^{\frac{1}{n'c}} - 1 \quad (2.16)$$

The total damage for the  $i$ -th reversal,  $D_i$ , is obtained as the sum of Eqs. 2.14, 2.15 and 2.16. That is,

$$D_i = D_{i,e} + D_{i,p} + D_{i,m} \quad (2.17)$$

where  $D_{i,e}$  = damage due to elastic strain amplitude,  $D_{i,p}$  = damage due to plastic strain amplitude, and  $D_{i,m}$  = damage due to mean stress alone [37].

The fatigue crack initiation life,  $N_i$ , is obtained by applying Miner's linear cumulative damage rule [41] and is taken as half of the number of reversals required such that the summation of the individual damage components,  $D_i$ , equals unity.

$$\sum_{i=1}^{2N_1} D_i = 1 \quad (2.18)$$

### 2.2.5 Combination of Requirements

The successful analysis of the fatigue behavior of the material at the root of a notch requires the development of

a mathematical model that is capable of reproducing the hysteresis loop shape. The model must adequately account for memory, cyclic hardening and softening, and mean stress relaxation.

Martin et al. [38] and Wetzel [67] proposed models for the computer simulation of the cyclic stress-strain curve. The rheological model developed by Martin [37,38] was extended by Jhansale and Topper [24] and later by Plummer [53] to simulate the cyclic response of A36 mild steel. The program was revised by Mattos [40] with the addition of Neuber control to determine the notch stresses and strains, and a procedure that computes damage on a reversal by reversal basis.

In previous studies [4,40] residual stresses were handled by means of a set-up cycle OAB (Fig. 2.1) such that after reversal AB the simulated stress at the notch root was equal to the residual stress  $\sigma_r$ . However, this procedure was found to give inconsistent values of initiation life for low residual stresses. A modification was thereby made such that the initial stress of the simulated stress-strain curve was equal to  $\sigma_r$ . Using the assumption that  $\sigma_r$  be not greater than the yield strength of the base material,  $\sigma_{ys}$ , the corresponding residual strain was computed as  $\sigma_r/E$ , where E is the modulus of elasticity of the weld material. The consistency achieved with this modification is shown in Fig. 2.2. As would be expected the fatigue crack initiation life increases for



compressive residual stresses at the notch root, and decreases for tensile residual stresses. The revised Plummer-Mattos computer program was used in this study to predict the fatigue crack initiation lives of notched crack gages and specimens with partial penetration groove welds.

## 2.3 Crack Gage Models

### 2.3.1 Crack Gage Stresses

The use of a crack gage to provide a reliable indication of fatigue crack initiation and early crack growth in a structural member requires the crack gage be bonded to the member in one form or another. The deformation of the structural member, the method of attachment, and the geometry and unbonded length of the gage all influence the amount of load transferred into the crack gage. Thus, the stress in the crack gage may vary somewhat from the actual stress in the structure at the attachment location.

Theoretically, the total displacement of a bonded, unnotched crack gage as shown in Fig. 2.3 may be determined as follows:

$$\delta_G = \delta_G' + 2\delta_G'' \quad (2.19)$$

where  $\delta_G$  = total crack gage displacement, and  $\delta_G'$  and  $\delta_G''$  = crack gage displacement in the reduced section and thick section, respectively. The elastic axial deformation is given from Hooke's law as:

$$\delta = \left(\frac{\sigma}{E}\right) L \quad (2.20)$$

where  $\sigma$  = applied stress,  $L$  = gage length, and  $E$  = modulus of elasticity. Consequently, the displacements in the reduced and thick sections of the crack gage are given as:

$$\delta_G' = \frac{P_G}{W t_R E_G} l_R \quad (2.21)$$

$$\delta_G'' = \frac{P_G}{W t_0 E_G} (l_U - l_R) \quad (2.22)$$

where  $P_G$  = load transferred into crack gage,  $E_G$  = modulus of elasticity of the crack gage material,  $l_R$  = length of the reduced section of the crack gage,  $l_U$  = total unbonded length of the crack gage,  $t_R$  = thickness of the reduced section,  $t_0$  = thickness of the thick section, and  $W$  = crack gage width. The total gage displacement may be expressed in terms of the stress in the reduced section of the crack gage by combining Eqs. 2.19, 2.21, and 2.22:

$$\delta_G = \frac{\sigma_G t_R}{E_G} \left[ \frac{1}{t_R} + \frac{1}{t_0} - \frac{1}{t_R} \right] \quad (2.23)$$

For the portion of the structure beneath the crack gage,

$$\delta_S = \left( \frac{\sigma_S}{E_S} \right) l_U \quad (2.24)$$

where  $\delta_S$  is the displacement in the structure beneath the crack gage. Assuming that a perfect bond exists between the crack gage and the structure, then the displacements that occur in the structure and the gage must be compatible:

$$\delta_S = \delta_G \quad (2.25)$$

The stress in the reduced section of the gage,  $\sigma_G$ , is obtained by substituting the elastic displacements (Eqs. 2.23 and 2.24) into the compatibility relationship (Eq. 2.25):

$$\sigma_G = \frac{(1_U/t_R) (E_G/E_S)}{\left[ \frac{1}{t_R} + \frac{1}{t_0} - \frac{1}{t_R} \right]} \sigma_S \quad (2.26)$$

There is a distinct advantage in adhesively bonding the fatigue crack gage to a structural member. The use of a structural adhesive avoids the introduction of potential fatigue crack initiation sites associated with welding and bolting. However, as a result of the creep and relaxation of structural adhesives, the assumption of perfect bonding between the crack gage and the structural member may not be perfectly valid. Hence, the actual stress in the crack gage must be modified as follows:

$$\sigma_G = F_g F_a \sigma_S \quad (2.27)$$

where  $F_g$  = geometry factor that is a function of the crack gage geometry, and  $F_a$  = load transfer factor that is a function of the adhesive. Assuming that the structural member and the crack gage are both fabricated from the same material ( $E_G / E_S = 1$ ) then the geometry factor is given as:

$$F_g = \frac{1 U / t_R}{\left[ \frac{1_R}{t_R} + \frac{1 U - 1_R}{t_0} \right]} \quad (2.28)$$

The load transfer factor,  $F_a$ , is a coefficient that accounts for the reduction in gage stress as a result of creep and relaxation of the adhesive. The value of  $F_a$  must be established experimentally by monitoring the strain in

the structure relative to that in the gage during a load test. In studies by Dumanis [8] and Ori and Grandt [48],  $F_a$  was found to be fairly constant over most of the loading cycle, indicating load independence. On the other hand, Ashbaugh and Grandt [2] found a linear load dependence of the load transfer ratio, although no relationship for the load transfer was given. Examination of the methods used to bond the crack gages to the structural members indicate that load independence of the load transfer factor may be achieved by fully heat curing the adhesive to minimize creep and relaxation. However, the use of heat curing is neither practical nor economical for crack gages which are bonded to the surface of large structural members.

### 2.3.2 Crack Gage Stress Intensity Factor

The empirical relationship developed by Paris [49,50] can be used to compute crack growth in the fatigue crack gage. However, in order to use the Paris expression, the stress-intensity factor range,  $\Delta K_I$ , for a crack originating from a notch in a crack gage must be known, as well as the crack growth material constants. The stress-intensity factor range,  $\Delta K_I$ , may be estimated in two different ways: applied load solution or applied displacement solution. Since the crack gage is adhesively bonded to the structural member, it is subjected to displacement constraints. Under these constraints, the applied displacement approach has

been shown to be much simpler than the applied load approach if the shape function for the geometry can be determined [8].

The stress intensity factor for a cracked, unnotched gage under displacement constraints is given by Dumanis [8] as:

$$K_{I_G} = \frac{\delta_G}{l_R} E_G \sqrt{\pi a} \beta \quad (2.29)$$

where  $\beta$  = shape function for displacement control that depends on  $a/W$ ,  $a$  = length of the edge crack in the gage, and  $\delta_G$  = total applied displacement in the gage. Substituting  $\delta_S$  for  $\delta_G$ , Eq. 2.29 becomes:

$$K_{I_G} = \sigma_S \left( \frac{E_G}{E_S} \right) \left( \frac{l_U}{l_R} \right) \sqrt{\pi a} \beta \quad (2.30)$$

This expression is relatively simple and requires knowledge only of the shape function  $\beta$  for a given gage configuration. The  $\beta$  values for the stress-intensity factor may be obtained from the solution given by Torvik [63], and are summarized in Table 2.1 for various  $a/W$  values and gage aspect ratios.

The displacement constraint stress-intensity factor given by Torvik [62] for short crack lengths ( $a/W$  ratio less than 0.1) is:

$$K_{I_G} = 1.12\sigma_S \left( \frac{E_G}{E_S} \right) \sqrt{\pi W} \sqrt{\frac{a}{W}} \quad (2.31)$$

The crack length,  $a$ , in Eqs. 2.30 and 2.31 is for an edge crack in an unnotched crack gage. If, however, the crack propagates from the root of an edge notch in the gage, then the crack length should include both the notch depth and actual crack length.

A computer program was developed to estimate fatigue crack propagation in the gage. The program utilized numerical integration of the Torvik stress-intensity solution in the Paris [49,50] crack growth power law.

### 2.3.3 Crack Gage Selection Procedure

As previously stated, the primary objective of this study is to investigate the feasibility of using a crack gage to predict the onset of fatigue crack growth in a structural member. To this effect, it was desired that the crack gage initiate a detectable crack before the detection of a fatigue crack in the structural member. In addition, a desired feature was to obtain complete fracture of the gage before fracture of the structural member occurred. The selected structural member was a transverse butt-joint welded specimen containing a full-length lack of penetration (LOP) discontinuity.

Fatigue crack initiation lives were predicted using the modified Plummer-Mattos computer program mentioned earlier (Sec. 2.2.5) and the fatigue properties of E60 electrode material and ASTM A36 mild steel [22,40].

The steps followed in the design of an A36 mild steel crack gage to predict the onset of fatigue crack growth from the LOP discontinuity in a structural member are summarized below:

1. In Fig. 2.4 a family of curves of the fatigue notch factor,  $K_f$ , versus the fatigue crack initiation life,  $N_I$ , for the structural member is presented. The curves were generated using the fatigue properties of E60 electrode material [22] since no information on the fatigue properties of AWS-E70S-6 wire electrode, which was used in welding the test specimens, was found. Tobe and Lawrence [60] have shown that for a given lack of penetration (LOP) discontinuity the maximum fatigue notch factor is given by Eq. 2.32.

$$K_{f_{\max}} = 1 + (c/A)^{0.5} \quad (2.32)$$

where,  $c$  = one half of the LOP depth and  $A$  = microstructural parameter. Using the computed  $K_{f_{\max}}$  and the applied stress level, the corresponding  $N_I$  was determined from Fig. 2.4.



2. Next, the stress in the crack gage due to applied stress level in the structural member was calculated from Eq. 2.27. From Fig. 2.5, the required value of  $K_f$  associated with the calculated crack gage stress range and the predicted  $N_I$  from step 1 above was then found for the A36 steel crack gage.
  
3. Finally, from Fig. 2.6, a notch root radius,  $r$ , and notch depth,  $d$ , was selected to obtain a  $K_f$  value equal to that given in Step 2. The notch depth  $d$  was chosen such that the corresponding  $K_f$  was either equal to or greater than the predicted  $K_f$  from step 2. This was to ensure that the crack gage initiated a crack before the presence of a crack was detected in the structural member.

## CHAPTER 3

## EXPERIMENTAL INVESTIGATION

3.1 General

The primary objective of this study is to investigate the feasibility of using a crack gage to detect the onset of fatigue crack initiation and early crack growth in steel members. A secondary objective is to further examine the effect of lack of penetration (LOP) discontinuities on the fatigue behavior of transverse butt-welded joints.

To achieve these objectives, three series of tests were conducted: Load Transfer tests, Basic Control tests, and Crack Gage/LOP tests. The purpose of the Load Transfer tests was to determine the fraction of the applied load transferred into the crack gages through the adhesive, and to evaluate the integrity of the adhesive under cyclic loading. The purpose of the Basic Control tests was to provide reference data for comparisons with the LOP tests. The purpose of the Crack Gage/LOP tests, which constituted the bulk of the experimental study, was to evaluate the performance of crack gages in detecting crack initiation, to evaluate the suitability of the mathematical models used in the crack gage design, and to detect the onset of early

crack growth in welded butt joints. Details concerning the fabrication, instrumentation, and testing of the specimens in the three series of tests are described in this chapter.

A 220,000-lb. (979 kN) MTS servo-controlled hydraulic testing machine in the Structural Engineering Laboratory at Purdue University was used to apply the required static or cyclic loading for the test specimens (Fig. 3.1). All of the tests were conducted in the load control mode at ambient room-temperature conditions. The loading frequency for the cyclic load tests was either 2.0 or 3.3 Hz; most of the tests were conducted at the latter frequency. The total fatigue life of the structural component was the number of cycles to complete fracture, and was recorded automatically by a counter on the control unit of the MTS machine.

## 3.2 Specimen Fabrication

### 3.2.1 Structural Component Fabrication

Depending on the test series, the structural component was either a plain plate member, a sound butt-joint double-V groove welded member, or a butt-joint double-V groove welded member containing a full-length lack of penetration (LOP) discontinuity, as shown in Fig. 3.2. All of the structural components were fabricated from 3/4-in. (19.05-mm) ASTM A36 steel plate. The physical properties

of the ASTM A36 steel obtained from coupon tests are presented in Table 3.1. The chemical composition of the ASTM A36 steel as obtained from a laboratory analysis is presented in Table 3.2.

#### 3.2.1.1 Plain Plate Member

The plain plate specimens were fabricated in the following manner:

1. 27-in. x 30-in. (675-mm x 750-mm) blanks were cut from a 6.75-ft. by 9-ft. (2.0-m by 2.75-m) steel plate such that the direction of rolling was parallel to the eventual longitudinal axis of the structural specimens (Fig. 3.3).
2. Twelve 4-in. (102-mm) wide x 27-in. (686-mm) long strips were flame cut from two blank panels.
3. The specimen strips were machined to the final specimen size (Fig. 3.2(a)) on a computer-controlled Hirco milling machine.

These specimens were used in the Load Transfer tests, and also in the first phase of the Basic Control tests.

#### 3.2.1.2 Welded Butt-Joint Member

The butt-joint, double-V groove welded members were fabricated in the following manner:

1. Same procedure as in Step 1 of the plain plate specimens.
2. The blanks were milled in half and beveled at one end of each of the halves. A 1/16-in. (1.6 mm) weld groove land was used for full penetration (sound) weld specimens. As shown in Fig. 3.4, the specimens with full length LOP discontinuities were fabricated by using weld groove lands of either 1/4-in. (6.4 mm) or 3/8-in. (9.5 mm).
3. The two halves were welded together using the gas metal arc (GMAW) process. A 0.045-in. (1.14-mm) diameter solid electrode wire (AWS Classification ER70S-6) was used in the welding process. The physical and chemical properties of the electrode wire as reported by the manufacturer's specifications are presented in Tables 3.1 and 3.2, respectively. A Meta-Lax vibration inducer, shown in Fig. 3.5, was used during the welding process to provide residual stress relief.
4. Finally, the weld reinforcement was ground off and the welded plate flame cut into 4-in. (100-mm) strips. The strips were then machined to the final specimen dimensions on a computer-controlled Hirco milling machine.

Prior to fabrication of the welded members, a trial

welding study was conducted to establish the welding procedures that produced the desired weld types. Appropriate combinations of voltage, current, gas flow rate, weld speed and land size were selected to fabricate complete penetration welds and welds with LOP depths of 0.125-in. (3.2-mm) and 0.250-in. (6.4-mm). The established procedures used in the fabrication of the welded members are summarized in Table 3.3.

As shown in Table 3.4, the LOP depths ranged from 0.133-in. to 0.231-in. (3.38-mm to 5.87-mm) for the LOPl-8 series, and from 0.220-in. to 0.342-in. (5.59-mm to 8.69-mm) for the LOPl-4 series. The variations in LOP depths across the width of the specimens are also presented in Table A.1. These variations are attributed primarily to the fact that welding was performed manually. Operator control was not nearly as consistent during the welding of the 30-in. (762-mm) wide plates as it was for the welding of the trial plates which had a maximum width of only 12-in. (305-mm).

### 3.2.2 Crack Gage Fabrication

The crack gages were fabricated from 3/16-in. (4.76-mm) thick ASTM A36 steel sheet, the physical properties of which are given in Table 3.1. The gages were fabricated such that the direction of rolling was parallel to the

longitudinal axis of the structural component. The 2-in. (50.8-mm) wide x 6-in. (152.4-mm) long blanks were cut initially from the sheet plate with a shearing machine. The blanks were then machined to the final gage configuration, shown in Fig. 3.6, on a computer controlled Hirco milling machine.

A fillet radius of 0.375-in. (9.5-mm) was used to reduce the likelihood of a fatigue crack initiating from the fillet region. The gage thickness was 0.03-in. (0.76-mm), the minimum thickness that could be machined without bending the gage out-of-plane as a result of tool pressure. This thickness also satisfies the recommendation by Smith [56] that the gage thickness should not exceed 20% of the thickness of the structural component to which the gage is to be bonded. The 2.0-in. (50.8-mm) gage width was selected to provide adequate surface area for bonding to the structural component. Finally, the length of the thin part of the gage was also selected as 2.0-in. (50.8-mm) so that the ratio  $l_R/W$  was equal to one. This ratio of  $l_R/W$  has been shown experimentally by Smith [56], and analytically by Torvik [63], to give a uniform rate of crack growth.

### 3.3 Load Transfer Tests

#### 3.3.1 Test Specimen

The Load Transfer test specimen consisted of a structural component (Fig. 3.2(a)) with a pair of unnotched crack gages adhesively bonded to the surface. The plain plate structural component was fabricated from 3/4-in. (19.05-mm) thick ASTM A36 steel plate as described in Sec. 3.2.1. The performance of two different structural adhesives, namely, Loctite Depend Adhesive and Dymax Engineering Adhesive 845, were evaluated in the Load Transfer tests. Both bonding agents required the application of an activator to one surface and the adhesive to the mating surface. The physical properties of the two adhesives as reported by the manufacturers' specifications are given in Table 3.5.

Preliminary tests indicated that careful surface preparation was necessary to maintain adequate bond integrity under fatigue loading. Consequently, the following procedure was adopted in bonding the crack gages to the structural components:

1. The surfaces to be bonded were roughened with grit 50 sand paper with the aid of a hand operated pneumatic belt sander, and then degreased with Chlorothene-Nu degreaser.



2. The surfaces were then cleaned with M-Prep Conditioner A and M-Prep Neutralizer, respectively.
3. Two beads of the adhesive, per 4-in<sup>2</sup> (25.8-cm<sup>2</sup>) area, were then applied to the surface of the structural component and the activator applied to the surface of the crack gage.
4. Immediately after contact was made between the crack gage and the structural component, two 0.30-lbs. (135-g) weights were placed at each end of the crack gage to distribute the adhesive evenly over the entire bonding area, and thereby, achieve a uniform bond thickness.

Average bond thicknesses of 0.010-in. (0.254-mm) and 0.004-in. (0.102-mm) were obtained for the Loctite Depend and Dynax Engineering adhesives, respectively. The larger bond thickness obtained for the Loctite Depend adhesive was due to its higher viscosity (Table 3.5).

A set-up guide was used to keep the crack gage in position during the bonding process. The set-up guide, which is shown in Fig. 3.7, consisted of small C-clamps and a 'horizontal movement restrainer' to hold the gages in the desired location as the adhesive cured.

### 3.3.2 Test Procedure

Prior to testing, strain gages were bonded to the test specimen surface as shown in Fig. 3.8. Micro-Measurements electrical resistance strain gages EA-06-250BG-120 and EA-06-125BT-120 were bonded to the structural component and crack gages, respectively.

The test specimen was statically loaded and unloaded from 0 to 45 kips (0 to 200 kN) in increments of 5 kips (22 kN) and the strain readings recorded after each load increment by means of a Vishay/Ellis 20 constant current strain indicator and switch and balance unit. The loading cycle was repeated twice. The 45 kip load (200 kN) produced a stress of approximately 30 ksi (207 MPa) on the gross area, and represented the maximum anticipated stress range to be used in the Crack Gage/LOP fatigue tests described in Sec. 3.5.

Subsequent to the initial static loading, the specimen was loaded cyclically from 0 to 45 kips (0 to 200 kN) for two million cycles to evaluate the bond integrity of the adhesive under cyclic loading conditions. At several pre-selected number of load applications, the test was temporarily stopped and the static test repeated to determine if a change in strain reading had occurred. A significant change in the strain reading would imply that the load transferred into the gage had changed, possibly as a result of cyclic debonding.

### 3.4 Basic Control Tests

#### 3.4.1 Test Specimen

Two different Basic Control test specimens were prepared. The first type was a plain plate specimen as shown in Fig. 3.2(a), while the second was a sound transversely welded butt-joint specimen as shown in Fig. 3.2(b). The plain plate specimens were tested to provide data on the fatigue behavior of the ASTM A36 steel plate from which all the structural components were fabricated. The soundly welded specimens were tested to provide data on the fatigue behavior of full penetration welded butt joints, and to provide a basis from which the effect of lack of penetration (LOP) discontinuities on welded butt joints could be evaluated.

#### 3.4.2 Test Procedure

The Basic Control test specimens were tested under zero-to-tension ( $R=0$ ) cyclic loading until complete fracture occurred. However, specimens that survived two million cycles of loading without any visual indication of fatigue damage were declared run-outs and retested at higher stress levels. The number of cycles to failure, the stress level, and the location from which fracture initiated were recorded for each test.

### 3.5 Crack Gage/LOP Fatigue Tests

#### 3.5.1 Test Specimen

The test specimen for the Crack Gage/LOP tests consisted of a structural component with a pair of crack gages adhesively bonded on opposite sides of the specimen surface - see Fig. 3.9. The structural component was a butt-welded flat plate member containing a full-width lack of penetration (LOP) discontinuity as shown in Fig. 3.2(c). The structural component was fabricated from 3/4 in. (19.05 mm) thick ASTM A36 steel plate as described in Sec. 3.2.1.

The weld at the sides of the structural component was etched using a two percent solution of nital. Etching enhanced the weld configuration and made it possible to measure the depth of the LOP discontinuity with a fine-graduated ruler. The measured values of the LOP depth were used in the design of a single edge notch at mid-height of one of the crack gages bonded to the structural component.

The notch type and dimensions were selected such that a crack was expected to initiate in the gage before the presence of a crack was detected in the structural component (Sec. 2.3.3). Although a crack gage can be designed for a specific application, in this study the gages were selected to satisfy a broad range of behavior. This was achieved by using either a sharp-vee notch, a U-groove notch or a smooth circular notch; the three notch

configurations are shown in Fig. 3.10. The root radius for each notch type was kept constant and only the notch depth varied for each application. In one application a smaller root radius was used in order to reduce the depth of the notch. The selected notch depths and radii are presented in Table 3.6.

On the basis of the Load Transfer tests, Dymax Engineering Adhesive 845 and 535 Activator was used for all structural bonding. The bonding procedure described in Sec. 3.3.1 was followed to attach the gages to the structural components.

### 3.5.2 Instrumentation

The results of primary interest in the Crack Gage/LOP tests included the fatigue crack initiation and total lives of both the structural component and the crack gages, advance of the crack in the gage, and the extent of fatigue damage in specimens that did not fracture.

The fatigue crack initiation life of the structural component was estimated experimentally by monitoring the reflection of an ultrasonic pulse from the LOP discontinuity. A 0.5" x 1.0" (12.7 mm x 25.4 mm) Panametrics A4035 ultrasonic transducer (2.25 MHz) mounted in a 70° wedge reflector (Fig. 3.11) was attached to the specimen to detect the onset of fatigue cracking. The transducer was

connected to a Panametrics 5055UA Ultrasonic Analyzer which was in turn connected to a Tektronix T912 10MHz Storage Oscilloscope. A Tektronix C-5C camera mounted on the oscilloscope enabled photographs of the ultrasonic pulse reflection from the LOP to be taken and compared.

Initially, it was intended to also estimate the crack initiation life by tracking the strain developed in electrical resistance strain gages bonded very closely to the LOP tip. Accordingly, Micro-Measurements EA-06-062AK-120 electrical resistance strain gages were attached to specimens LOPl-8-1, LOPl-8-3 and LOPl-8-4. The cyclic loading was periodically interrupted and a Vishay/Ellis 20 constant current strain indicator and switch and balance unit was used to read the strain levels during a static loading cycle. However, no indication of fatigue crack initiation could be deduced from the recorded strains and, as such, the procedure was not continued for the remaining tests. Examination of the fractured surfaces indicated that the cracks often initiated near mid-length of the LOP discontinuity, a factor which is undoubtedly related to the inability of the surface mounted strain gages to detect the onset of fatigue crack initiation.

Crack initiation and propagation in the crack gages was observed by means of a low-power traveling tele-microscope. The tele-microscope was mounted on a Velux unislide A2500 assembly at the end of which was attached a Hewlett Packard optical shaft encoder with a digital

readout to measure the crack length in the gage. A photograph of the tele-microscope and accompanying instrumentation is shown in Fig. 3.12.

### 3.5.3 Test Procedure

Prior to testing, the specimen was placed in the horizontal position and the LOP discontinuity monitored with an ultrasonic transducer mounted in a  $70^{\circ}$  wedge reflector. Household three-in-one oil was used as a transmitting medium. The wedge reflector was moved back and forth along the longitudinal axis of the specimen in the vicinity of the LOP discontinuity, until a position that gave the maximum reflection of the ultrasonic pulse from the LOP was observed.

The position of the wedge reflector was then lightly marked on the specimen. The oil was wiped off and the specimen degreased with Chlorothene-Nu degreaser. Finally, the edges of the marked area representing the position of the wedge reflector, were taped with several passes of heavy-duty Scotch Tape thereby creating a tight fitting slot for the wedge reflector. This procedure was necessary to ensure that the wedge reflector was placed at the same location throughout the test. The wedge reflector was held in place by a wide rubber band.

The specimen was then gripped under the load control mode of the MTS testing machine. A static load, equivalent

to the maximum load to be applied during the fatigue test, was introduced so that the LOP discontinuity was opened as fully as possible. An initial polaroid photograph of the ultrasonic reflection from the LOP was then taken using the camera mounted onto the oscilloscope. The specimen was unloaded and the fatigue test started using a loading frequency of 3.3 Hz. All of the specimens were subjected to a zero-to-tension cyclic loading, except specimen LOP1-4-4 which was loaded from 5-22.5 ksi. (34.5-155.0 MPa).

At several pre-selected number of load applications the cyclic loading was stopped and the maximum cyclic load was applied statically. The ultrasonic transducer/wedge reflector was then placed in position and the ultrasonic pulse reflection from the LOP monitored and photographed. Monitoring of the ultrasonic pulse reflection was continued until significant changes in the reflected waveforms were observed.

The area around the notch in the crack gage was observed frequently with the aid of a low-power tele-microscope until a crack was observed. To facilitate detection of the crack a light film of oil was applied to the area surrounding the notch. As the crack opened and closed after initiation, the oil was drawn in and squished out in sequence with the frequency of loading leaving bubbles on the surface of the gage. The crack length in the gage was recorded from the digital readout (Sec. 3.5.2) and the number of loading cycles obtained from the counter on



the control unit of the MTS machine. The number of cycles necessary to completely fracture the crack gage was also recorded.

The majority of the specimens were cyclically loaded to complete fracture. However, some of the specimens survived two million cycles loading or more. These specimens were removed from the testing machine and broken statically in a bend test. These specimens were first notched in the plane of the LOP discontinuity to ensure that the location of fracture was through the LOP, and thus, permit inspection of the weld and the LOP discontinuity.

Finally, the ends of the fractured specimens were machined off approximately one inch from the point of fracture and the depth of the LOP discontinuity measured at five different locations across the width of the specimen as shown in Fig. A.1 of Appendix A. The measured values of the LOP depths are presented in Table A.1. The two ends of each fractured LOP specimen were also placed side by side and photographed. The photographs of the fracture surfaces are presented in Figs. B.1 and B.2 of Appendix B, for the LOPl-8 and LOPl-4 series, respectively.

## CHAPTER 4

## DISCUSSION AND EVALUATION OF TEST RESULTS

4.1 General

In this chapter the results of the experimental investigation are presented and discussed. Data of primary interest that was collected during the specimen tests include strain measurements, gage crack lengths, polaroid photographs of the ultrasonic pulse reflection from the lack of penetration (LOP) discontinuities, and measurements of the LOP sizes. The data from the tests are presented in tabular form; where possible, graphical representation of the data is also provided.

In Sec. 4.2 the results of the Load Transfer tests are presented and the performance of the Depend and Dymax engineering adhesives evaluated.

In Sec. 4.3 the fatigue test results for the plain plate, sound weld, and LOP test series are presented and discussed. The test data are also compared with data reported in the literature for similar tests. The effect of LOP discontinuities on the fatigue life of mild steel weldments is discussed also.

The results of the Crack Gage tests are presented and

discussed in Sec. 4.4. The observed fatigue lives are compared with the fatigue lives computed using the mathematical models outlined in Chapter 2.

Finally, a comparison between the crack gages and the LOP specimens to which they were bonded is presented in Sec. 4.5.

#### 4.2 Load Transfer Test Results

The strain data from the Load Transfer tests were obtained from strain gages bonded to the crack gages and the structural component. The strain gage locations are shown in Figure 3.8. The test was stopped at several pre-selected number of load applications so that a static load cycle could be applied to obtain the strain readings. Plots of the gage strain values versus applied stress for various number of loading cycles are presented in Figs. 4.1 and 4.2 for the Depend adhesive, and in Figs. 4.3 and 4.4 for the Dymax adhesive. These plots show the progressive reduction in gage strain with increase in the number of applied loading cycles, as well as the introduction of compressive strains in the gages.

Strain values at zero load, prior to the application of the static load cycle, versus the number of applied loading cycles are presented in Figs. 4.5 and 4.6 for the Depend and Dymax adhesives, respectively. Gages 1 and 2

refer to the electrical resistance strain gages bonded to the specimen surface at mid-width, while Gages 3 and 4 refer to the strain gages at mid-width on the crack gages (Fig. 3.8). The corresponding plots of the strain readings at the maximum applied load are shown in Figs. 4.7 and 4.8.

In Fig. 4.5 it can be observed that compressive strains of approximately 400 and 20 microstrain had been induced in crack gages 1 and 2 (strain gages 3 and 4), respectively, for the Depend adhesive after 2 million cycles of loading. These values correspond to compressive stresses of 11.6 ksi (80 MPa) and 0.6 ksi (4.1 MPa), respectively. For the Dymax adhesive, the maximum compressive strains induced in crack gages 1 and 2 after 2 million cycles of loading were 60 and 300 microstrain, corresponding to compressive stresses of 1.7 ksi (12 MPa) and 8.7 ksi (60 MPa), respectively.

These results initially indicate the possibility of bending in the structural component or in the crack gages. However, minor variations of the strain readings on opposite sides of the structural component (Gages 1 and 2, Figs. 4.5-4.8) indicate that, within the limits of experimental error, the factors leading to the introduction of bending in the crack gages are localized. Consequently, variations in the gage strains may be attributed to deformation of the adhesives, out-of-planeness of the crack gages, or a combination thereof. Since the maximum applied stress of 30 ksi (207 MPa) was well below the yield

strength of the crack gage material (43.8 ksi (302 MPa)), the compressive stresses are not the result of residual stresses from yielding of the gages. Consequently, the compressive effects can be attributed solely to deformation of the adhesives.

To determine the strain transfer ratio, the gage strain is normalized with respect to the structure strain. For cases where the structure and the crack gage are of the same material, then the stress transfer ratio will equal the strain transfer ratio. The strain transfer ratio is plotted against the number of applied loading cycles as shown in Figs. 4.9 and 4.10 for the Depend and Dymax adhesives, respectively. From Fig. 4.9 it is observed that the load transfer ratio for the Depend adhesive decreases rapidly with increase in the number of applied loading cycles. The maximum strain transfer ratios were 0.80 and 0.75 during the first static loading for crack gages 1 and 2 (sides 1 and 2), respectively, and only 0.40 and 0.44 after 2 million cycles.

The performance of the Dymax adhesive was significantly better than that of the Depend adhesive, with respect to the percentage of the strain transferred to the crack gage as shown in Fig. 4.11. The maximum values of the strain transfer ratio for the first loading cycle were 1.09 and 1.29 for crack gages 1 and 2, respectively. These values remained fairly constant up to about 100,000 cycles of loading and then decreased linearly to 0.77 and 0.66,

respectively, after 2 million cycles. As stated previously, the decrease in the strain transfer ratio is believed to be the result of deformation of the adhesives. The superior performance observed with the Dymax adhesive can be attributed to its low viscosity of 3,000 cps compared to 70,000 cps for the Depend adhesive - see Table 3.5. The lower viscosity of the Dymax adhesive resulted in an average bond thickness of 0.004-in. (0.010 mm) compared with 0.010-in. (0.254 mm) for the Depend adhesive. Thus, it is expected that the large bond thickness for the Depend adhesive will cause more deformation than the Dymax adhesive, leading to a lower strain transfer ratio, as was observed.

Based on the limited experimental data and evaluation discussed above, the Dymax adhesive was selected for use in bonding all further crack gages to the structural components. For analytical purposes, average values of the strain transfer ratio based on the number of applied loading cycles were used. It should be noted that the strain transfer ratio includes the geometric effect of the crack gage,  $F_G$ , as given by Eq. 2.28. For the crack gage configuration selected,  $F_G = 1.19$ . Hence, the true strain transfer factor for the Dymax adhesive,  $F_a$ , is given by the value of the inherent strain transfer ratio divided by  $F_G$ . The strain transfer ratio and the corresponding strain transfer factor for the Dymax adhesive are presented in Table 4.1 for different ranges of applied loading cycle.

### 4.3 Plain Plate, Sound Weld and LOP Fatigue Test Results

#### 4.3.1 Results of the Fatigue Tests

The results of the plain plate, sound weld, and the LOP fatigue tests are presented in Tables 4.2, 4.3 and 4.4, respectively. Plots of the applied stress range versus fatigue life on a log-log scale (S-N curves) for these data are shown also in Figs. 4.12 to 4.15. In these diagrams the solid lines represent the mean value of the observed data computed using a least squares best-fit method.

Specimens which were declared runouts, indicated by the arrows in Figs. 4.12 to 4.15, as well as the data obtained from their re-test, indicated by the solid symbols in Figs. 4.12 and 4.13, were excluded from the least squares best-fit analysis. The re-test values were not included in the regression analysis because the fatigue strengths may have been affected by the prior loading history. The fatigue strengths at 100,000, 500,000, 1 million, and 2 million cycles were computed from the least squares best-fit equations and are presented in Table 4.5.

In Fig. 4.16 a summary comparison of the mean regression curves as obtained from the fatigue test results is presented. By comparing the plain plate and the sound weld S-N results, it is clear that the use of welding significantly reduces the fatigue strength for long lives (greater than 100,000 cycles). Moreover, further reductions in the

fatigue strength are obtained when LOP discontinuities are present.

#### 4.3.2 Discussion and Analysis of Test Results

##### 4.3.2.1 Plain Plate Specimens

A total of ten specimens were tested in the plain plate test series. The results of these fatigue tests (Table 4.2 and Fig. 4.12) indicate very little scatter and excellent correlation of the fatigue life with the applied stress range. A linear regression analysis of the data (excluding data from runouts and re-tests) indicated a standard error of estimate of 0.096 and a correlation coefficient of -0.986. It should be noted that only two data points were available for each stress range.

Although the results of the re-tests matched the results of the tests at the higher stress ranges, no absolute conclusions could be drawn as to what effect understressing had on the fatigue resistance of the re-tested specimens. The fatigue resistance of specimen PPL-1R appears to have been improved slightly by understressing: 126,800 cycles compared with 74,900 and 96,700 cycles for specimens PPL-4 and PPL-5, respectively. However, the fatigue resistance of re-tested specimens PPL-8R and LTT-1R, 274,500 cycles, fell between the fatigue resistance of specimens PPL-6 and PPL-7: 312,500 and 257,300 cycles,



respectively. Thus it would appear that understressing below the fatigue limit did not have a significant effect on the fatigue resistance of the re-tested specimens. This conclusion is further supported by the fact that specimens PPL-8R and LTT-1R both had a fatigue life of 274,500 cycles when cycled at 47 ksi (324 MPa) even though they were initially tested at stress ranges of 35 ksi and 30 ksi (241 MPa and 207 MPa), respectively.

#### 4.3.2.2 Sound Weld Specimens

The results of the sound weld fatigue tests shown in Fig. 4.13 typify the scatter associated with fatigue test data. The standard error of estimate obtained from a regression analysis of the data (excluding data from runouts and re-tests) was 0.210, with a correlation coefficient of -0.805.

The weld reinforcement of the sound weld specimens was removed and the weld surface was ground flush with the specimen surface. However, as shown in Table 4.3, all the specimens fractured through the weld toe, indicating that the stress raisers present at the weld toe were more severe than at the fillets of the specimens.

Specimen SWD-12 survived 2.19 million applications of cyclic loading at a stress range of 27 ksi (186 MPa) without any indication of fatigue damage, and was declared a runout. However, the specimen fractured after 178,400

cycles when re-tested at a stress range of 42 ksi (290 MPa). This compares favorably with the fatigue lives of specimens SWD-1 (260,100 cycles), and SWD-2 (176,100 cycles) indicating that specimen SWD-12R did not suffer any significant fatigue damage as a result of being initially tested at a lower stress range.

Very scattered porosity was present in some of the sound welds. However, the porosity apparent on the fracture surface was especially severe in specimens SWD-15 and SWD-16. It is not evident if the fatigue lives of these two specimens were adversely affected by the porosity since they fell within the normal scatter of the data (Fig. 4.13).

The mean fatigue resistance of the sound weld specimens was lower than that of the plain plate specimens, especially in the long-life region (Fig. 4.16). As shown in Table 4.5, the fatigue strengths of the plain plate specimens at 100,000 and 2 million cycles were 52.8 ksi and 39.5 ksi (364 MPa and 272 MPa), respectively. The corresponding values for the sound weld specimens were 49.2 ksi and 21 ksi (347 MPa and 135 MPa), or 93.2 and 53.2 percent of the plain plate fatigue strengths. The applied stress ranges in the short-life region of the plain plate and sound weld fatigue tests were either around or greater than the yield strength of the ASTM A36 mild steel material. As a result of the large (plastic) strains in the specimens, the fatigue lives are expected to be

comparable in the short-life region, even though the stress raisers at the weld toe of the sound weld specimens may be more severe than the stress raisers at the fillets of the plain plate specimens. However, in the long-life region where the strains are low (primarily elastic), the stress raisers present at the weld toe of the sound weld specimens have a more pronounced effect than the fillet of the plain plate specimen resulting in the marked difference in the fatigue strengths.

#### 4.3.2.3 LOP Specimens

A total of twenty-nine LOP specimens were tested at stress ranges ranging from 12 ksi (82.7 MPa) to 30 ksi (207 MPa). As shown in Figs. 4.14 and 4.15, there was considerable scatter in the results. The standard error of estimate obtained from a linear regression analysis of the data was 0.315 for the LOP1-8 series, and 0.348 for the LOP1-4 series. The corresponding correlation coefficients were -0.697 and -0.737, respectively.

Originally, it was intended to have LOP depths of 0.125-in. (3.38 mm) and 0.250-in. (6.35 mm) for the LOP1-8 series and LOP1-4 series, respectively. However, as shown in Table 3.4 the actual LOP depths ranged from 0.133-in. to 0.231-in. (3.18 mm to 5.87 mm) for the LOP1-8 series, and from 0.220-in. to 0.342-in. (5.59 mm to 8.69 mm) for the LOP1-4 series. Variations in the LOP depth across the

width of the specimens were commonly observed for all of the specimens. Values of the LOP depth as measured on the fracture surface are summarized in Table A.1. As discussed in Sec. 3.2.1, these variations can be attributed to the fact that the welding was performed manually. The use of an automatic welding process would have produced more uniform LOP depths since there would have been consistent control of the electrode gun tip.

As evident in Figure 4.16, the fatigue strengths of the LOP specimens were significantly lower than the fatigue strengths of the plain plate and sound weld specimens. Several researchers [9,18,31,45,60,65,69] have noted the deleterious effect of lack of penetration (LOP) discontinuities on the overall fatigue strength. Moreover, it can be observed in Fig. 4.16 that the slopes of the S-N curves for the sound weld and the LOPl-8 series are identical, but steeper than the slope of the S-N curve for the LOPl-4 series. The fatigue strengths of the LOPl-8 and the LOPl-4 specimens at 100,000 cycles were 37.3 ksi (257 MPa) and 27.4 ksi (189 MPa), respectively. However, as a result of the flatter slope of the S-N curve for the LOPl-4 series, the fatigue strength of both the LOPl-8 and LOPl-4 specimens at 2 million cycles was 17.0 ksi (117 MPa). This can be attributed to the fact that in the short-life region, where the greater percentage of the life is spent in crack propagation, the cracks have a smaller thickness to propagate through in the LOPl-4 specimens as a result of

their larger LOP depths. Thus, the LOPl-4 specimens would be expected to have shorter lives in the short-life region. However, in the long-life region a greater portion of life is spent in crack initiation, and as a result the smaller thickness of the LOPl-4 specimens would have less effect on the total life. The total fatigue lives of the LOPl-8 and LOPl-4 specimens will thus be expected to be comparable in the long-life region.

One of the objectives of this study was to estimate what fraction of the total life of the LOP specimens was spent in crack initiation. This was achieved experimentally by monitoring the ultrasonic pulse reflection from the LOP discontinuity as described in Sec. 3.5.3. The fatigue crack initiation life was taken as the number of cycles required to produce a definite change in the reflection of the ultrasonic pulse from the LOP discontinuity. For example, an initiation life of 45,000 cycles can be inferred from the sequence of polaroid photographs in Fig. 4.17 for Specimen LOPl-4-3. Since the LOP discontinuity was sub-surface, the crack length at which a change in the ultrasonic pulse reflection was observed could not be measured. Hence, it should be emphasized that the crack size corresponding to this definition of initiation life is unquestionably different from the 0.01-in. (0.25 mm) crack size that is often used in crack propagation calculations.

The changes in the ultrasonic pulse reflection from the LOP discontinuity were in most instances significant

enough to allow firm conclusions to be drawn regarding the crack initiation life of a specimen. However, in a few cases the changes were not clear, and careful examination of the peaks and valleys of the pulse reflections were required to estimate the crack initiation life. No estimation of the crack initiation life could be made for Specimens LOP1-8-7 and LOP1-4-14 because the ultrasonic pulse reflection for these specimens did not change. Polaroid photographs of the ultrasonic pulse reflection for specimen LOP1-4-14 are shown in Fig. 4.18.

Several factors may have affected the use of ultrasonics to estimate the crack initiation lives of the LOP specimens: the pressure exerted on the transducer, the position of the transducer, and the quality of the weld. For each of the test specimens the position of the ultrasonic transducer that gave the maximum reflection of the ultrasonic pulse was clearly defined, as described in Sec. 3.5.3. Also, a single wide rubber band was used to hold the transducer in place each time a scan was taken. Hence, it is believed that the pressure exerted on the transducer and its position on the specimen were kept fairly constant for each ultrasonic reading. The repeatability of the ultrasonic signals prior to crack initiation supports the belief that consistent transducer placement between readings was achieved. Porosity in some of the welds and the uneven surfaces of the discontinuities were also believed to have introduced noise in the ultrasonic pulse reflection

from the LOP. Erratic signals at times made it difficult to draw firm conclusions from the polaroid photographs of the reflection. However, the overall performance of the ultrasonic transducer in detecting the onset of crack initiation from the LOP discontinuities was generally satisfactory.

The fatigue crack initiation life for each of the LOP specimens was predicted using revised version of the computer program developed by Mattos et al. [40]; the predicted values are presented in Table 4.6. To compute the predicted values, initial compressive residual stresses of 26 ksi (179 MPa) and 13 ksi (89.6 MPa) were assumed to exist at the tip of the LOP discontinuities in the LOPl-8 and LOPl-4 specimens, respectively. These values correspond to two-thirds and one-third of the yield strength of the ASTM A36 base material, and are based on the idealized through-thickness residual stress distribution presented in Fig. 4.19.

A comparison of the initiation lives estimated by ultrasonics and predicted analytically are presented in Fig. 4.20. From this figure it is observed that the estimated initiation lives were generally lower than the predicted lives. It can also be observed from Table 4.6 that the onset of crack initiation from the LOP discontinuities as detected by ultrasonics occurred within 19% of the total life for most of the specimens. The ratio was approximately 37% for LOPl-4-16, mainly as a result of its

low total life (41,100 cycles).

#### 4.3.3 Comparison of Test Results with Other Studies

The results of the fatigue tests were compared with the results of similar tests by other researchers [9,45,54] and are presented in Figs. 4.21 to 4.23. In Fig. 4.21 it can be observed that the S-N curve for the plain plate specimens tested in the current study has a flatter slope than the S-N curve for the results reported in the data bank by Munse et al. [54]. The fatigue strengths at 100,000 cycles are comparable; however, at 2 million cycles, the fatigue strength determined in the current study is slightly higher than the fatigue strength reported in the data bank, 39.5 ksi (272 MPa) versus 32.1 ksi (221 MPa). The data bank results are based on a combination of fatigue tests for A7, A36 and A373 mild steels. These steels generally have slightly lower yield strengths than the ASTM A36 mild steel used in the current study. Thus, the ASTM A36 mild steel used in the current study would be expected to have slightly better fatigue properties than the average values for the steels in the data bank.

The fatigue strength of the transverse butt-joint weld specimens tested in the current study was slightly higher at all stages of life than that reported in the data bank - see Fig. 4.22. However, the S-N curve for the sound weld tests conducted by Ekstrom and Munse [9] had a flatter



slope and differed significantly from the S-N curves obtained in this study and from the data bank. The differences in fatigue strength between the results of the current study and the data bank results may be attributed to the higher fatigue characteristics of the E70 wire electrode used in the current study compared with the E60 electrodes used in the data bank study. The difference in fatigue strength obtained in the study by Ekstrom and Munse [9] can be attributed to the fact that some of the specimens were tested with negative stress ratios. The effective stress range for these specimens will therefore be less than the applied stress range, and as such, the fatigue lives of these specimens will be increased.

The results of the LOP fatigue tests compare reasonably with the results obtained by Ekstrom and Munse [9] and by Newman and Dawes [45], as shown in Fig. 4.23. Although the LOP discontinuities in the specimens tested by Newman and Dawes [45] did not extend throughout the plate width, only the 3/4" x 1/16" LOP series had a notably higher fatigue strength in the long-life region. This result is consistent with the findings of Guyot et al. [18] for welds with partial width LOP discontinuities. However, the S-N curve for the 1-1/4" x 1/16" LOP series tested by Newman and Dawes [45] was slightly below the S-N curve for the LOP1-8 series tested in the current study. The results presented in Fig. 4.23, as well as the results of other LOP studies [9,18,31,45,60,65,69], illustrate the extremely

poor fatigue strength of welds which contain LOP discontinuities when compared with the fatigue resistance of comparable sound welds.

#### 4.4 Crack Gage Test Results

The fatigue lives of the crack gages which were attached to the welded specimens in the LOP study are presented in Table 4.7. Both the observed fatigue lives and the analytically predicted fatigue lives are presented.

Three different notch types were used for the entire range of expected fatigue crack initiation lives: smooth circular notches, sharp vee-notches and U-groove notches (Fig. 3.11). Circular notches with radii of 0.250-in. (7.36 mm) and depths of either 0.200-in. or 0.275-in. (5.08 mm or 6.99 mm) were used for crack gages designed to initiate cracks after 2 million cycles. As noted in Table 4.7, these crack gages, (CG1-8-1 to CG1-8-3 and CG1-4-1 and 2) performed as they were designed, as no detectable crack initiation was observed at the gage notch root after 2 million cycles of loading.

For LOP specimens in which a very short initiation life was expected (less than 20,000 cycles), sharp vee-notches 0.20-in. (5.08 mm) deep were used. For the applied loading the vee-notched crack gages, CG1-8-10 to CG1-8-12 and CG1-4-13 to CG1-4-16, all had initiation lives less

than or equal to 2,000 cycles, which was consistently less than the predicted initiation lives. The observed crack initiation lives demonstrate that notched crack gages can be designed to rapidly initiate a crack in the presence of an extreme fatigue loading condition. As a result of the relatively short lives of the LOP specimens to which crack gages CG1-4-13 to CG1-4-16 were bonded, the gages did not fracture completely prior to failure of the welded LOP specimens. The cracks in gages CG1-4-13 and CG1-4-15 propagated through 88% and 81% of the gage width, respectively, but the crack in CG1-4-16 propagated through only 26% of the width before the LOP specimen failed. The extent of damage in gages CG1-4-13 and CG1-4-15 was very significant, and thus, these gages were considered to have performed excellently. From the crack growth data for gages CG1-4-13 through CG1-4-16, it appears that gage CG1-4-16 would have experienced similar damage levels as did gages CG1-4-13 through CG1-4-15 had it survived about 150,000 cycles of loading. The other vee-notched gages, CG1-8-11 through CG1-8-13, all performed excellently, and failed prior to failure of the structural components to which they were bonded.

For LOP specimens in which the expected initiation lives fell between 20,000 and 2 million cycles, U-groove notches with depths of 0.250-in., 0.300-in., or 0.400-in. (6.35 mm, 7.62 mm or 10.16 mm) were used. A constant root radius of 0.125-in. (3.18 mm) was used for all grooves,

except for gages CG1-4-3, CG1-4-7, and CG1-4-8 where the root radius was 0.063-in. (1.59 mm). A smaller root radius was used in the design of the latter gages to limit the depth of the notch to 0.400-in. (10.16 mm); a root radius of 0.125-in. (3.18 mm) would have resulted in a notch of depth 0.600-in. (15.2 mm) to initiate a crack as desired. Three U-groove gages, CG1-8-6, CG1-4-10, CG1-4-12, had initiation lives corresponding to 65.4%, 87.6% and 75.6% of the predicted values, respectively. Nine of the crack gages, CG1-8-4,8,9 and 13 and CG1-4-4,5,6,9 and 11, had initiation lives ranging from 104% to 149% of the predicted values. The ratios for CG1-8-5, CG1-4-7, and CG1-4-8 ranged from 192% to 270%. Only gage CG1-8-7 had an initiation life greater than 300% of the predicted value (379%). However, this gage experienced severe out-of-plane bending during the cyclic test, which probably reduced the effective tensile stress transferred into the gage, and caused the crack to initiate much later than predicted (580,000 versus 153,000 cycles).

In Fig. 4.24 a plot of the analytically predicted versus the experimentally estimated initiation life for all the crack gages is presented. As shown in the figure, the predicted initiation lives were in most instances less than the experimentally estimated lives.

The performance of gage CG1-8-7 illustrates two of the potential problems associated with the use of the crack gage to detect the onset of fatigue damage in structural

members, namely, out-of-plane bending, and variations in stress in the gage with cyclic life. Out-of-plane bending of the gage may be the result of out-of-planeness or inadequate stiffness of the thin part of the gage. The latter can be addressed easily by increasing the thickness of the thin part of the gage. Out-of-planeness of the gage can be attributed to unsymmetrical machining and the application of excessive pressure on the thin part of the gage during various handling processes. These can be addressed by careful machining and handling of the gages. None of the gages tested, apart from CG1-8-7, experienced notable out-of-plane bending.

At each stress level only one set of identical crack gages was used. The notch in the gages were of the same type, and had the same depth and root radius. Given the random nature of fatigue behavior, the initiation lives within each set of identical gages cannot be attributed solely to differences in strain transfer. However, examination of the crack growth data presented in Figs. 4.25 to 4.31 indicates that in each set the gages experienced different crack growth rates. The variation in crack growth rates reflects the different stresses experienced by the gages, mainly as a result of possible variations in the adhesive thicknesses, which as discussed earlier in Sec. 4.2 does affect the strain transfer ratio.

Smith [56] and Torvik [63] have demonstrated that the crack growth rate in a gage with a reduced section of

square configuration, subjected to displacement constraints, is approximately constant. This behavior was observed also in the gages tested in the present study, as indicated by the typical gage crack length versus number of loading cycles plot presented in Fig. 4.32. Prior to fracture, however, the crack growth rates normally increased as indicated by the non-linear region in Fig. 4.32. For a given set of gages, the average stress intensity factor of each gage will give a indication of the stress experienced by that gage. As a result of the linear relationship between crack length and number of loading cycles, the average crack growth rate,  $da/dn$ , was computed from a linear regression analysis of the crack growth data, excluding data in the non-linear region. The average stress intensity factor for the gage was then computed by means of the Paris relationship [49,50]. The crack growth constants  $C = 3.6 \times 10^{-10}$  and  $m = 3.0$  for ASTM A36 mild steel were used [55]. The computed stress intensity factors are presented in Table 4.8.

From Table 4.8 it is observed that the vee-notched gages had consistent average stress intensity factors, 37.13, 36.12, and 36.30  $\text{ksi}\sqrt{\text{in}}$  for gages CG1-8-10 to CG1-8-12, respectively, and 30.29, 32.67, 32.41 and 31.52  $\text{ksi}\sqrt{\text{in}}$  for gages CG1-4-13 to CG1-4-16, respectively. This indicates that in each set the gages experienced very similar stresses. As presented in Figs. 4.27 and 4.31, the measured crack growth data for the vee-

notched gages were predicted very well, indicating that the actual gage stresses were identical nearly to the stresses obtained from the strain transfer analysis. Gages CG1-8-4,6 and 9 and CG1-4-5,6,8,11 and 12 also are well behaved, implying that the actual gage stresses were predicted very well from the strain transfer analysis. However, the crack growth prediction for Gages CG1-8-5,7,8 and 13 and CG1-4-3,4 and 7 is not as good, and the actual gage stresses appear to be slightly less than those obtained from the strain transfer analysis. This conclusion is of particular interest in the case of CG1-8-7 because as mentioned earlier, this gage experienced severe out-of-plane bending and was expected to have an actual gage stress less than that obtained from the strain transfer analysis.

From Figs. 4.25 to 4.31 it is also observed that in most instances the predicted crack growth curves are conservative. This is also illustrated in Fig. 4.33 where the predicted propagation lives are plotted against the observed lives.

The predicted total fatigue life for each specimen was obtained by summing the predicted crack initiation life and the predicted crack propagation life. The total fatigue lives of the gages were predicted fairly well, although somewhat conservatively, as shown in Fig. 4.34.

#### 4.5 Comparison of Crack Gages with LOP Specimens

In this study the development of a detectable crack in the crack gages was desired to occur concurrently with the development of a detectable crack in the LOP specimens to which they were bonded. To evaluate the performance of the gages in this regard, the experimentally estimated gage initiation lives were plotted, as shown in Fig. 4.35, against the ultrasonic estimate of the initiation lives for the LOP specimens. In Fig. 4.35 it is observed that the experimentally estimated gage initiation lives were in most instances greater than the experimentally estimated LOP initiation lives. Thus, it would appear that the gages were not very effective in detecting the onset of crack growth in the LOP specimens. However, it should be emphasized that the gages were designed on the basis of the analytical prediction of the LOP initiation lives, which as shown in Fig. 4.20 were also greater than the experimentally estimated LOP initiation lives.

To further clarify the above statement, the experimentally estimated gage initiation lives were plotted against the analytically predicted LOP initiation lives as presented in Fig. 4.36. Given the random nature of fatigue behavior and the fact that the analytically predicted LOP initiation lives were not exact, the correlation achieved between the estimated gage initiation lives and the analytical prediction of the initiation lives for the LOP



specimens is considered excellent. Thus, it can be concluded that the gage designs were effective.

Finally, in Fig. 4.37 a comparison is made between gage total life and LOP total life. The solid symbols shown in Fig. 4.37 indicate tests in which the LOP specimen failed prior to complete fracture of the gage (Sec. 4.4). The symbols with the arrows indicate tests in which the gage failed, but in which the LOP specimen did not (runout tests). Excluding the solid symbols, in Fig. 4.37 it is observed that in all instances the gage failed before failure of the LOP specimen occurred. This satisfies the desired gage design requirement that the gage should fracture completely through before fracture of the LOP specimen occurred. In an actual service application, complete fracture (or significant damage) of a gage would provide further warning of potential fatigue damage in the structural detail being monitored.

## CHAPTER 5

## PRACTICAL APPLICATION OF CRACK GAGE CONCEPT

5.1 General

The objective of the fatigue crack gage study reported herein is to examine the feasibility of a method that provides a clear indication of fatigue crack initiation and early, subcritical crack growth at a given detail in a structural steel element. Previous investigators have used crack gage configurations which were pre-cracked so that all of the fatigue life of the gage was spent in propagation of the crack. A modification of the crack gage concept is to use a notched gage with no pre-crack. Thus, in this application the crack gage notch can be designed such that it will initiate a detectable crack in the crack gage concurrent with the development of a detectable fatigue crack in the structural member. Alternately, the crack gage may be designed such that it is significantly damaged prior to the development of a detectable fatigue crack in the structural member. The latter approach would require more crack propagation in the crack gage than the former method, and may be more desirable when infrequent visual inspection is used.

In this chapter the steps involved in the design of a crack gage are outlined in Sec. 5.2, and numerical examples that illustrate crack gage design are presented in Sec. 5.3. Finally, recommendations for the design of a crack gage are presented in Sec. 5.4.

## 5.2 Crack Gage Design

A fatigue crack gage can be designed for use with most structural steel members, provided a reasonable estimate of the fatigue notch factor,  $K_f$ , for the detail can be obtained. Design of the crack gage for a given structural detail involves proper correlation of the fatigue crack initiation lives for the gage and the detail. The following procedure, which is summarized also in a flow chart format in Fig. 5.1, outlines the steps necessary to design a fatigue crack gage:

1. Determine the fatigue notch factor for the structural detail,  $K_{fS}$ . Peterson's equation [51,52] is frequently used to estimate  $K_f$ :

$$K_f = 1 + \frac{K_t - 1}{1 + A/r} \quad (5.1)$$

where  $K_t$  = theoretical stress concentration factor,  
 $r$  = notch radius, and

$$A = 0.001(300/\sigma_u)^{1.8} \text{ inches} \quad (5.2)$$

with  $\sigma_u$  = ultimate tensile strength, in ksi.

2. Estimate the fatigue crack initiation life of the structural detail,  $N_{I_S}$ , using the fatigue notch factor,  $K_{f_S}$ , the given load history, and the appropriate low-cycle fatigue properties of the structural member. The relationship between  $K_f$  and  $N_I$  for ASTM A36 steel is shown in Fig. 5.2 for four different constant-amplitude remote loading stress ranges. A computer-based solution, consistent with the low-cycle fatigue requirements previously described, is needed to estimate  $N_{I_S}$ .
3. Adjust the crack gage initiation life to suit the crack gage design philosophy. If the initiation lives are to be matched directly, then no adjustment is necessary and  $N_{I_G} = N_{I_S}$ . However,  $N_{I_G}$  can be selected to be less than  $N_{I_S}$  to permit the gage crack to grow to an appropriate size.
4. Use the estimate of  $N_{I_G}$  to obtain the fatigue notch factor for the gage,  $K_{f_G}$ . (Again, Fig. 5.2 may be used if the gage is A36 steel.) It is necessary to determine the crack gage aspect ratio,  $l_G/W$ , and the adhesive characteristics,  $F_a$ , when evaluating the gage fatigue notch factor.

5. Adjust the notch depth,  $d$ , and notch radius,  $r$ , to provide the appropriate  $K_{fG}$  value. For illustration purposes, a slot with a circular radius, as shown in Fig. 5.3, is the notch type selected for the crack gage. The relationship between  $K_{fG}$  and the notch root radius for a crack gage fabricated from ASTM A36 steel is summarized in Fig. 5.4 for various values of the notch depth.

As noted above, it may be desirable from an inspection standpoint to permit the gage crack to propagate to a particular size. A gage crack large enough for visual detection certainly would be logical. The number of loading cycles to achieve a particular crack size can be computed using Eqs. 2.30 and 2.31 in conjunction with the Paris crack growth equation.

### 5.3 Numerical Examples

A fillet welded tee joint, as shown in Fig. 5.5, has been chosen to illustrate the fatigue crack gage selection procedure. It is assumed that the connection is fabricated using ASTM A36 steel and is designed to resist a zero-to-tension cyclic loading of 16.67 ksi (115 MPa). Two numerical examples are given to illustrate different crack gage design philosophies. Also, the sensitivity of the crack

gage design to loadings different from the design loading is evaluated.

### 5.3.1 Example 1

In this example, the crack gage is designed such that fatigue crack initiation in the gage and the tee joint occur simultaneously. Consequently, the initiation of a crack in the gage would signal the inspector that the tee joint has experienced a loading sequence that is sufficiently severe to cause the formation of a fatigue crack.

The first step involves estimation of the fatigue notch factor for the structure. A finite element analysis of the joints reported by Gurney [17] indicates that the stress concentration factor for a load-carrying fillet welded member with a weld toe angle of  $45^\circ$  is 4.0. If this value, along with a weld toe radius of 0.03 to 0.04 in. (0.76 to 1.02 mm), is used in Eqs. 5.1 and 5.2, the resulting range in  $K_{fS}$  values is 2.8 to 3.0. Consequently, the fatigue notch factor for the structure,  $K_{fS}$ , is assumed to be 3.0.

Second, the crack initiation life of the structural detail must be estimated. The fatigue crack initiation life for an A36 steel member with  $K_{fS} = 3.0$  and  $\sigma_S = 16.67$  ksi (115 MPa) is 815,000 cycles. This value may be computed using an appropriate computer solution, or it may be

obtained approximately from Fig. 5.2.

Third, no adjustment in the initiation life is needed since the crack gage and the structure are to initiate a crack simultaneously. Consequently,  $N_{I_G} = N_{I_S}$ .

Fourth, the required value of the fatigue notch factor for the crack gage will be determined. The crack gage geometry in the unbonded region will be assumed square with  $l_U/W = 1.0$ . Moreover, the thick section of the gage will be fully bonded giving  $l_U = l_R$ ; for this condition  $F_g = 1.0$ . Finally, it is assumed that the characteristics of the adhesive are known and that  $F_a = 0.9$ . Consequently, the crack gage stress given by Eq. 2.27 is 15.0 ksi (103 MPa). From Fig. 5.2 we find that  $K_{f_G} = 3.35$  is needed to provide  $N_{I_G} = 815,000$  cycles.

Finally, the notch geometry parameters must be selected to provide the appropriate  $K_{f_G}$  value. Fig. 5.4 can be used to determine the necessary crack gage notch. For example, a gage with  $r = 0.15$ -in. (3.8 mm) and  $d = 0.20$ -in. (5.1 mm) produces the appropriate  $K_{f_G}$  value. It should be noted that other combinations of  $r$  and  $d$  would also provide the desired  $K_{f_G}$  value.

### 5.3.2 Example 11

In this example, the crack gage will be designed to be

"significantly damaged" before crack initiation in the structure occurs. This scheme provides further warning since the gage will initiate a crack before a crack forms in the tee joint. The "significantly damaged" condition is assumed to correspond to a crack that has propagated 0.50-in. (12.7 mm) across the gage width; a crack of this size can be detected easily using visual inspection.

As in the first example,  $K_{fS} = 3.0$  and  $N_{IS} = 815,000$  cycles. However, in this example the initiation life of the gage is adjusted as follows:

$$N_{IG} = N_{IS} - N_{PG} \quad (5.3)$$

Using Eqs. 2.30 and 2.31, in conjunction with the crack growth constants for A36 steel, the propagation life of the gage,  $N_{PG}$ , for  $d = 0.20$ -in. (5.1 mm) is estimated to be 459,000 cycles. Consequently, from Eq. 5.3 the value of  $N_{IG}$  is given as 356,000 cycles. From Fig. 5.2, a value of  $K_{fG} = 3.84$  is selected to obtain this value of  $N_{IG}$ .

The notch geometry parameters must be selected to reflect the gage fatigue notch factor. Consequently, notch values of  $r = 0.10$ -in. (2.5 mm) and  $d = 0.20$ -in. (5.1 mm) are selected from Fig. 5.4. It can be noted that a notch radius, smaller than that required in the previous example, was necessary to provide for the higher  $K_{fG}$  value.

The gage design should be selected to match the



inspection philosophy. The thoroughness and frequency of the inspection program should be considered when correlating the critical damage level in the crack gage to fatigue crack initiation in the structural detail. The method used in the first example may be preferable if the structure is inspected frequently, while the method in the latter example may be better for inspection programs that require only occasional inspections.

### 5.3.3 Sensitivity Analysis

In a survey on bridges [64], the actual stresses experienced by girders were found to be considerably lower than the design stresses. If a crack gage is bonded to a structural joint which experiences a stress range significantly different from the design stress range, the crack initiation life of the gage, as well as that of the joint, will change. For the crack gage to function as desired, it must still be able to initiate and propagate a detectable fatigue crack prior to the development of a detectable fatigue crack in the structural joint. Moreover, the fatigue crack initiation life of the gage must change in the same proportion that crack initiation life of the structure changes when subjected to a stress range different than the design stress range. In other words, the gage must be able to function independent of the applied remote loading.

To examine the sensitivity of the crack gage design to loadings different than the design loading, the fatigue crack initiation lives of the tee joint and the crack gage designed in Example I were evaluated at two other stress levels. It was assumed that the actual stress experienced at the joint was (a) 10 ksi (69 MPa) and (b) 20 ksi (138 MPa), instead of 16.67 ksi (115 MPa). The corresponding gage stresses are (a) 9 ksi (62 MPa) and (b) 18 ksi (124 MPa), instead of 15 ksi (103 MPa). For a joint stress of 10 ksi (69 MPa) the fatigue crack initiation lives of the tee joint and the crack gage are  $2.82 \times 10^7$  and  $2.71 \times 10^7$  cycles, respectively. The corresponding lives for a joint stress of 20 ksi (138 MPa) are 330,000 and 323,000 cycles, respectively. In both cases the crack gage initiates a fatigue crack before the tee joint, and thus still functions as desired.

The above sensitivity analysis was extended to the design in Example II. The crack propagation life of the gage when subjected to a joint stress of 10 ksi (69 MPa) was estimated to be  $1.86 \times 10^6$  cycles; the corresponding crack propagation life for a joint stress of 20 ksi (138 MPa) was estimated to be 232,000 cycles. The fatigue crack initiation life of the tee joint at the two stresses are the same as above,  $2.82 \times 10^7$  and 330,000 cycles, respectively. Thus, the required fatigue crack initiation life for the gage would be  $2.64 \times 10^7$  and 98,000 cycles, respectively. For a gage with  $K_{fG} = 3.84$  as obtained in Example

11, the fatigue crack initiation lives are  $8.39 \times 10^6$  and 173,000 cycles for joint stress ranges of 10 ksi (69 MPa) and 20 ksi (138 MPa), respectively. Thus, at the lower stress range the gage would still function as designed, although a fatigue crack would be initiated much earlier than expected ( $8.39 \times 10^6$  versus  $2.64 \times 10^7$  cycles). However, at the higher stress the design philosophy would not be satisfied since a fatigue crack would initiate in the gage later than required (173,000 versus 98,000 cycles).

The sensitivity analyses described above illustrates the importance of knowing and using the actual expected stress in the design of a gage. If the actual stress and design stress are expected to be considerably different, then matching fatigue crack initiation for the gage with crack initiation for the structural detail will provide satisfactory results.

#### 5.4 Recommendations for Design

Based on the findings of this study the following recommendations are made when considering the notch design of a crack gage:

1. For fatigue crack initiation lives less than 20,000 cycles, gages with sharp, vee-shaped notches may be used. A notch depth of 0.20-in. (5.08 mm) is sufficient for most purposes.

2. For fatigue crack initiation lives between 20,000 cycles and  $2.0 \times 10^6$  cycles, gages with U-shaped notches provide the best performance. The notch depth and root radius should be selected in accordance with the procedure outlined in Sec. 5.2.
3. For initiation lives greater than  $2.0 \times 10^6$  cycles, gages with a gentle circular notch can be used. Again, the procedure outlined in Sec. 5.2 should be used to select the appropriate notch dimensions.
4. If the actual stress range at the structural detail being monitored is expected to be considerably different from the design stress range, then the crack gage should be designed by directly matching crack initiation in the gage with crack initiation in the structural detail.

## CHAPTER 6

## SUMMARY AND CONCLUSIONS

6.1 Summary

The primary objective of this research was to experimentally investigate the feasibility of using a crack gage to detect the onset of fatigue crack initiation and early crack growth in structural steel details. A secondary objective was to further examine the effect of lack of penetration (LOP) discontinuities on the fatigue behavior of transverse butt-welded joints.

Twenty-nine notched crack gages, adhesively bonded to twenty-nine LOP specimens were tested under a zero-to-tension cyclic loading with stress range values between 12 ksi (82.7 MPa) and 30 ksi (207 MPa). In addition, ten plain plate and sixteen sound butt-welded specimens were tested under a zero-to-tension fluctuating load to provide reference data for comparisons with the LOP tests. Two load transfer tests were conducted to evaluate the performances of Loctite Depend and Dymax engineering adhesives, and also to determine the fraction of the applied load transferred into the crack gages through the

adhesives.

The crack gage fatigue test results are compared with analytical predictions of the fraction of cyclic life spent in crack initiation and crack propagation. The plain plate, sound weld and LOP fatigue test results from this study are compared with those from three other studies. Finally, recommendations for crack gage design are discussed, and two examples are provided to illustrate the crack gage design procedure.

## 6.2 Conclusions

The following conclusions are based on the limited number of experimental tests and the analytical evaluations presented in this report.

1. Adhesively bonded notched crack gages can be used as visual inspection aids to provide a reasonable indication of fatigue crack initiation and early crack growth at a given detail in a structural steel member.
2. Notched crack gages can be designed to satisfy a broad range of expected crack initiation lives in structural steel details subjected to fatigue loading:

(a) For a structure that is inspected frequently, the notch can be designed such that it initiates a detectable crack in the crack gage concurrent with the development of a detectable fatigue crack in the structural member.

(b) For a structure that is inspected less frequently, notched crack gages can be designed such that they are "significantly damaged" before crack initiation in the structure occurs. The presence of a crack across a significant portion of the gage width, which is easy to detect visually, will provide further warning of potential crack initiation and growth in the structure. For this crack gage design philosophy, however, the applied stress range must be well known.

(c) Shallow circular notches can be used to provide fatigue crack initiation lives greater than 2 million cycles. For expected crack initiation lives between 20,000 cycles and 2 million cycles, U-shaped notches are recommended. For initiation lives less than 20,000 cycles, which are unlikely for most practical situations, sharp vee-notches should be used.

(d) A square configuration for the reduced portion of the crack gage,  $l_R/W=1.0$ , will provide a fairly uniform crack growth rate in an adhesively bonded gage.

(e) The Torvik stress intensity factor solutions [63], together with knowledge of the stress transferred into a crack gage, can be used to obtain a reasonable prediction of the crack growth in the gage.

3. Lack of penetration (LOP) discontinuities significantly reduce the fatigue strength of a weld. The reduction in strength due to LOP is obvious when compared to the fatigue strength of plain plate or sound weld specimens. For example, the fatigue strength, relative to plain plate material, of sound transverse butt welds and butt welds with LOP discontinuities at 100,000 cycles and 2 million cycles were found as follows: 93 and 53 percent for sound weld material; 71 and 43 percent for welds with 1/8-in. (3.2 mm) LOP discontinuities; and 52 and 43 percent for welds with 1/4-in. (6.4 mm) LOP discontinuities.
4. The onset of crack initiation at the LOP discontinuities as detected by ultrasonics occurred



within 19% of the total life for most of the specimens.

5. An adhesive with low viscosity, such as Dymax Engineering Adhesive 845, was found to perform better under cyclic load than a similar adhesive with higher viscosity. However, the strain transfer characteristics of the adhesive must be known to obtain reasonable estimates of the stress transferred into the crack gage. A bonding process that limits the extent of deformation within the adhesive will improve the strain transfer characteristics of the adhesive.

### 6.3 Recommendations For Future Work

The tests and analyses presented in this report have demonstrated that it may be feasible to use notched crack gages as visual inspection aids to provide a reasonable indication of crack initiation and early crack growth in steel structures. However, further research is required to improve upon the design features and procedures to make the crack gage more versatile. The following suggestions for future research and study are recommended to improve the understanding of crack gage behavior and to test their suitability for actual implementation and use under service

conditions.

1. Since most practical load applications will be significantly different from the constant amplitude loading used in the experiments conducted in this study, the performance of notched crack gages under complex load histories should be evaluated.
2. The crack gage experiments described herein were conducted under controlled environmental conditions in a laboratory and do not reflect the environmental conditions experienced by actual structures. It is conceivable that the performance of a crack gage under actual environmental conditions, such as high humidity and the extreme ranges of temperature that occur from summer to winter, may differ from that observed in the laboratory. The question of paramount importance is: How does a crack gage perform under actual environmental and service conditions? This question can be addressed only through the direct application and monitoring of crack gages on actual structural steel members which are subjected to cyclic loadings, such as bridges and offshore structures. Such a study would not only provide useful data on the performance of crack gages in the field, but would also provide information regarding adhesive and material effects that could be

used in the design of a more versatile crack gage.

3. Further research to evaluate the load transfer and deformation characteristics of the structural adhesives will provide a more accurate evaluation of the stresses induced in the crack gages.

Table 2.1 Shape Function Values for Stress-Intensity Factor of Edge-Cracked Gage Subjected to Displacement Constraints [63]

a/W	$\beta$		
	$1_{U/W} =$		
	0.5	1.0	2.0
0.1	0.848	1.028	1.094
0.2	0.606	0.854	1.053
0.3	0.489	0.717	0.991
0.4	0.417	0.615	0.887
0.5	0.373	0.540	0.798
0.6	0.341	0.489	0.724
0.7	0.320	0.453	0.666
0.8	0.303	0.432	0.615
0.9	0.290	0.417	0.572

Table 3.1 Physical Properties of ASTM A36 Steel and AWS ER70S-6 Solid Electrode Wire

Material	Yield Strength (ksi)	Ultimate Strength (ksi)	Reduction in area (percent)	Remarks
ASTM A36 Steel (3/4 in. plate)	39.0	71.5	55.8	Average of two tests
ASTM A36 Steel (3/16 in. plate)	43.8	68.9	48.4	"
AWS ER70S-6	60.0	72.0	-	Values reported by electrode manufacturer

Table 3.2 Chemical Properties of ASTM A36 Steel and AWS ER70S-6 Solid Electrode Wire

Element	Chemical Composition, %	
	ASTM A36 Steel <sup>a</sup>	AWS ER70S-6 Solid Electrode Wire <sup>b</sup>
Carbon	0.23	0.07-0.15
Manganese	0.90	1.40-1.85
Silicon	0.05	0.80-1.15
Phosphorus	0.039	0.025
Sulfur	0.012	0.035
Nickel	<0.05	-
Chromium	0.10	-
Titanium	<0.01	-
Columbium	<0.01	-
Copper	<0.05	0.50
Molybdenum	<0.05	-
Aluminum	<0.008	-
Vanadium	<0.01	-

a - Obtained from a laboratory chemical analysis on steel shavings.

b - Obtained from electrode manufacturer specifications.

Table 3.3 Welding Parameters

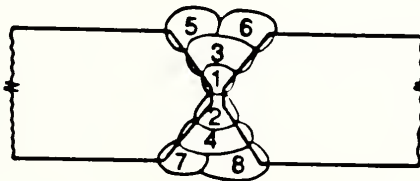
Weld Type	Pass #	Voltage (volts)	Current (amps)	Wire Feed Speed Setting <sup>a</sup>
Sound <sup>b</sup>	1-2	29	290	2.5
	3-8	24	230	1.25
Lack of Penetration	1-2	33	320	2.5
	3-6	24	230	1.25

a - Setting on a Linear 1 Hobart welding machine.

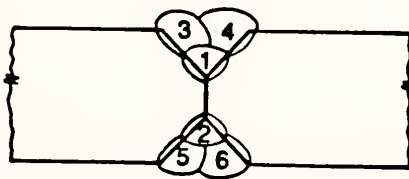
b - First pass was background before second pass was placed.

Shielding gas :- 98% Argon, 2% Oxygen at a flow rate of 42 cfh.

### WELD PASS SEQUENCES



Sound Weld



Lack of Penetration (LOP)

Table 3.4 Structural Component Details

Specimen ID	(2)		(1)		Gross Area in. <sup>2</sup>	Net Area in. <sup>2</sup>	(1) --- (2) percent
	Specimen Width in.	Specimen Thickness in.	LOP Width in.	LOP Width in.			
LOPI-8-1	2.000	.758	.168	.168	1.516	1.180	22.2
LOPI-8-2	2.020	.755	.172	.172	1.525	1.178	22.8
LOPI-8-3	2.010	.770	.167	.167	1.548	1.212	21.7
LOPI-8-4	2.000	.759	.177	.177	1.518	1.164	23.3
LOPI-8-5	2.008	.756	.173	.173	1.518	1.171	22.9
LOPI-8-6	2.008	.765	.158	.158	1.536	1.219	20.7
LOPI-8-7	1.998	.750	.133	.133	1.499	1.233	17.7
LOPI-8-8	2.016	.751	.196 <sup>a</sup>	.196 <sup>a</sup>	1.514	1.119	26.1
LOPI-8-9	1.998	.754	.187	.187	1.506	1.133	24.8
LOPI-8-10	2.000	.759	.221	.221	1.518	1.076	29.1
LOPI-8-11	1.997	.759	.223	.223	1.516	1.070	29.4
LOPI-8-12	2.006	.763	.231	.231	1.531	1.067	30.3
LOPI-8-13	1.997	.755	.159	.159	1.508	1.190	21.1

<sup>a</sup> - Measured from etched sides. Specimen did not fail through the LOP.



Table 3.4 (continued)

Specimen ID	(2)		(1)		Gross Area in. <sup>2</sup>	Net Area in. <sup>2</sup>	(1) --- (2) percent
	Specimen Width in.	Specimen Thickness in.	LOP Width in.				
LOP1-4-1	2.010	.740	.231	1.487	1.023	31.2	
LOP1-4-2	1.998	.747	.260	1.493	0.973	34.8	
LOP1-4-3	2.001	.750	.276	1.501	0.948	36.8	
LOP1-4-4	2.005	.750	.291	1.504	0.920	38.8	
LOP1-4-5	2.010	.751	.220	1.510	1.067	29.3	
LOP1-4-6	1.923	.747	.239	1.436	0.977	32.0	
LOP1-4-7	1.880	.750	.230	1.410	0.978	30.7	
LOP1-4-8	1.973	.746	.296	1.472	0.888	39.7	
LOP1-4-9	2.010	.743	.292	1.493	0.907	39.3	
LOP1-4-10	1.990	.749	.296	1.491	0.901	39.5	
LOP1-4-11	1.999	.743	.342	1.485	0.802	46.0	
LOP1-4-12	2.010	.745	.319	1.497	0.856	42.8	
LOP1-4-13	2.006	.747	.309	1.498	0.879	41.4	
LOP1-4-14	2.003	.760	.283	1.522	0.955	37.2	
LOP1-4-15	2.008	.749	.296	1.504	0.910	39.5	
LOP1-4-16	2.016	.759	.300	1.530	0.925	39.5	

Table 3.5 Adhesive Properties

Property	NAME OF ADHESIVE	
	LOCTITE DEPEND	DYMAX 845
Color	Clear	Amber
Viscosity	70,000 cps	3,000 cps
Handling Strength	1-2 minutes	45-60 seconds
Full Cure	4-24 hours	24 hours
Peel Strength	28 lb/in. (4800 N/m)	30 lb/in. (5140 N/m)
Tensile Shear Strength	2700 psi. (19 MPa)	3500 psi. (24 MPa)
Thermal Range	-60 to 250° F	-65 to 400° F

Table 3.6 Crack Gage Details

Specimen ID	Notch Type	$r_R$ (in.)	$r_N$ (in.)	$d_N$ (in.)
CG1-8-1	Circular	.030	.250	.200
CG1-8-2	"	.029	.250	.200
CG1-8-3	"	.030	.250	.200
CG1-8-4	U-Groove	.028	.125	.300
CG1-8-5	"	.029	.125	.300
CG1-8-6	"	.029	.125	.250
CG1-8-7	"	.030	.125	.250
CG1-8-8	"	.030	.125	.300
CG1-8-9	"	.030	.125	.250
CG1-8-10	Vee	.027	.010 <sup>a</sup>	.200
CG1-8-11	"	.030	.010 <sup>a</sup>	.200
CG1-8-12	"	.030	.010 <sup>a</sup>	.200
CG1-8-13	U-Groove	.030	.010 <sup>a</sup>	.200
CG1-4-1	Circular	.029	.250	.275
CG1-4-2	"	.031	.250	.275
CG1-4-3	U-Groove	.028	.063	.400
CG1-4-4	"	.030	.125	.300
CG1-4-5	"	.030	.125	.300
CG1-4-6	"	.030	.125	.300
CG1-4-7	"	.030	.063	.400
CG1-4-8	"	.029	.063	.400
CG1-4-9	"	.031	.125	.400
CG1-4-10	"	.029	.125	.400
CG1-4-11	"	.030	.125	.400
CG1-4-12	"	.030	.125	.400
CG1-4-13	Vee	.029	.010 <sup>a</sup>	.205
CG1-4-14	"	.028	.010 <sup>a</sup>	.207
CG1-4-15	"	.029	.010 <sup>a</sup>	.207
CG1-4-16	"	.030	.010 <sup>a</sup>	.208

$W = 2.0$  in.,  $L_T = 6.0$  in.,  $L_R = 2.0$  in., and  $L_U = 2.375$  in. for all crack gages.

<sup>a</sup> - Radius for maximum  $K_f$  = Peterson's material parameter, A

Table 4.1 Average Strain Transfer Ratios and Factors

Number of Cycles	Average Load Transfer Ratio	Average Load Transfer Factor, $F_a$
0-20,000	1.05	0.88
> 20,000	0.90	0.76

Table 4.2 Control Test Results - Plain Plate Specimens

Specimen Number	Stress Range (ksi)	Freq. (Hz)	Cycles to Failure	Location of Fracture
PPL-1 <sup>a</sup>	35.0	3.3	2,000,000	--
PPL-1R <sup>b</sup>	54.0	2.0	126,800	Fillet
PPL-2	42.0	3.3	1,436,500	"
PPL-3	42.0	3.3	984,300	"
PPL-4	54.0	2.0	74,900	Straight sec.
PPL-5	54.0	2.0	96,700	Fillet
PPL-6	47.0	2.0	312,500	"
PPL-7	47.0	2.0	257,300	Straight sec.
PPL-8 <sup>a</sup>	35.0	3.3	2,000,000	--
PPL-8R <sup>b</sup>	47.0	2.0	274,500	Fillet
LTT-1 <sup>a</sup>	30.0	3.3	2,000,000	--
LTT-1R <sup>b</sup>	47.0	2.0	274,500	Fillet
LTT-2 <sup>a</sup>	30.0	3.3	2,000,000	--

a - Test declared a runout

b - Specimen previously tested at a lower stress range

Specimens designated LTT were used in the Load Transfer Function Tests.

Table 4.3 Control Test Results - Sound Weld Specimens

Specimen Number	Stress Range (ksi)	Cycles to Failure	Location of Fracture
SWD-1	42.0	260,100	Weld toe
SWD-2	42.0	176,100	"
SWD-3	42.0	88,600	"
SWD-4	37.0	378,100	"
SWD-5	37.0	224,600	"
SWD-6	37.0	186,700	"
SWD-7	37.0	176,000	"
SWD-8	32.0	461,400	"
SWD-9	32.0	1,055,700	"
SWD-10	32.0	874,800	"
SWD-11	27.0	824,000	"
SWD-12 <sup>a</sup>	27.0	2,190,000	--
SWD-12R <sup>b</sup>	42.0	178,400	Weld toe
SWD-13	27.0	424,200	"
SWD-14	27.0	920,700	"
SWD-15 <sup>c</sup>	24.0	800,400	"
SWD-16 <sup>c</sup>	24.0	782,200	"

a - Test declared a runout

b - Specimen previously tested at a lower stress range

c - Fractured weld surface had severe porosity

Table 4.4 LOP Fatigue Test Results

Specimen ID	Gross Stress Range (ksi)	Net Stress Range (ksi)	Total Fatigue Life (cycles)	Remarks
LOP1-8-1	15	19.3	>2,000,000	Runout
LOP1-8-2	15	19.4	>2,000,000	Runout
LOP1-8-3	15	19.2	>2,000,000	Runout
LOP1-8-4	25	32.6	324,000	
LOP1-8-5	25	32.4	296,000	
LOP1-8-6	20	25.2	847,400	
LOP1-8-7	20	24.3	>3,640,000	Runout
LOP1-8-8	25	33.8	2,250,000	
LOP1-8-9	20	26.6	556,400	
LOP1-8-10	30	42.3	227,100	
LOP1-8-11	30	42.5	146,900	
LOP1-8-12	30	43.0	215,800	
LOP1-8-13	20	25.3	1,598,000	
LOP1-4-1	12	17.5	>2,000,000	Runout
LOP1-4-2	12	18.4	>2,000,000	Runout
LOP1-4-3	22.5	35.6	484,800	
LOP1-4-4	17.5	28.6	539,900	
LOP1-4-5	17.5	24.8	>2,000,000	Runout
LOP1-4-6	17.5	25.7	2,991,600	
LOP1-4-7	22.5	32.5	524,100	
LOP1-4-8	22.5	37.3	1,288,100	
LOP1-4-9	20	33.0	607,900	
LOP1-4-10	20	33.1	>2,272,000	Runout
LOP1-4-11	20	37.1	959,500	
LOP1-4-12	20	35.0	516,000	
LOP1-4-13	25	42.6	163,300	
LOP1-4-14	25	39.8	295,300	
LOP1-4-15	25	41.3	122,300	
LOP1-4-16	25	41.3	41,100	

Table 4.5 Summary of Fatigue Strengths (Stress Range)

	FATIGUE STRENGTH (ksi)			
	Plain Plate	Sound Weld	LOP1-8 Series	LOP1-4 Series
F <sub>100,000</sub>	56.5	62.5	44.9	30.6
F <sub>500,000</sub>	45.2	30.3	24.3	21.2
F <sub>1,000,000</sub>	42.2	24.4	20.2	18.9
F <sub>2,000,000</sub>	39.5	19.6	16.8	16.9

Table 4.6 Predicted and Estimated LOP Initiation Lives

Specimen ID	Analytical Predicted Initiation Life (cycles)	(1)	(2)	(1)
		Ultrasonic Estimated Initiation Life (cycles)	Total Fatigue Life (cycles)	---
				(2)
LOP1-8-1	1,300,000	>2,000,000	>2,000,000	-
LOP1-8-2	1,190,000	>2,000,000	>2,000,000	-
LOP1-8-3	1,330,000	100,000	>2,000,000	-
LOP1-8-4	33,140	50,000	324,000	0.154
LOP1-8-5	34,740	35,000	296,000	0.118
LOP1-8-6	166,420	105,000	847,400	0.124
LOP1-8-7	257,560	a	>3,640,000	-
LOP1-8-8	26,940	50,000	2,250,000	0.022
LOP1-8-9	110,000	50,000	556,400	0.090
LOP1-8-10	8,650	3,000	227,100	0.013
LOP1-8-11	8,510	7,500	146,900	0.051
LOP1-8-12	7,990	4,000	215,800	0.019
LOP1-8-13	163,770	60,000	1,598,000	0.038
LOP1-4-1	4,160,000	71,500	>2,000,000	-
LOP1-4-2	2,360,000	1,445,000	>2,000,000	-
LOP1-4-3	23,330	45,000	484,800	0.093
LOP1-4-4	86,910	100,000	539,900	0.185
LOP1-4-5	176,800	50,000	>2,000,000	-
LOP1-4-6	142,600	50,000	2,991,600	0.017
LOP1-4-7	34,210	25,000	524,100	0.048
LOP1-4-8	20,200	10,000-	1,288,100	<0.001
		20,000		
LOP1-4-9	39,190	80,000	607,900	0.132
LOP1-4-10	38,030	10,000	>2,272,000	-
LOP1-4-11	27,720	20,000	959,500	0.021
LOP1-4-12	32,240	20,000	516,000	0.039
LOP1-4-13	10,990	3,000	163,300	0.018
LOP1-4-14	13,000	a	295,300	-
LOP1-4-15	11,950	5,000-	122,300	0.041-
		10,000		0.082
LOP1-4-16	11,650	15,000	41,100	0.365

a - Initiation life could not be estimated from polaroid photographs.

> - Indicates test was declared a runout after that many cycles.



Table 4.7 Predicted and Observed Crack Gage Lives

Specimen ID	Gage Stress (ksi)	INITIATION LIFE		PROPAGATION LIFE		TOTAL LIFE	
		Predicted	Observed	Predicted	Observed	Predicted	Observed
(cycles)							
CG1-8-1	13.50	3,200,000	>2,000,000	979,500	a	4,180,000	-
CG1-8-2	13.50	3,200,000	>2,000,000	979,500	a	4,180,000	-
CG1-8-3	13.50	3,200,000	>2,000,000	979,500	a	4,180,000	-
CG1-8-4	26.25	22,120	23,000	122,840	127,000	144,940	150,000
CG1-8-5	26.25	22,120	52,000	122,840	217,000	144,940	269,000
CG1-8-6	18.00	153,000	100,000	396,050	270,000	549,050	370,000
CG1-8-7	18.00	153,000	580,000	396,050	516,300	549,050	1,096,300
CG1-8-8	26.25	22,120	33,000	122,840	200,000	144,940	233,000
CG1-8-9	18.00	153,000	190,000	396,050	335,000	549,050	525,000
CG1-8-10	31.50	2,160	1,500	77,100	93,100	79,260	94,600
CG1-8-11	31.50	2,160	1,500	77,100	94,300	79,260	95,800
CG1-8-12	31.50	2,160	2,000	77,100	99,500	79,260	101,500
CG1-8-13	18.00	153,000	207,000	396,050	500,500	549,050	708,000

a - Crack gage had not initiated a detectable crack at the end of the test

Table 4.7 (continued)

Specimen ID	Gage Stress (ksi)	INITIATION LIFE		PROPAGATION LIFE		TOTAL LIFE	
		Predicted	Observed	Predicted	Observed	Predicted	Observed
		(cycles)					
CGI-4-1	10.80	5,540,000	>2,000,000	1,800,000	a	7,340,000	-
CGI-4-2	10.80	5,540,000	>2,000,000	1,800,000	a	7,340,000	-
CGI-4-3	23.62	8,320	16,000	157,500	248,200	165,820	264,200
CGI-4-4	15.75	208,000	232,000	571,000	539,500	779,000	-
CGI-4-5	15.75	208,000	220,000	571,000	580,000	779,000	800,000
CGI-4-6	15.75	208,000	282,000	571,000	520,000	779,000	802,500
CGI-4-7	23.62	8,320	19,000	157,500	363,000	165,820	382,000
CGI-4-8	23.62	8,320	22,500	157,500	194,500	165,820	217,000
CGI-4-9	18.00	68,520	90,000	355,930	607,900	424,450	-
CGI-4-10	18.00	68,520	60,000	355,930	765,000	424,450	825,000
CGI-4-11	18.00	68,520	94,000	355,930	271,800	424,450	365,800
CGI-4-12	18.00	68,520	51,800	355,930	356,500	424,450	408,300
CGI-4-13	26.25	4,760	2,000	132,900	163,300	137,660	-
CGI-4-14	26.25	4,760	1,500	132,900	137,900	137,660	139,400
CGI-4-15	26.25	4,760	1,000	132,900	122,300	137,660	-
CGI-4-16	26.25	4,760	1,000	132,900	41,100	137,660	-

a - Crack gage had not initiated a detectable crack at the end of the test

b - Specimen failed before crack gage was completely fractured

Table 4.8 Computed Stress Intensity Factors Based on Average Measured Crack Growth Rates

Specimen ID	$\Delta K_{avg}$ (ksi- $\sqrt{in}$ )
CG1-8-4	31.97
CG1-8-5	27.69
CG1-8-6	25.34
CG1-8-7	20.67
CG1-8-8	27.90
CG1-8-9	22.76
CG1-8-10	37.13
CG1-8-11	36.12
CG1-8-12	36.30
CG1-8-13	20.67
CG1-4-3	25.41
CG1-4-4	14.32
CG1-4-5	19.49
CG1-4-6	21.51
CG1-4-7	21.90
CG1-4-8	27.74
CG1-4-9	15.75
CG1-4-10	17.80
CG1-4-11	24.55
CG1-4-12	23.00
CG1-4-13	30.29
CG1-4-14	32.67
CG1-4-15	32.41
CG1-4-16	31.52

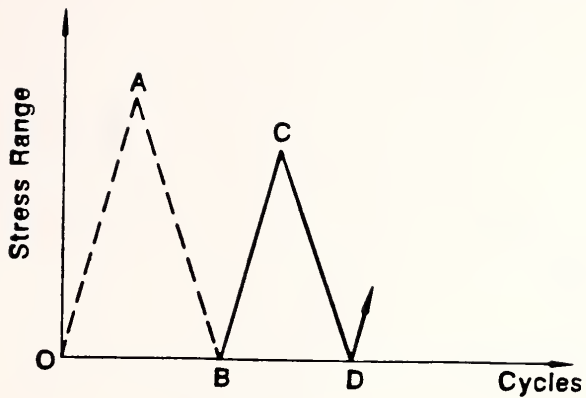


Figure 2.1 Set-Up Cycle for Compressive Residual Stress

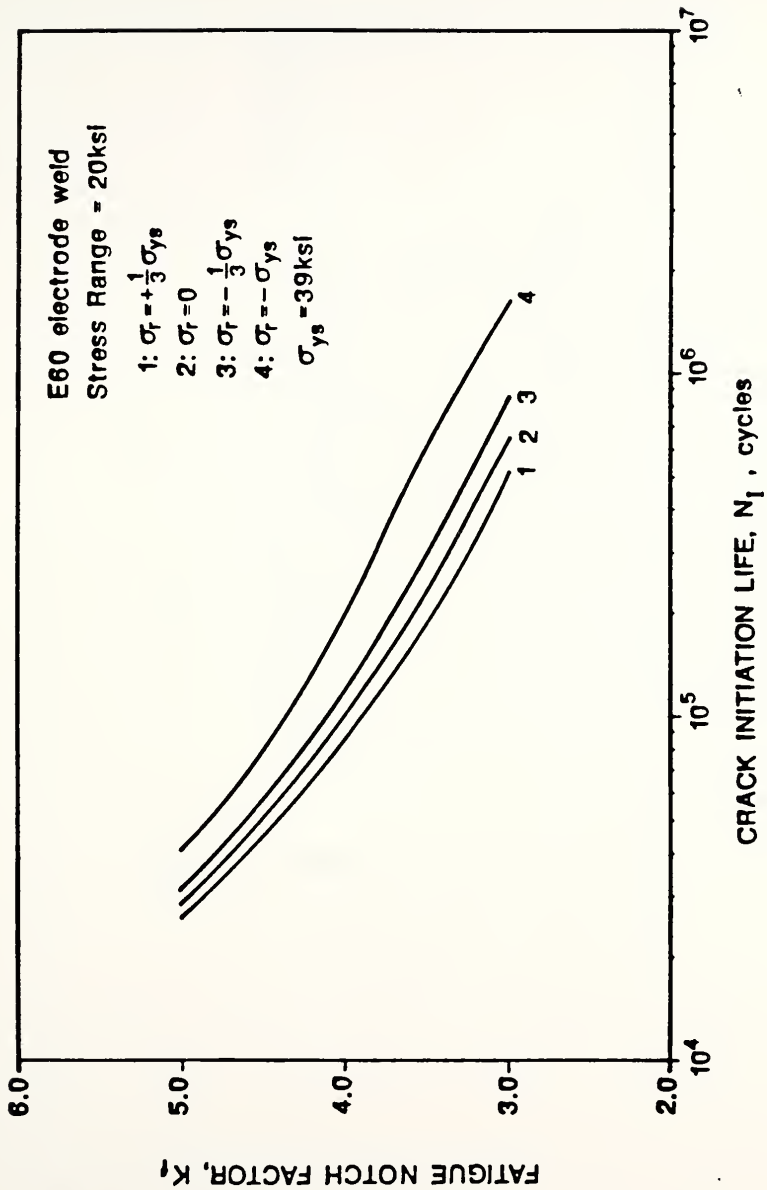


Figure 2.2 Fatigue Notch Factor versus Initiation Life for Different Residual Stress Values

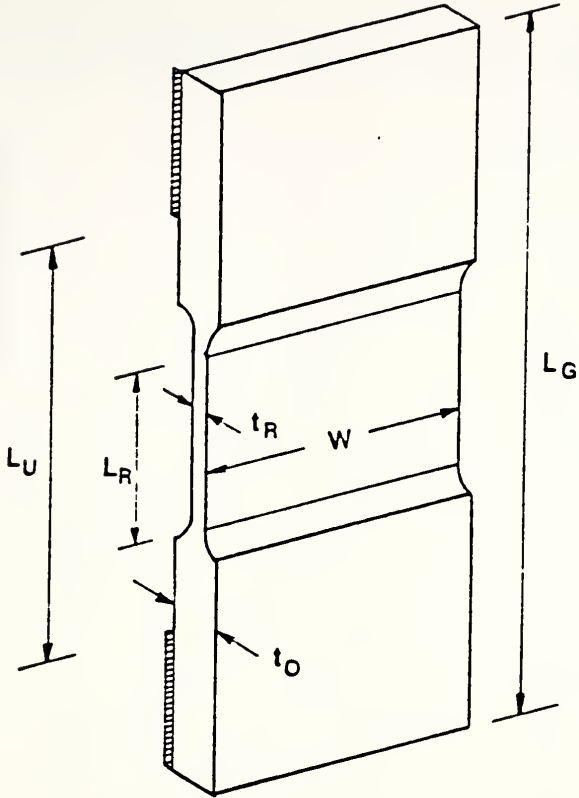
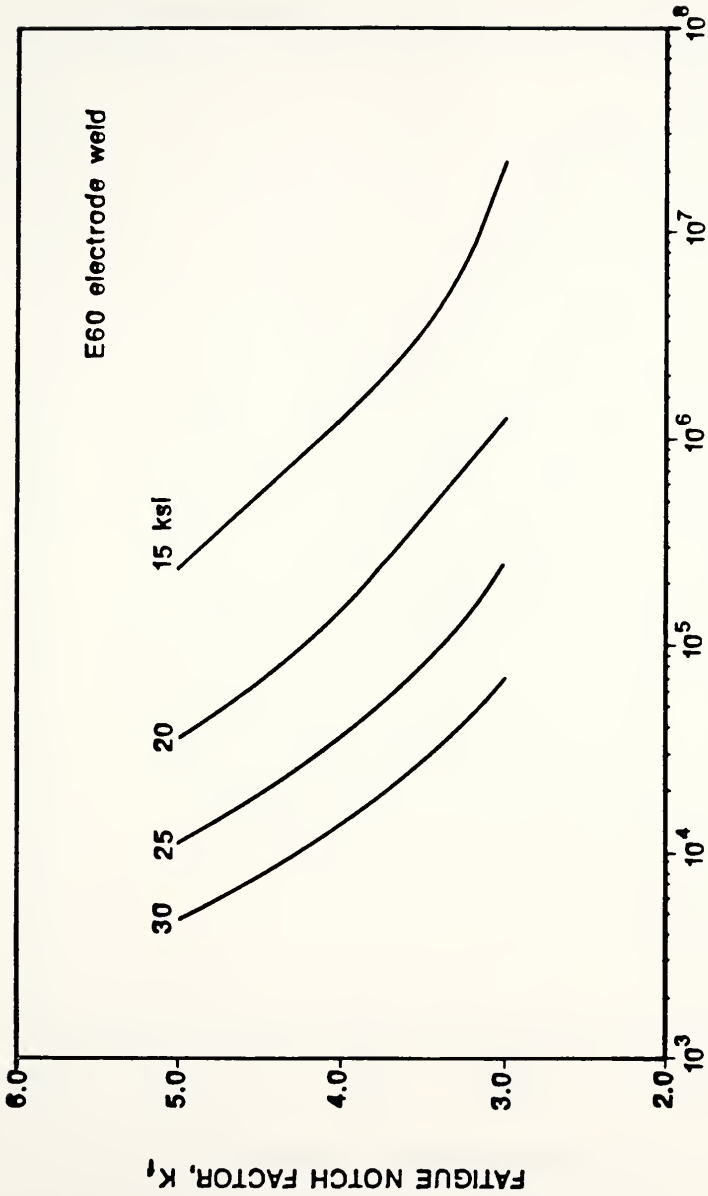


Figure 2.3 General Crack Gage Dimensions



CRACK INITIATION LIFE,  $N_i$ , cycles

Figure 2.4 Fatigue Notch Factor versus Initiation Life for Different Stress Ranges (E60 weld metal)

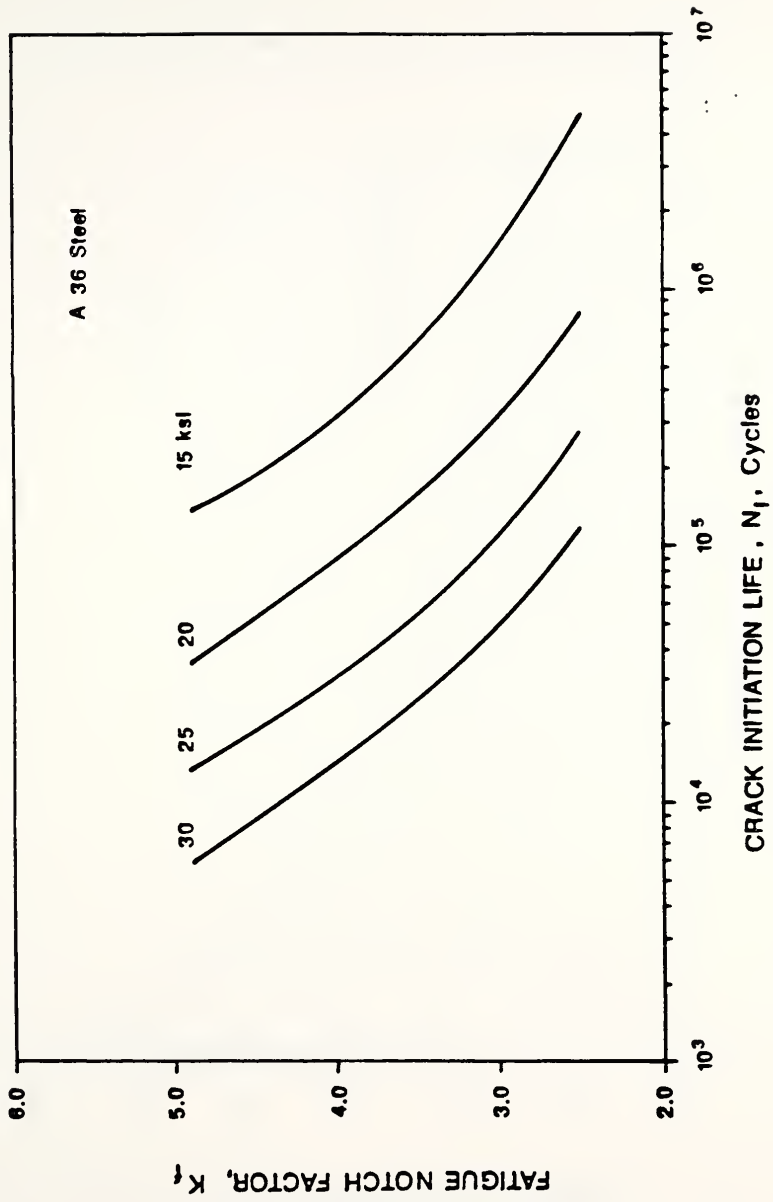


Figure 2.5 Fatigue Notch Factor versus Initiation Life for Different Stress Ranges (A36 steel)



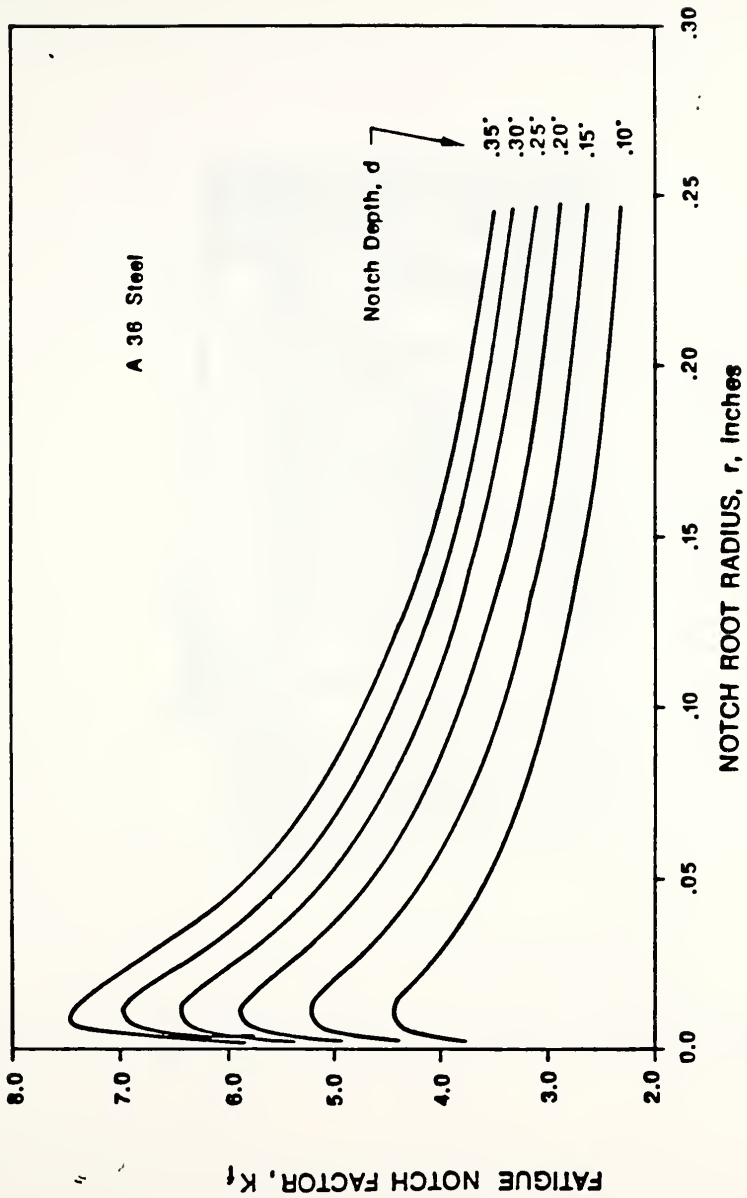


Figure 2.6 Fatigue Notch Factor versus Notch Root Radius for Different Notch Depths (A36 steel)

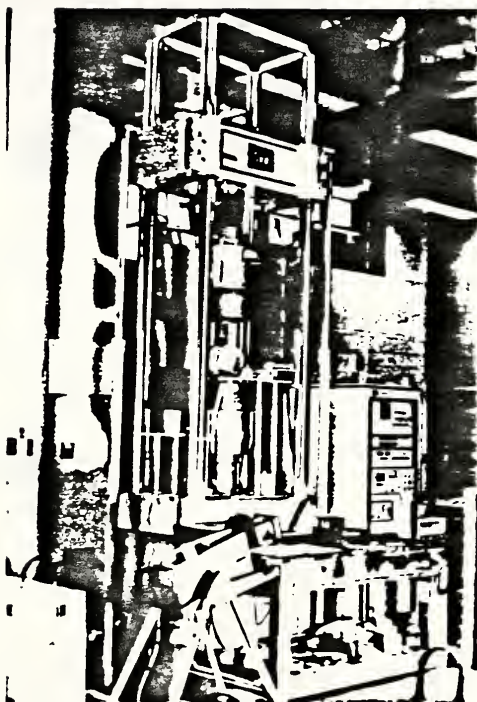


Figure 3.1 220,000 lb. (979 kN) Fatigue Testing Machine

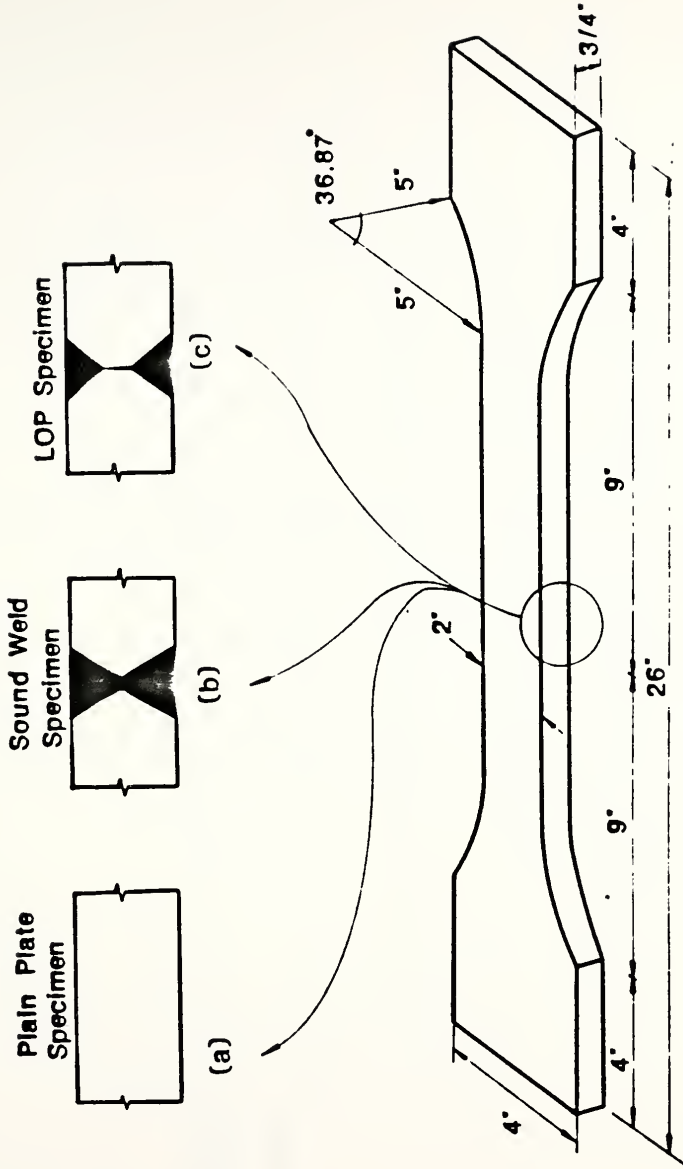


Figure 3.2 Structural Component Dimensions

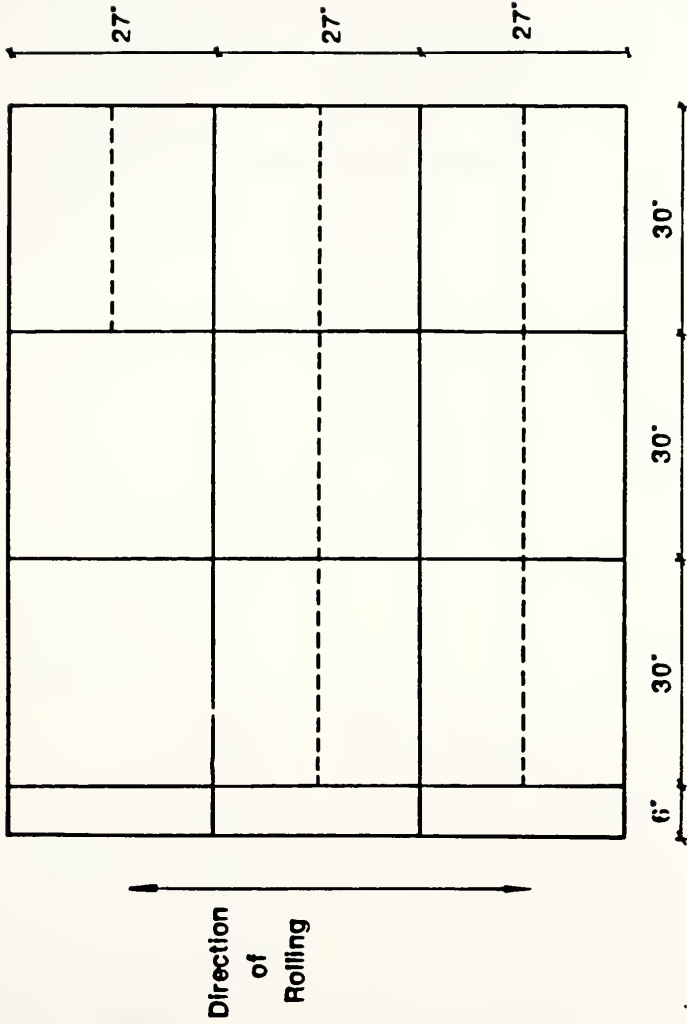
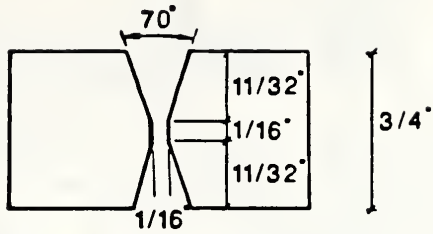
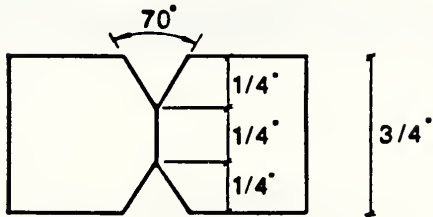


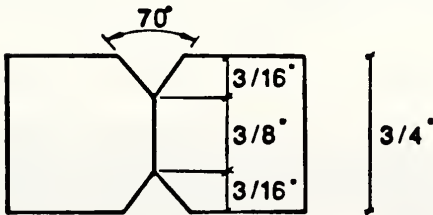
Figure 3.3 Cutting of Steel Plate for Specimen Preparation



(a) Sound Weld Specimen



(b) LOPI-8 Specimen

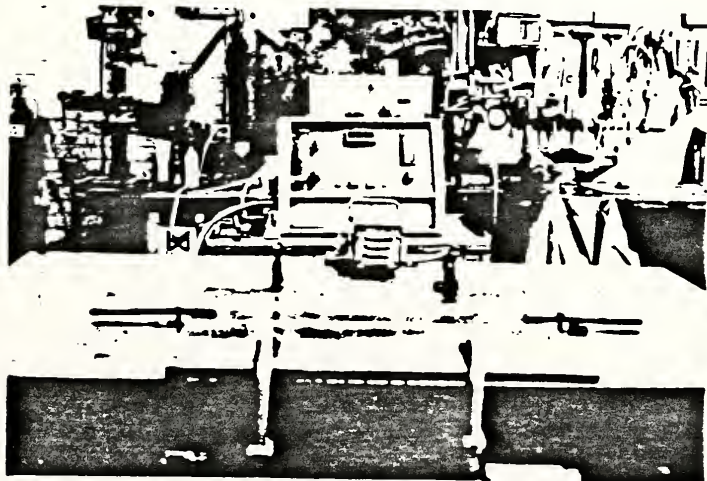


(c) LOPI-4 Specimen

Figure 3.4 Weld Groove for Sound and Lack of Penetration Welds



(a) Setting Vibration Frequency



(b) Welding Set-Up showing Vibration Inducer

Figure 3.5 Meta-Lax Vibration Inducer

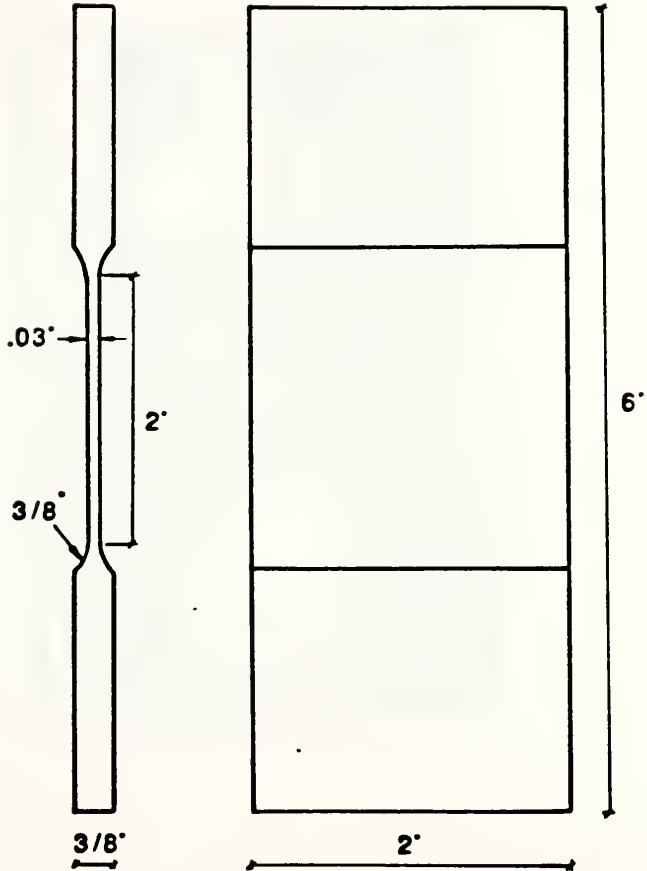


Figure 3.6 Blank Crack Gage Dimensions



**Figure 3.7 Set-Up Guide used in Bonding Process**



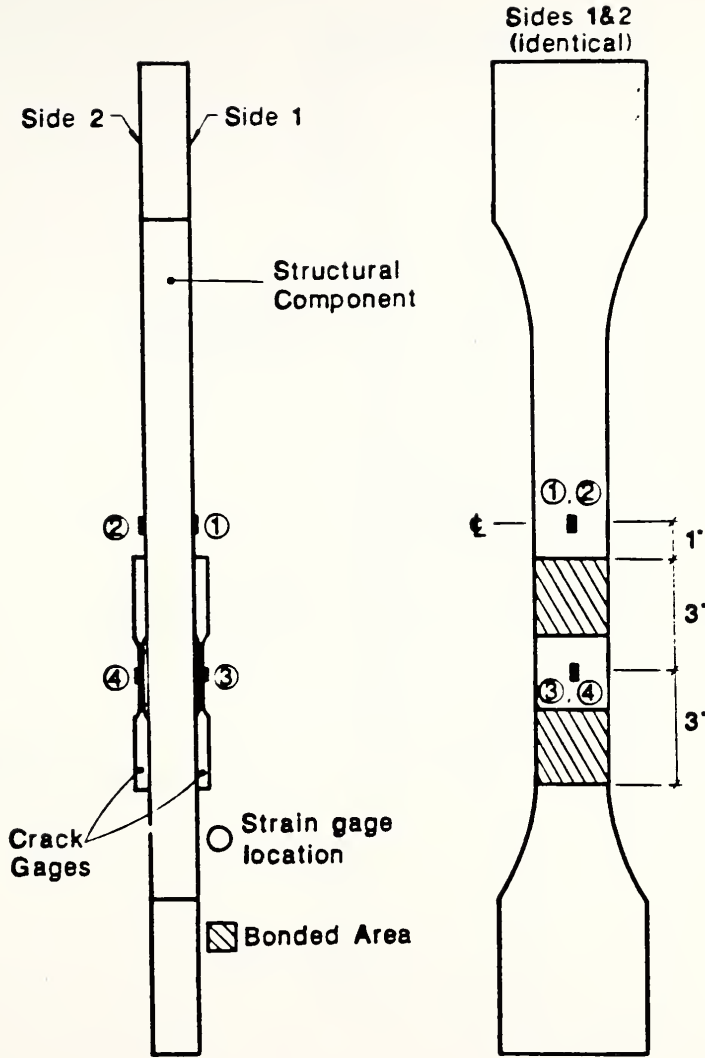


Figure 3.8 Load Transfer Specimen showing Strain Gage Locations

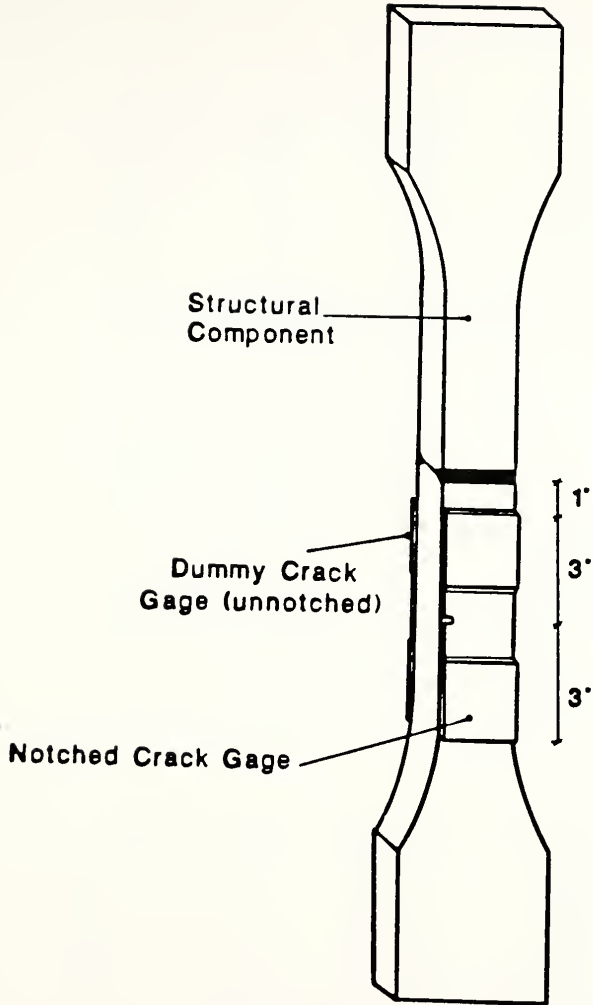


Figure 3.9 LOP Test Specimen with Bonded Crack Gages

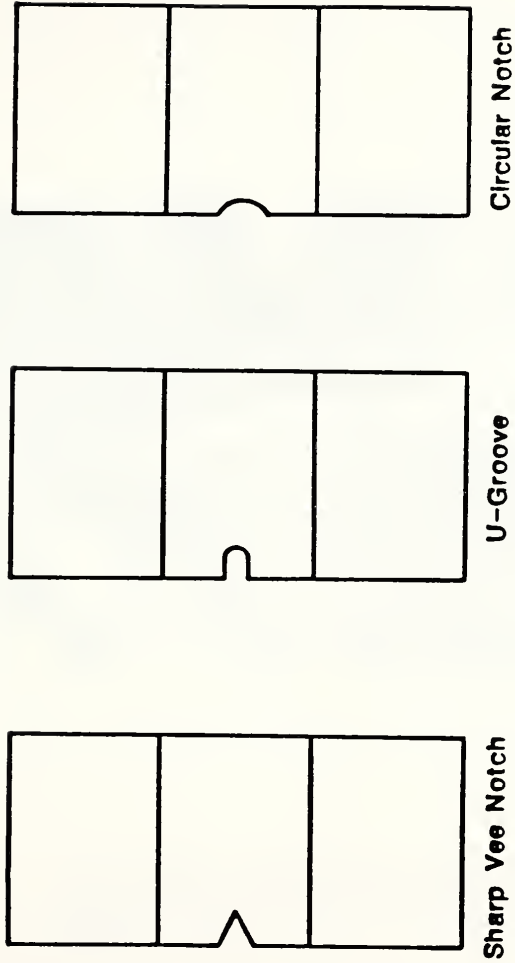
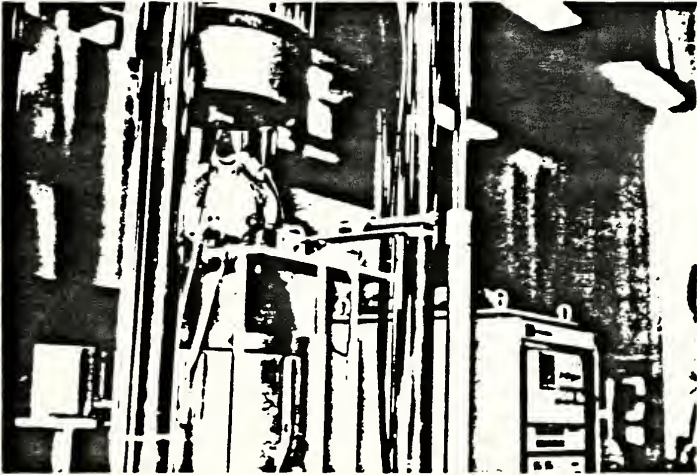


Figure 3.10 Types of Notched Crack Gages



**Figure 3.11** Ultrasonic Transducer, Signal Conditioner, and Oscilloscope used in Scanning the LOP Welds



**Figure 3.12 Crack Growth Measurement Instrumentation**

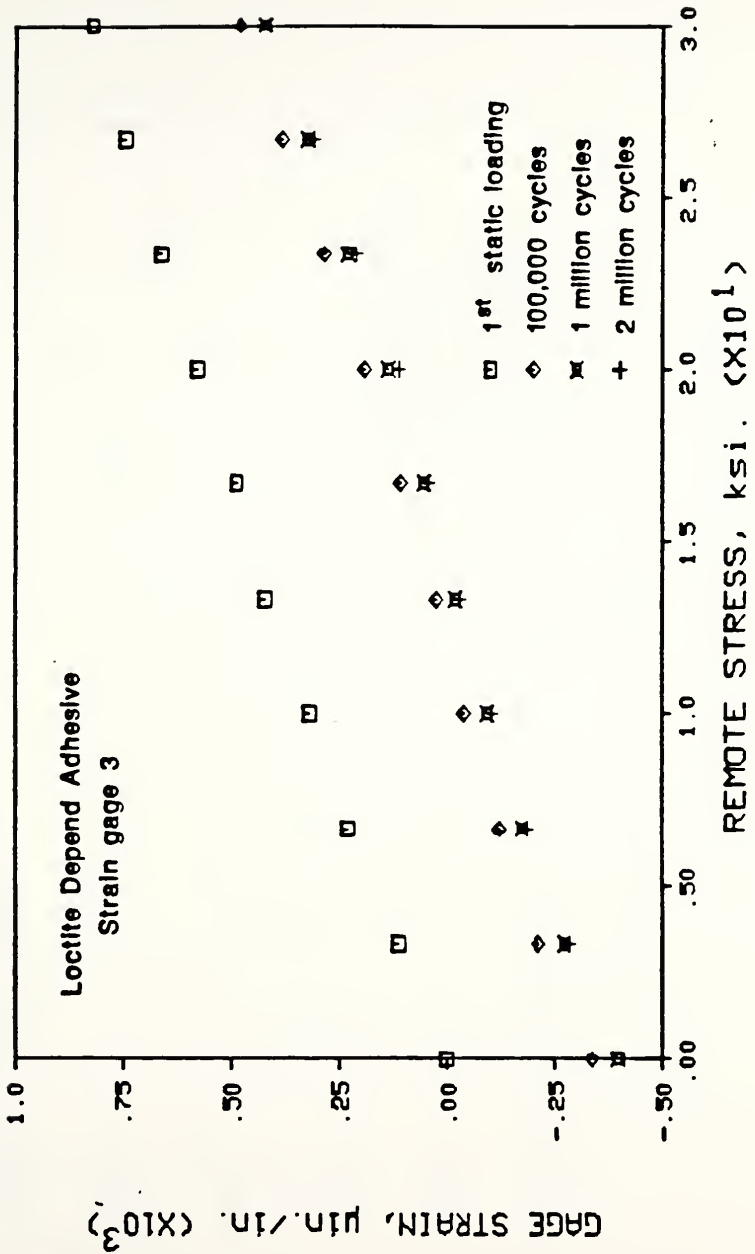


Figure 4.1 Crack Gage Strain versus Remote Stress for Loctite Depend Adhesive (Side 1)

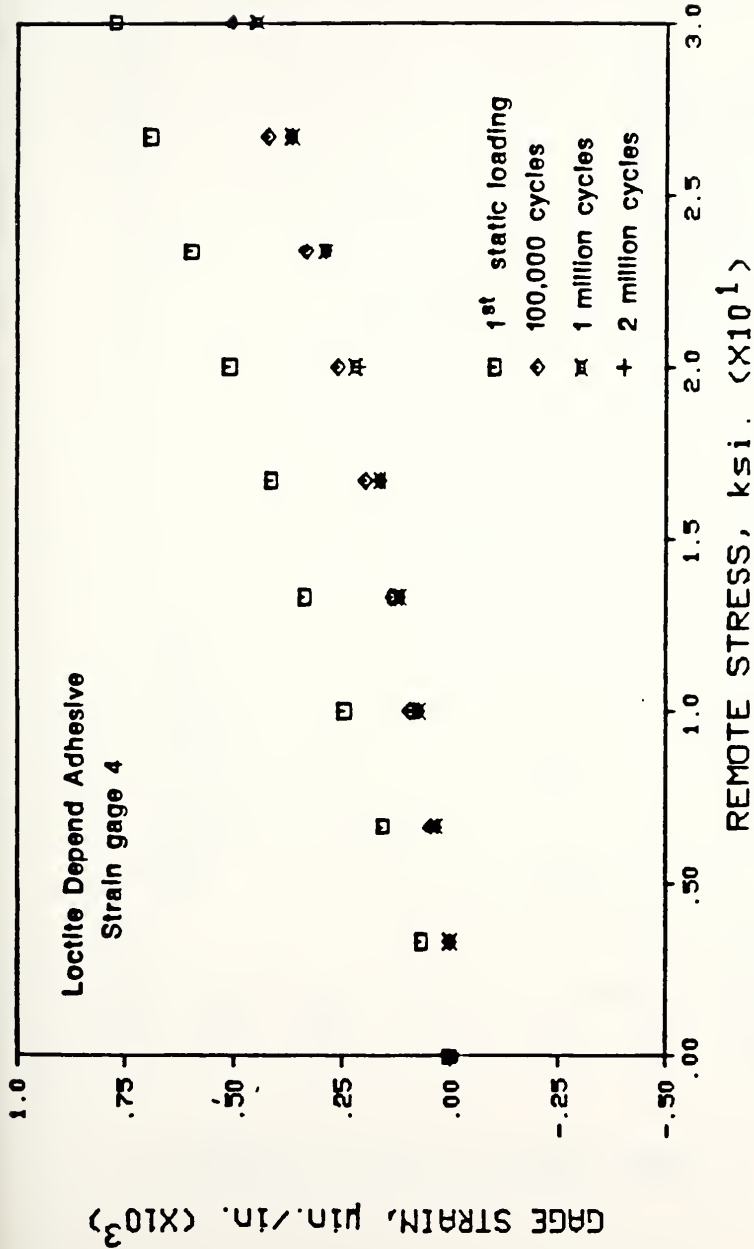


Figure 4.2 Crack Gage Strain versus Remote Stress for Loctite Depend Adhesive (Side 2)

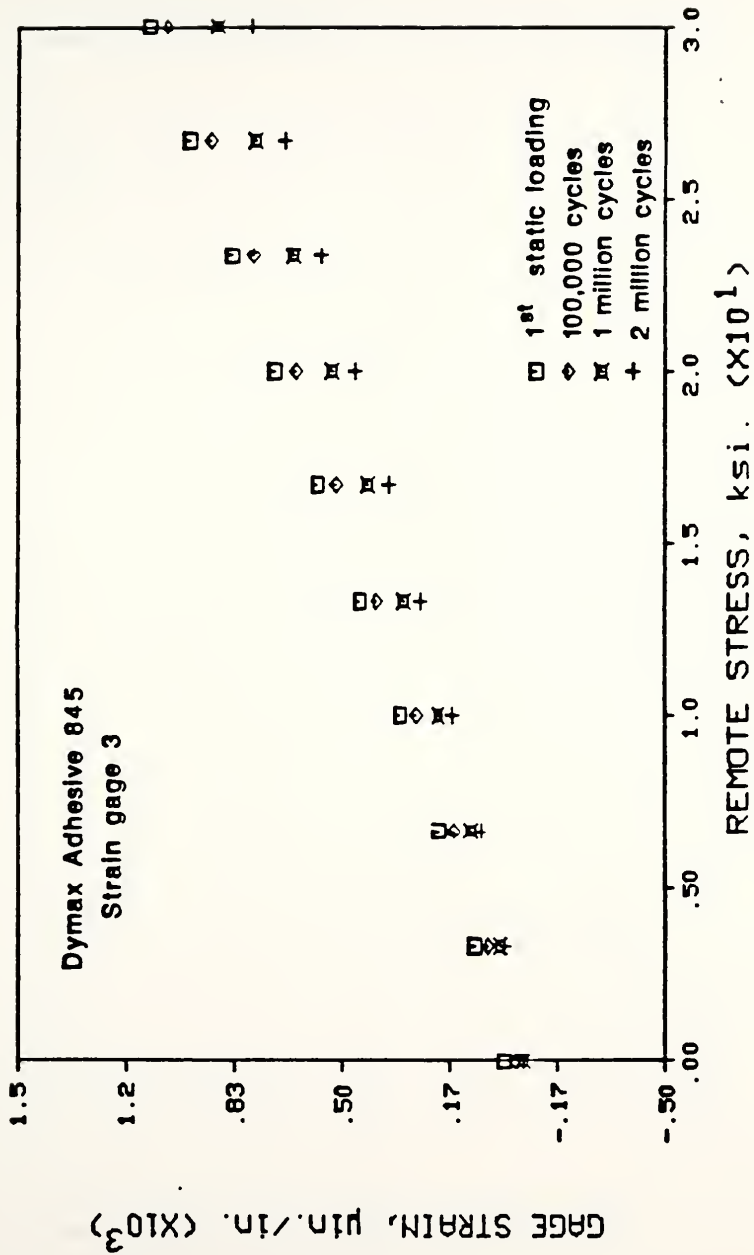


Figure 4.3 Crack Gage Strain versus Remote Stress for Dymax Adhesive 845 (Side 1)



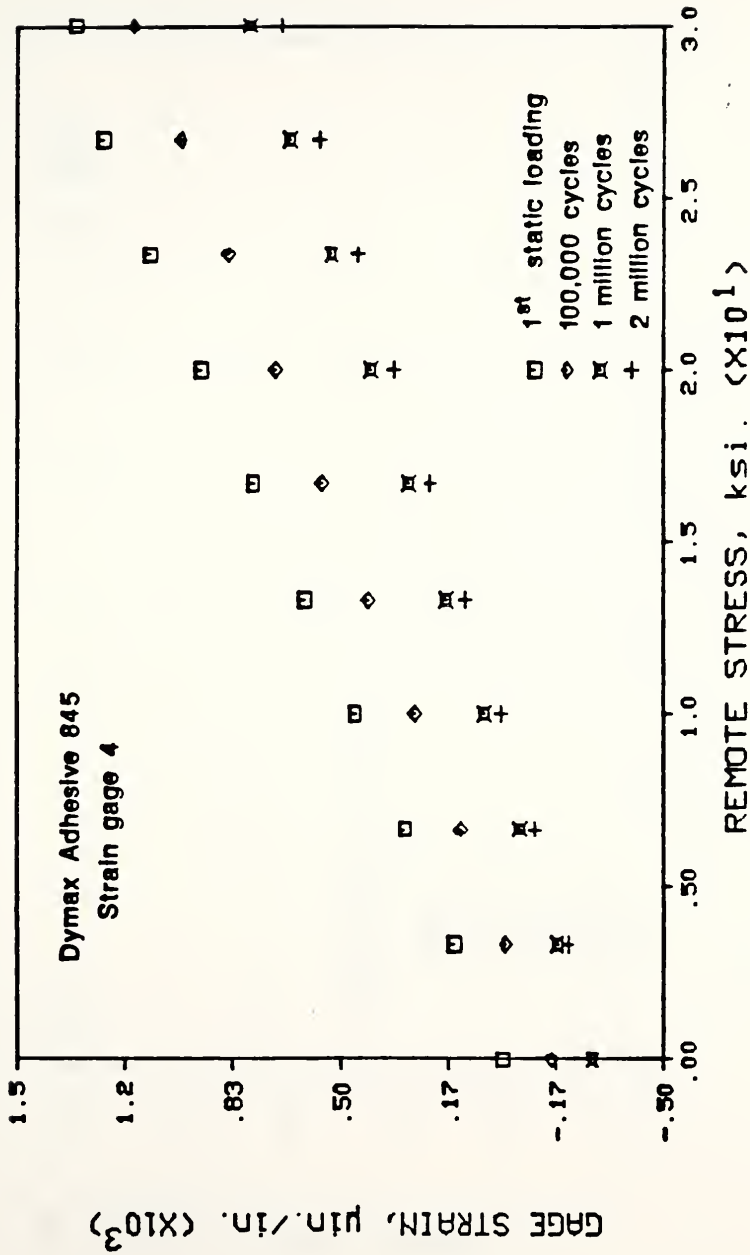


Figure 4.4 Crack Gage Strain versus Remote Stress for Dymax Adhesive 845 (Side 2)

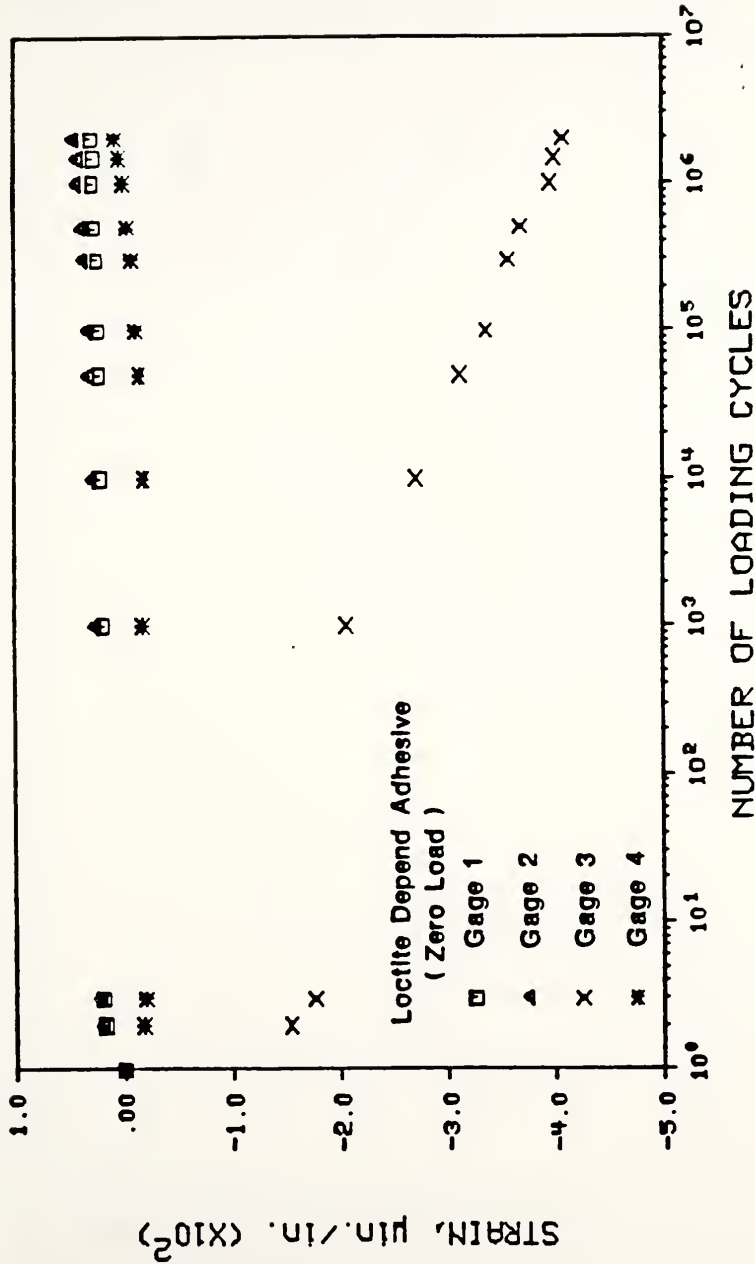


Figure 4.5 Crack Gage and Component Strain at Zero Load versus Number of Loading Cycles (Loctite Depend Adhesive)

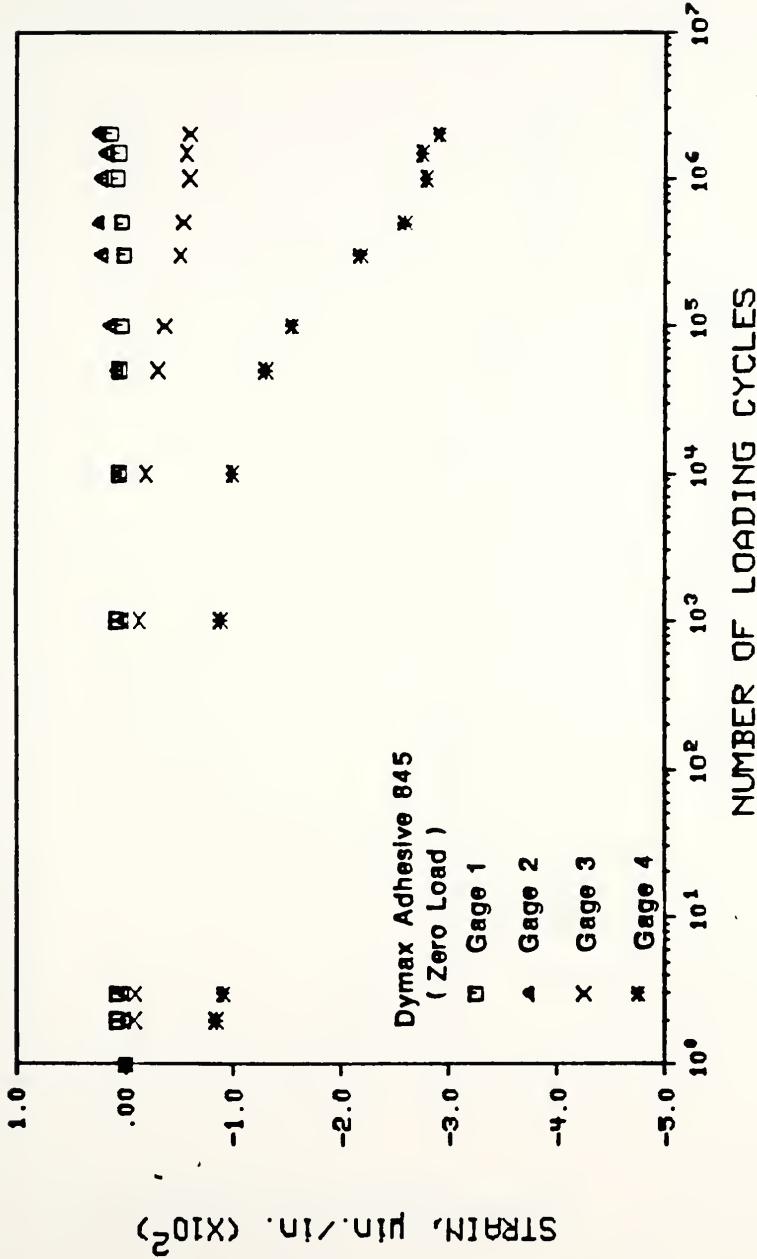


Figure 4.6 Crack Gage and Component Strain at Zero Load versus Number of Loading Cycles (Dymax Adhesive 845)

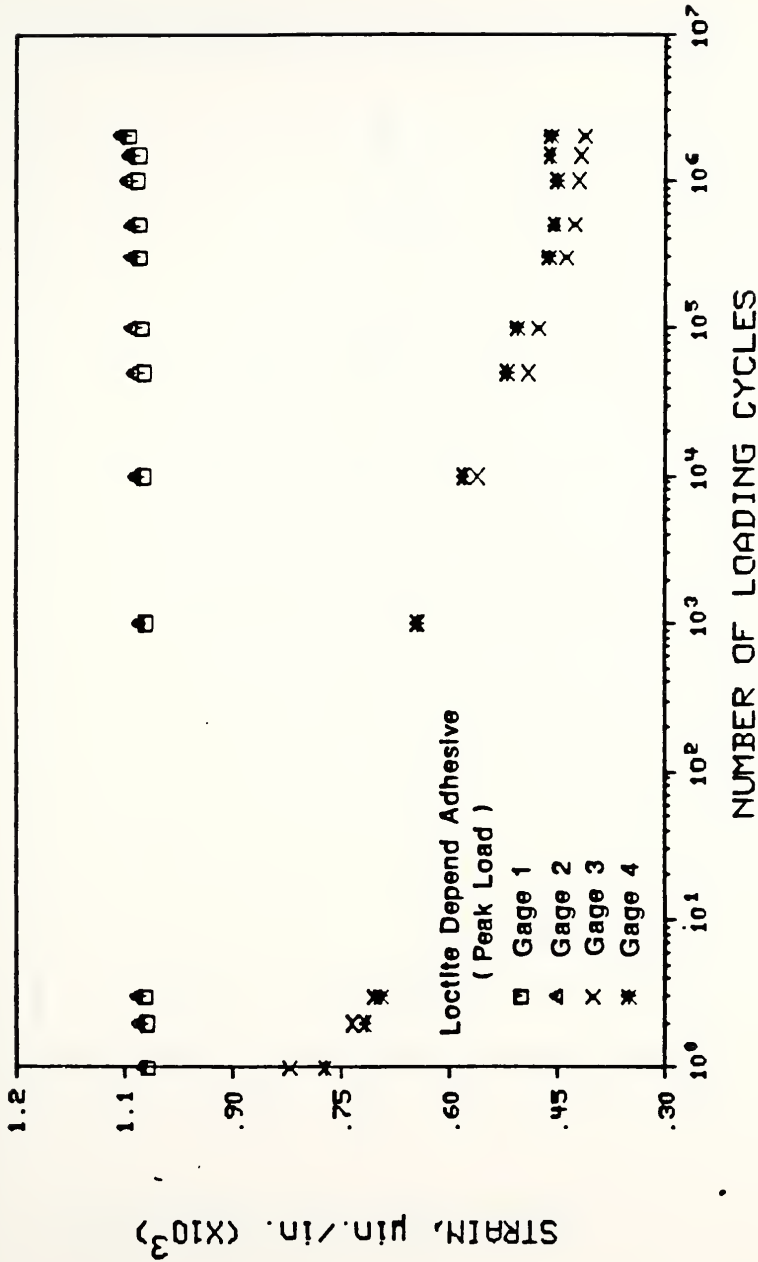


Figure 4.7 Crack Gage and Component Strain at Peak Load versus Number of Loading Cycles (Loctite Depend Adhesive)

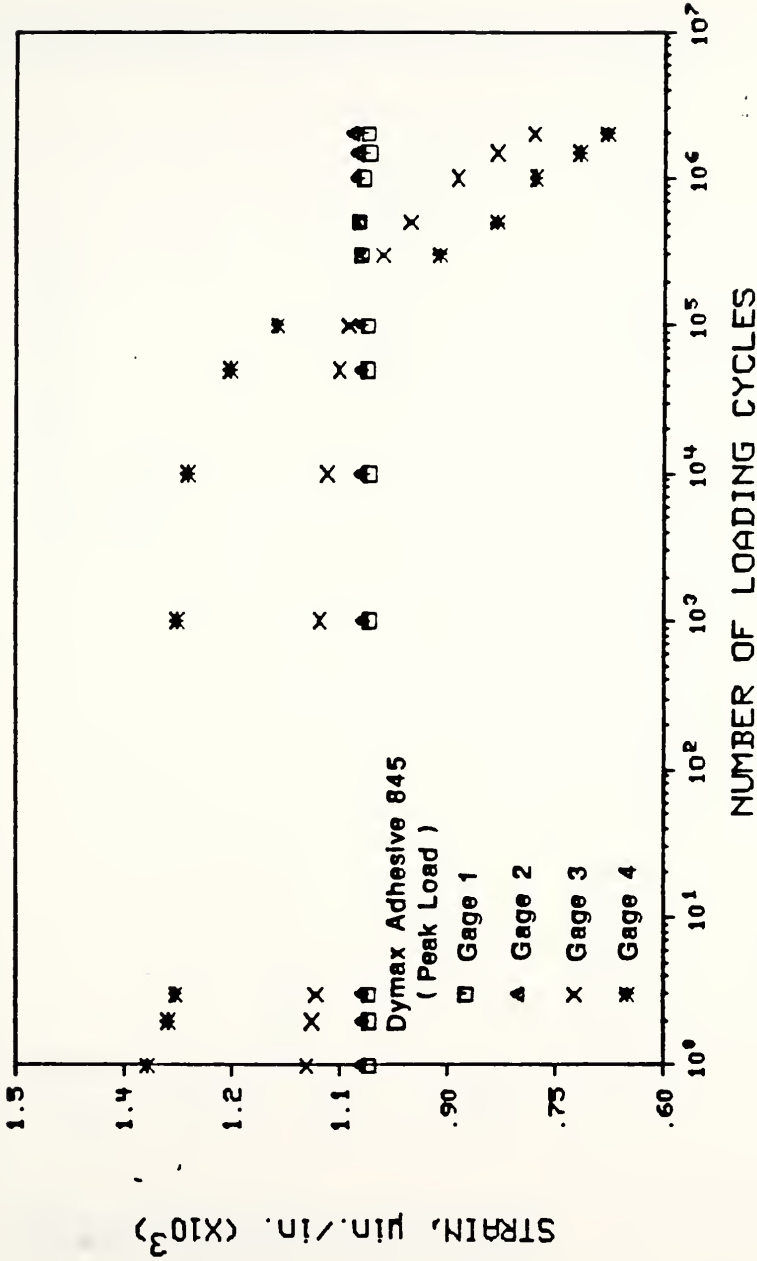


Figure 4.8 Crack Gage and Component Strain at Peak Load versus Number of Loading Cycles (Dymax Adhesive 845)

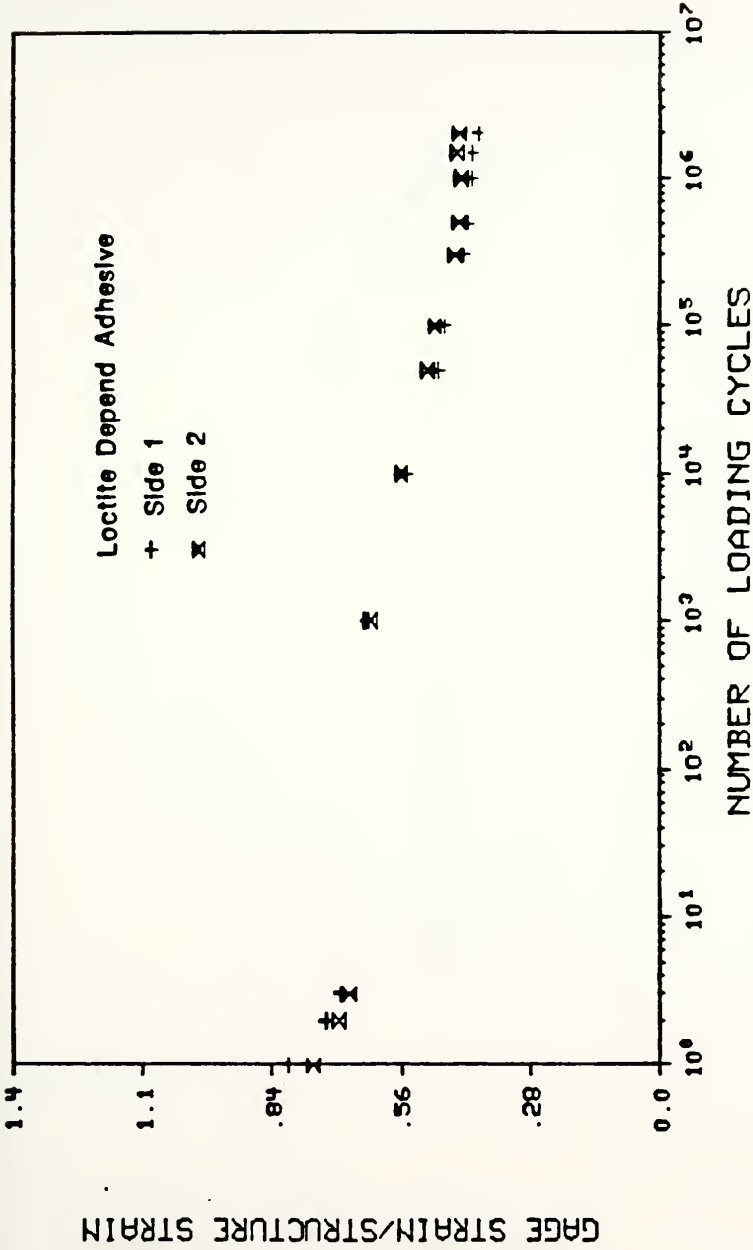


Figure 4.9 Relation between Strain Transfer Ratio and Number of Loading Cycles (Loctite Depend Adhesive)

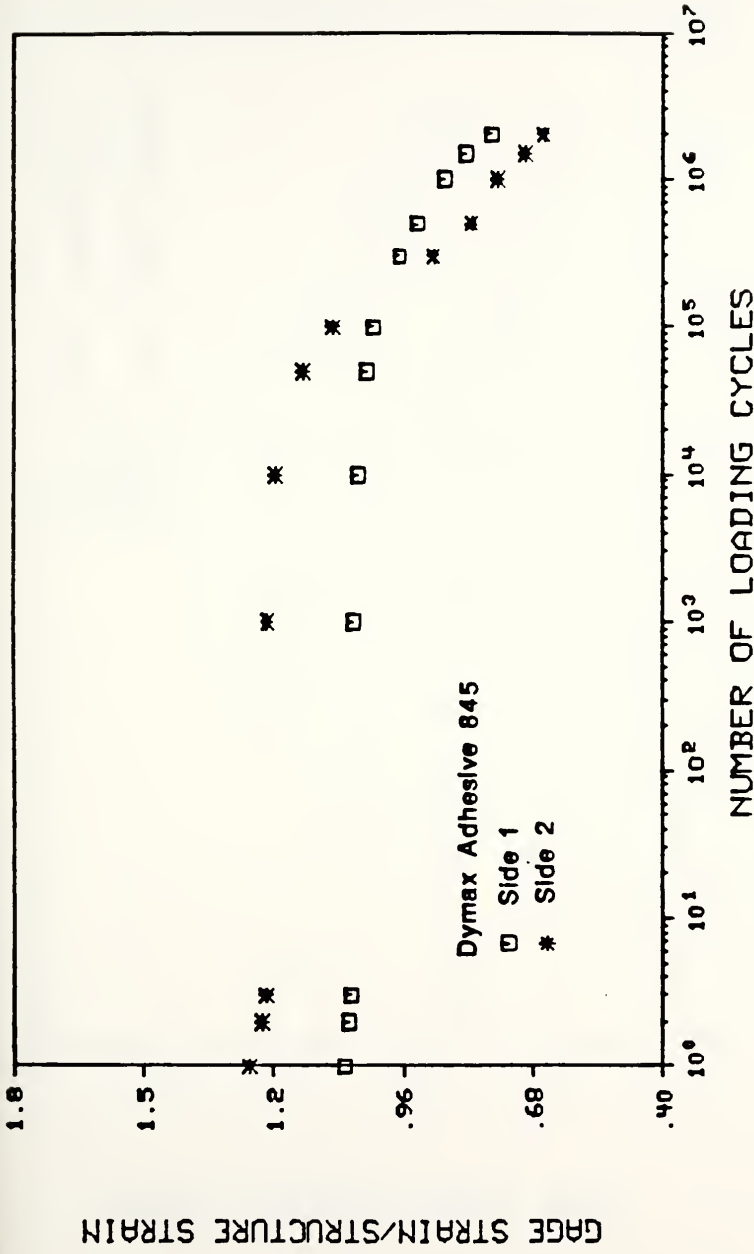


Figure 4.10 Relation between Strain Transfer Ratio and Number of Loading Cycles (Dymax Adhesive 845)

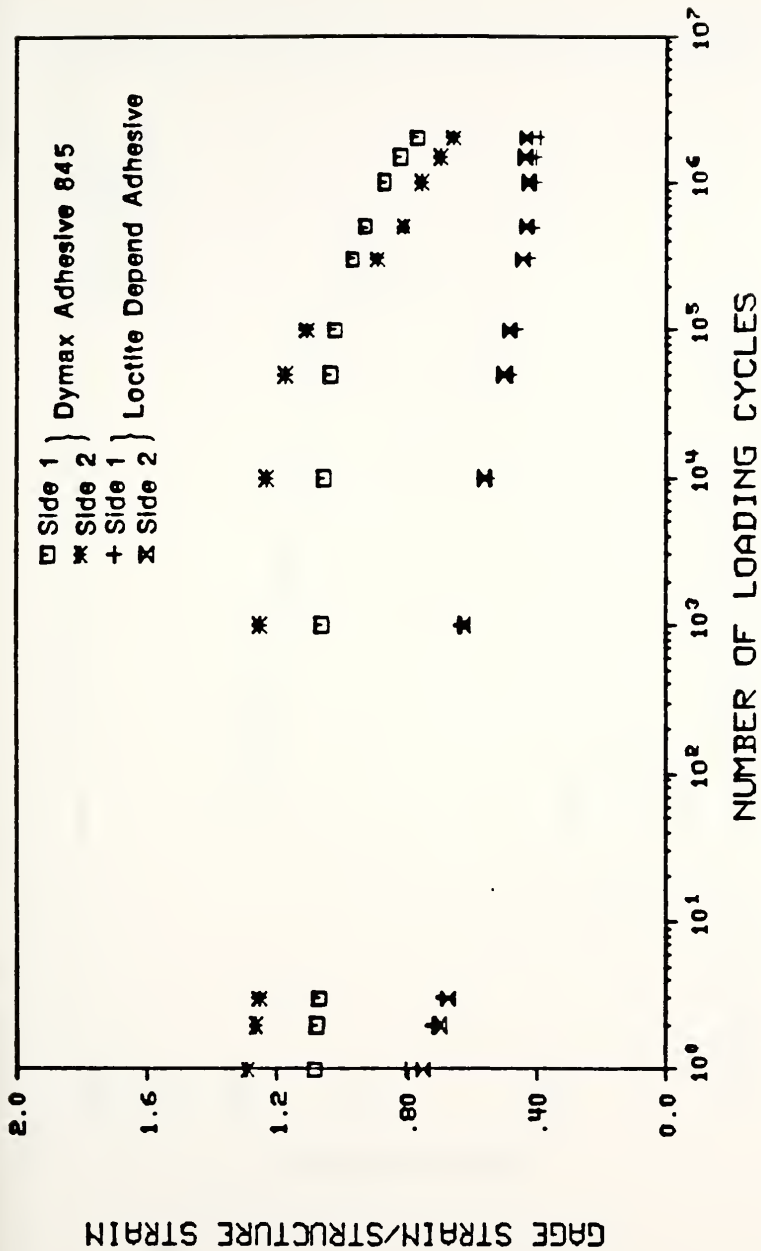


Figure 4.11 Strain Transfer Ratio Comparison for Dymax 845 and Loctite Depend Adhesives



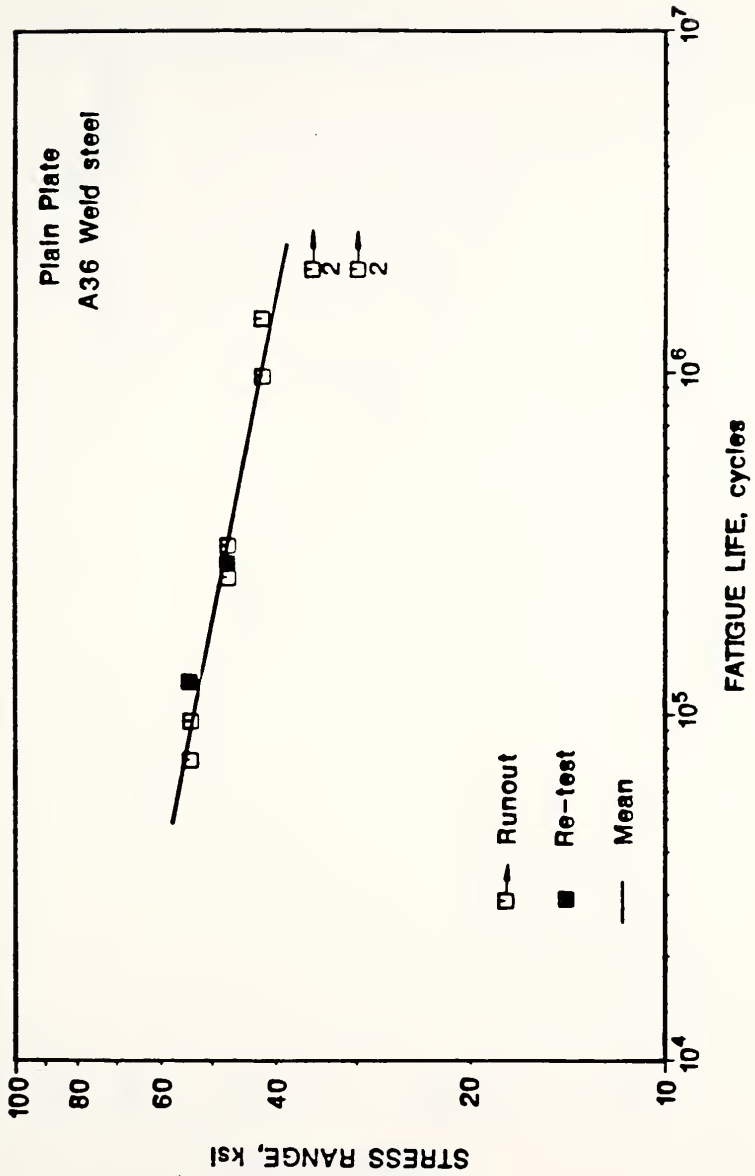


Figure 4.12 S-N Curve for Plain Plate Specimens

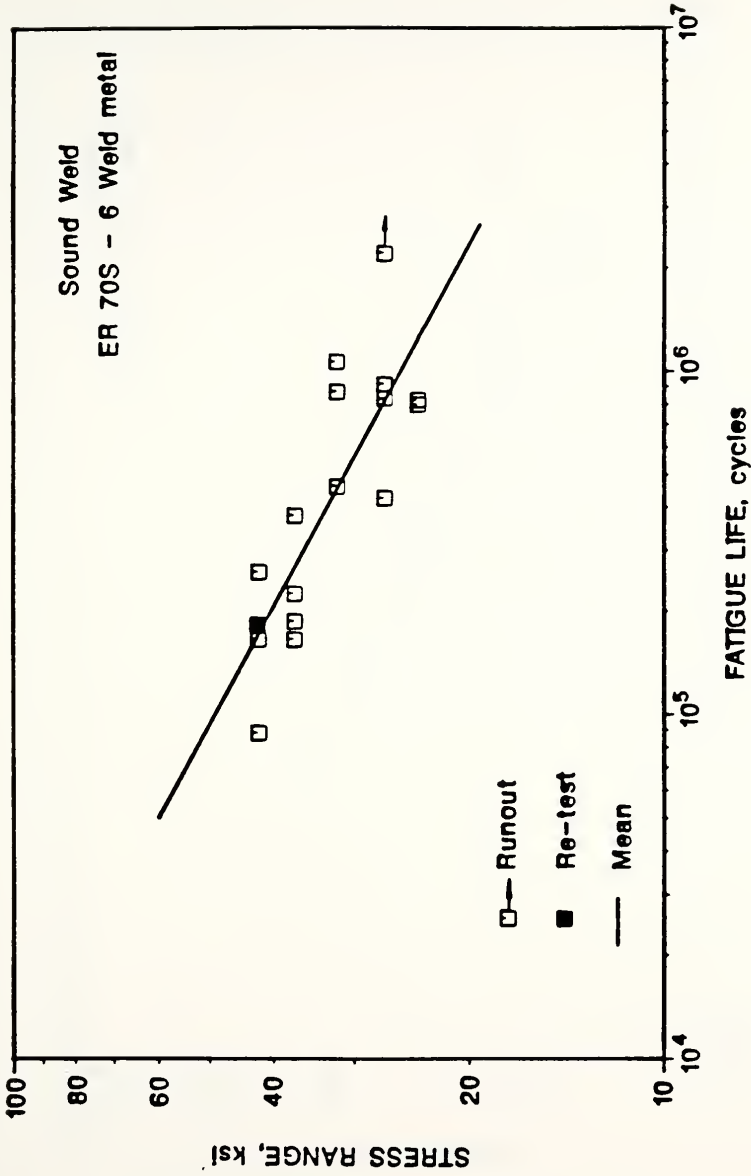


Figure 4.13 S-N Curve for Sound Weld Specimens

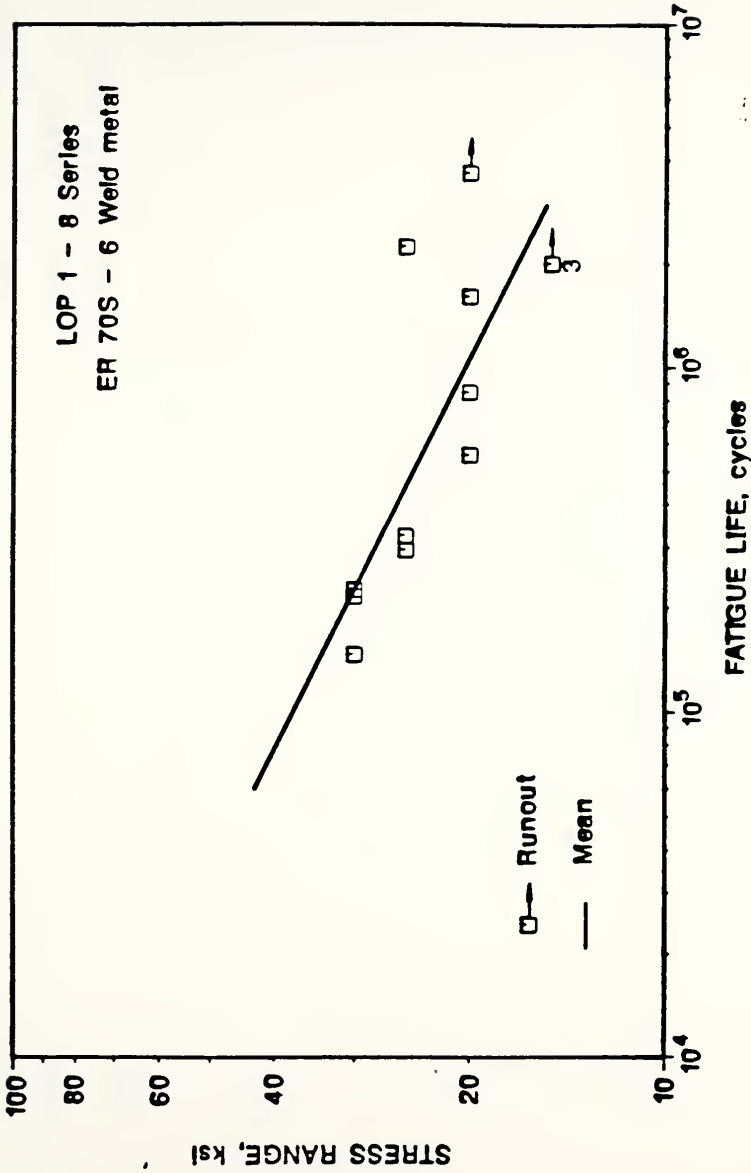


Figure 4.14 S-N Curve for LOP1-8 Specimens

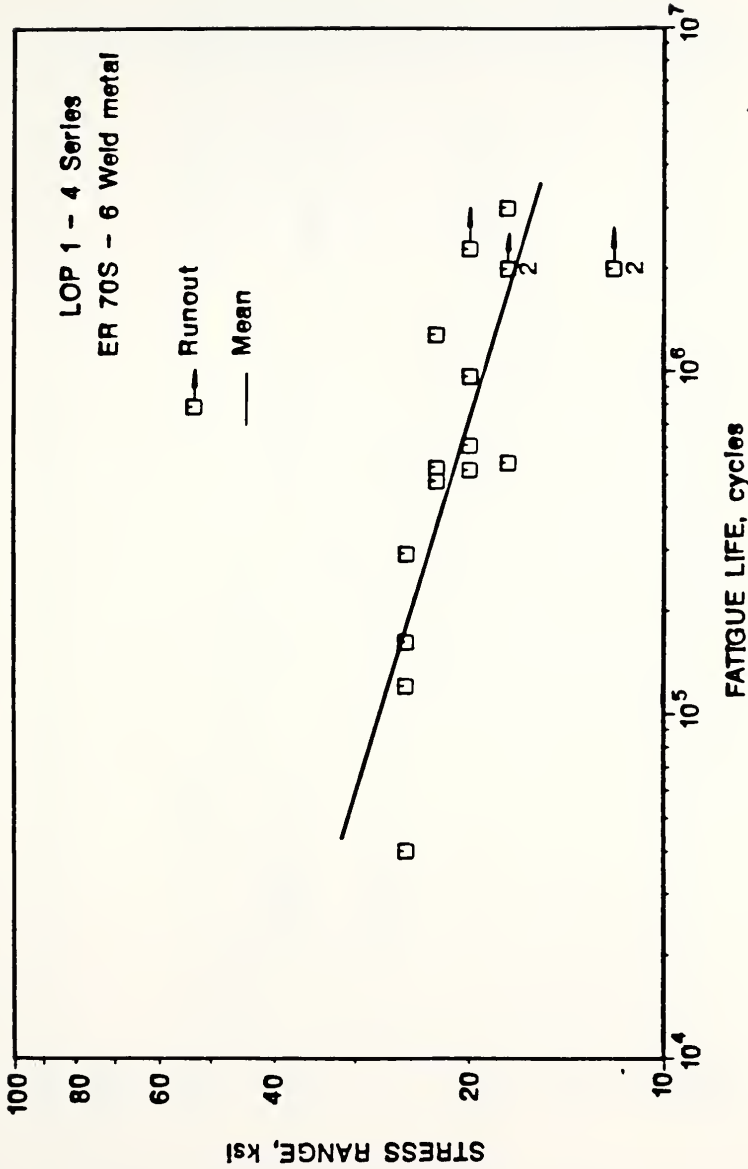


Figure 4.15 S-N Curve for LOP1-4 Specimens

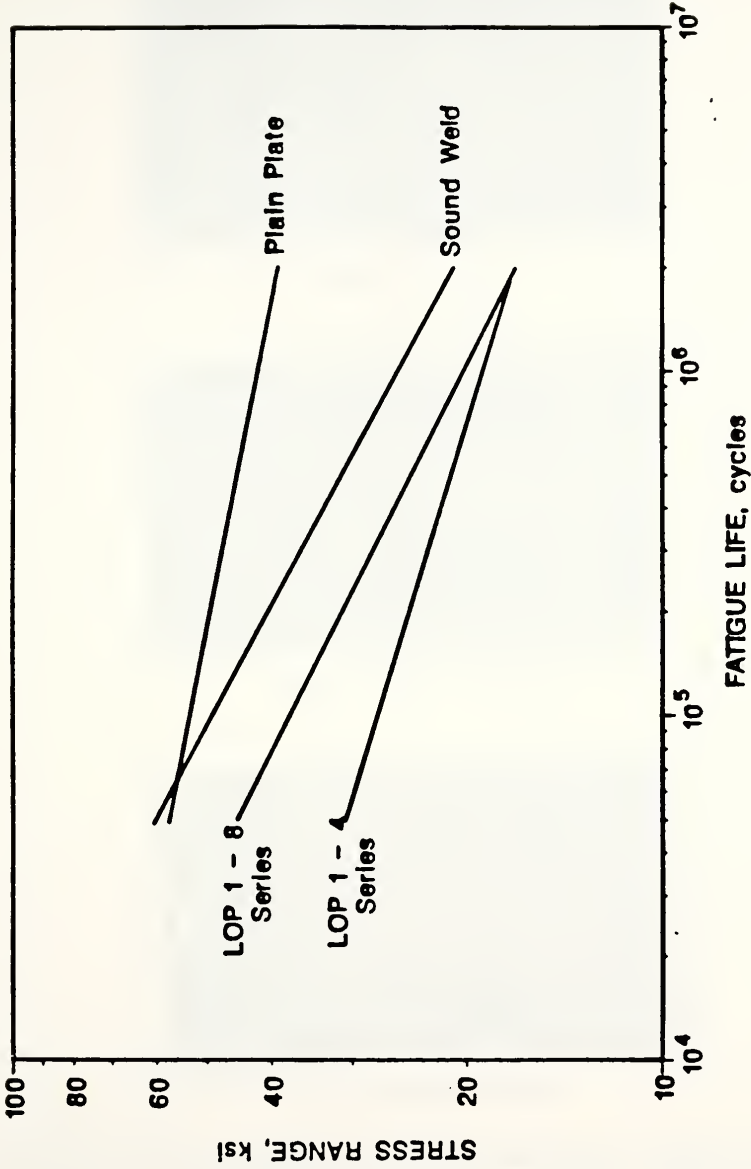
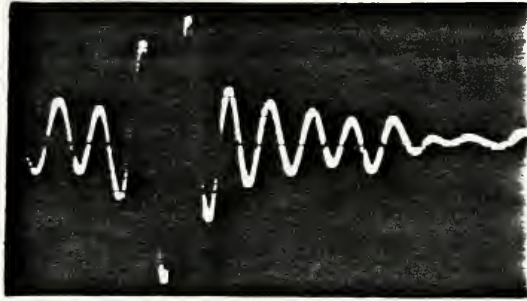
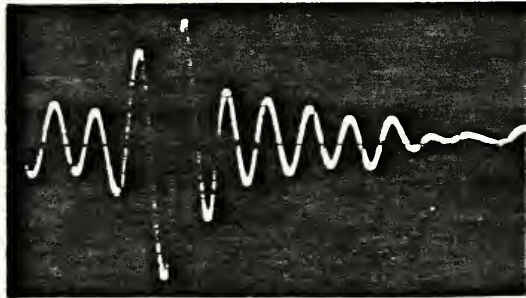


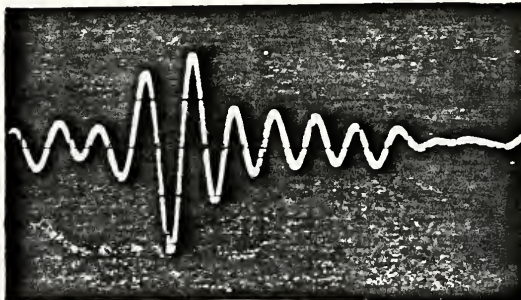
Figure 4.16 Comparison of Mean Fatigue Strength for Plain Plate, Sound Weld, and LOP Tests



(a) 1 cycle

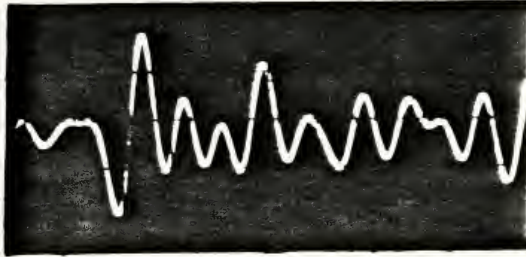


(b) 15,000 cycles

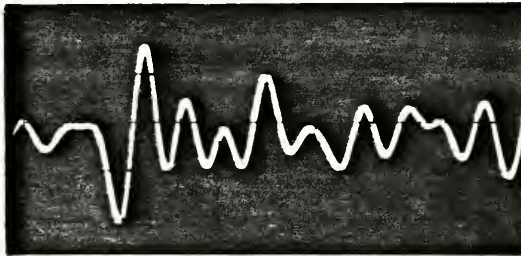


(c) 45,000 cycles

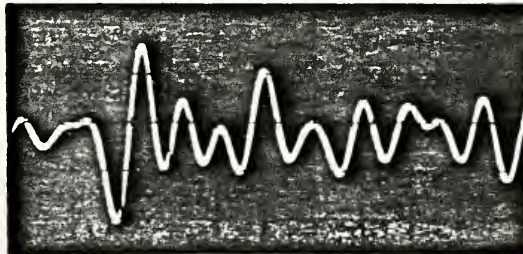
Figure 4.17 Ultrasonic Pulse Reflections from Lack of Penetration Discontinuity (LOP1-4-3)



(a) 0 cycle



(b) 5,000 cycles



(c) 50,000 cycles

Figure-4.18 Ultrasonic Pulse Reflections from Lack of Penetration Discontinuity (LOP1-4-14)

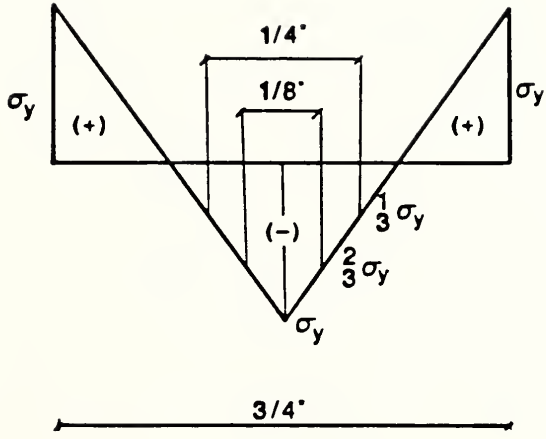


Figure 4.19 Idealized Residual Stress Distribution



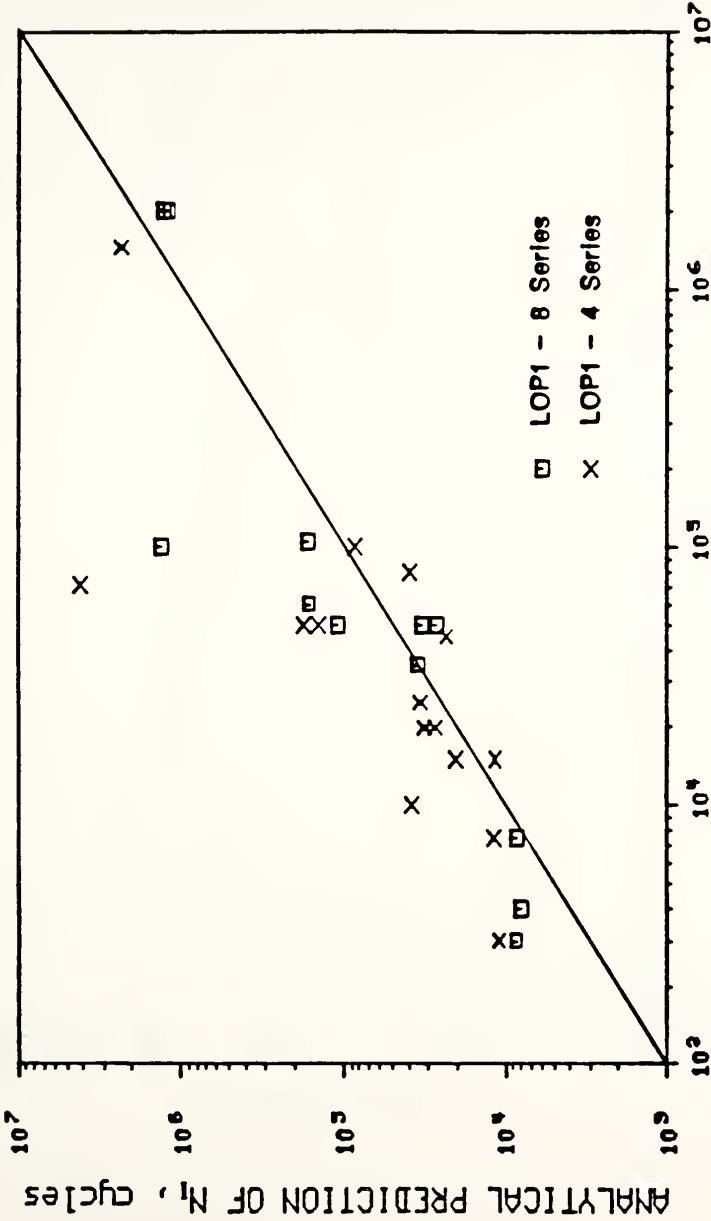


Figure 4.20 Comparison between Analytically Predicted and Ultrasonic Estimate of Initiation Life

ULTRASONIC ESTIMATE OF  $N_i$ , cycles

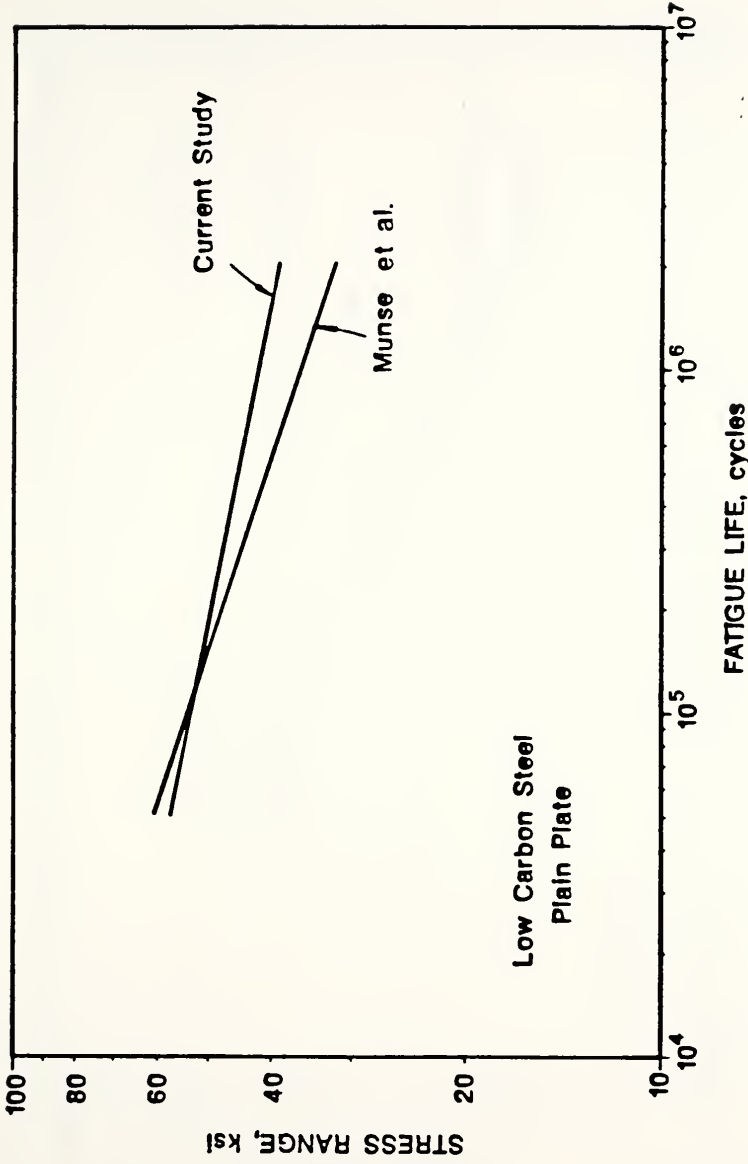


Figure 4.21 Comparison of Mean Fatigue Strength for Plain Plate Tests

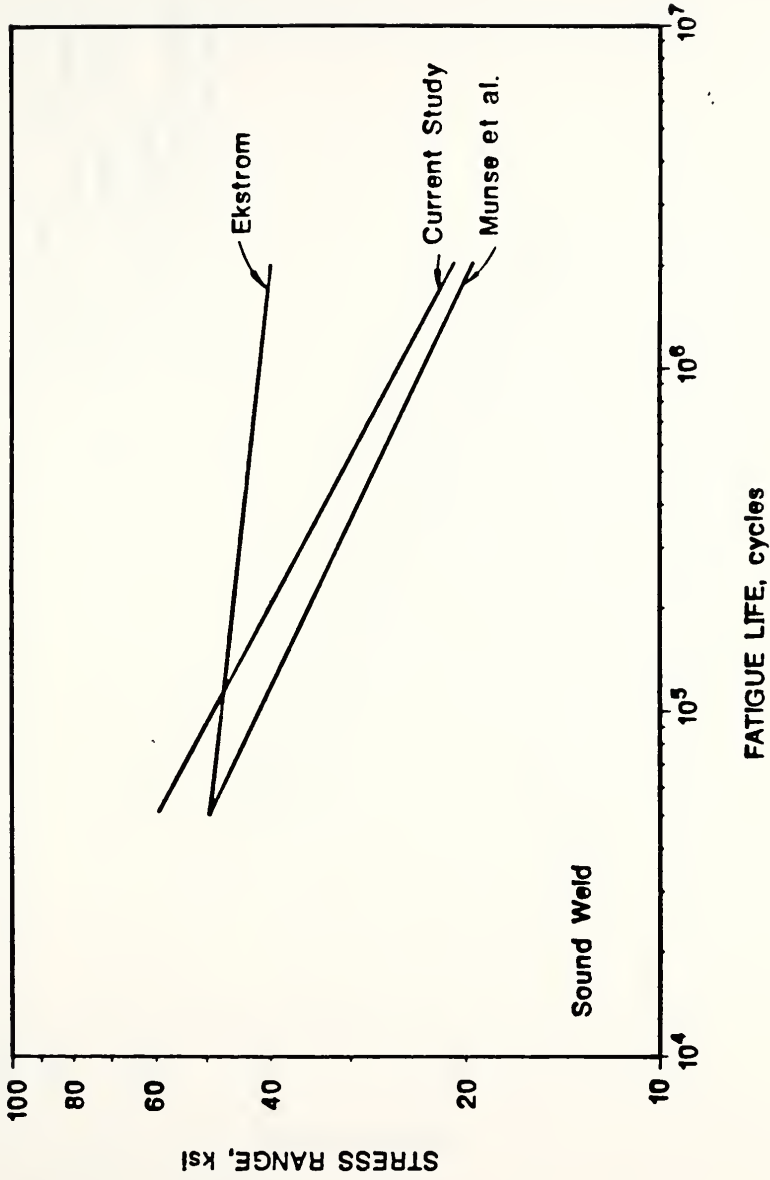


Figure 4.22 Comparison of Mean Fatigue Strength for Sound Weld Tests

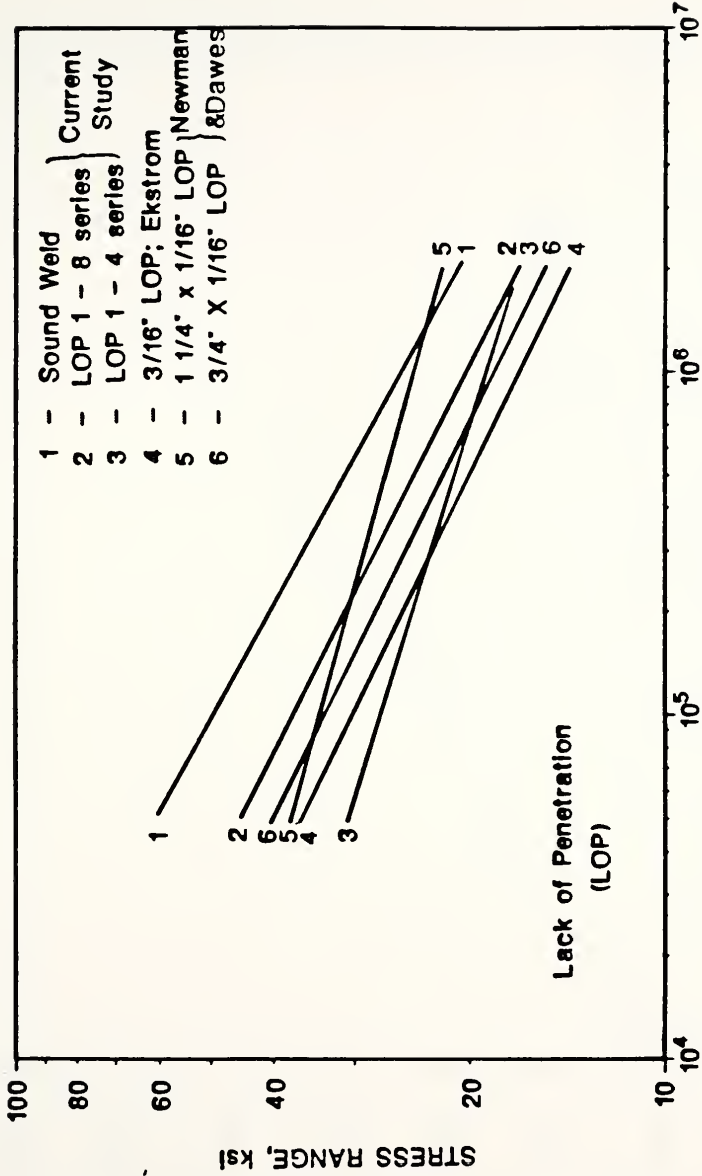


Figure 4.23 Comparison of Mean Fatigue Strength for Lack of Penetration Tests

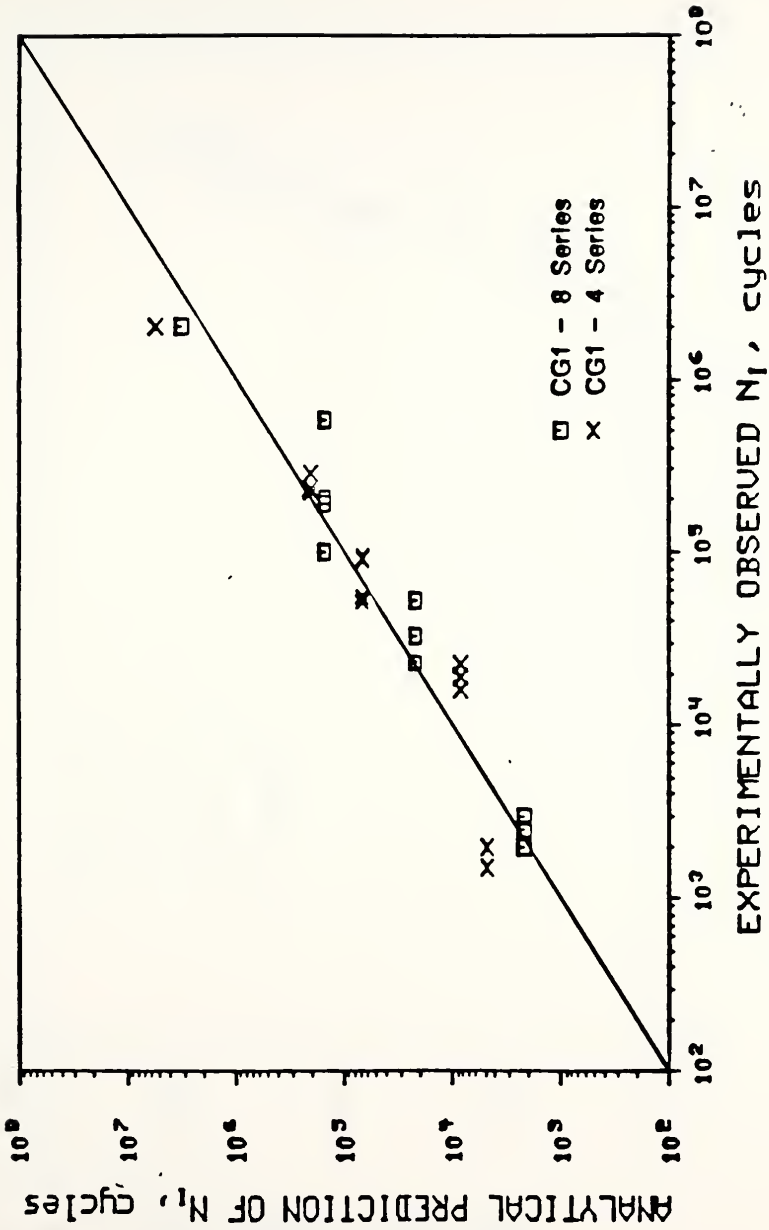


Figure 4.24 Comparison between Analytically Predicted and Experimentally Estimated Initiation Life of Gages

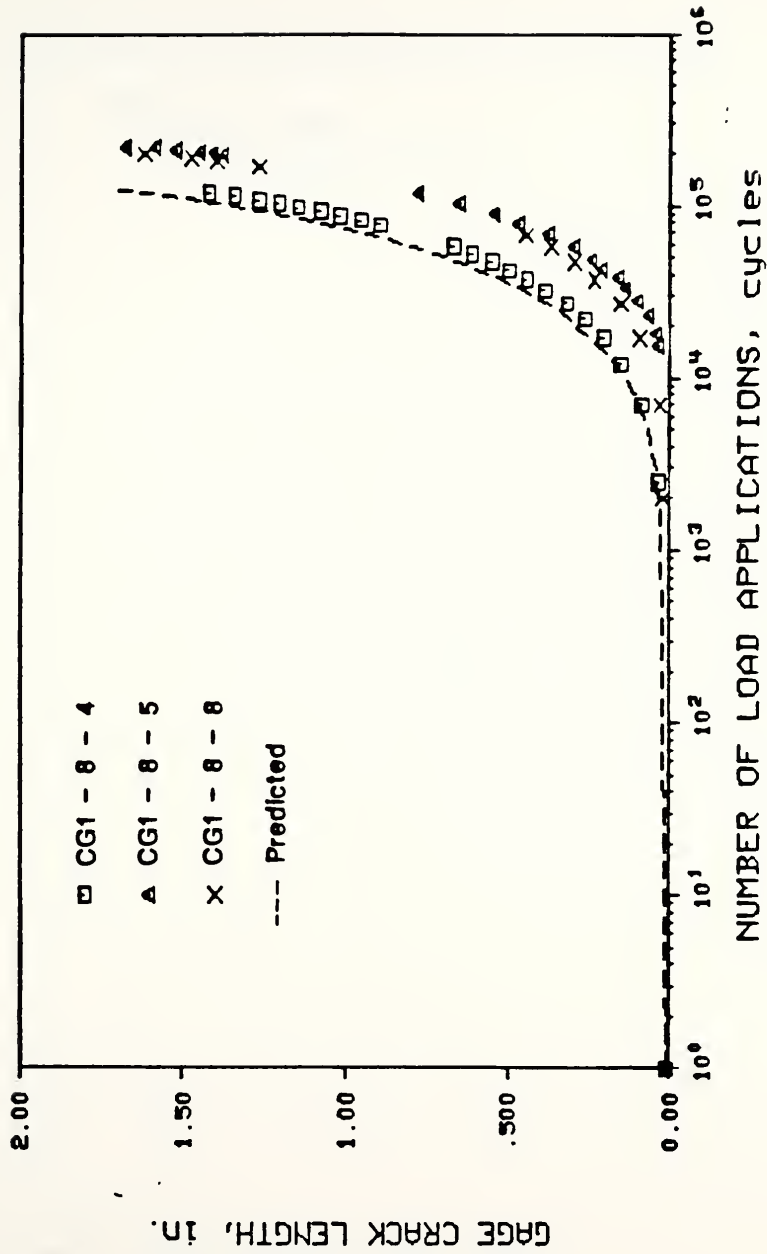


Figure 4.25 Observed and Predicted Crack Growth for Gages CG1-8-4, CG1-8-5 and CG1-8-8

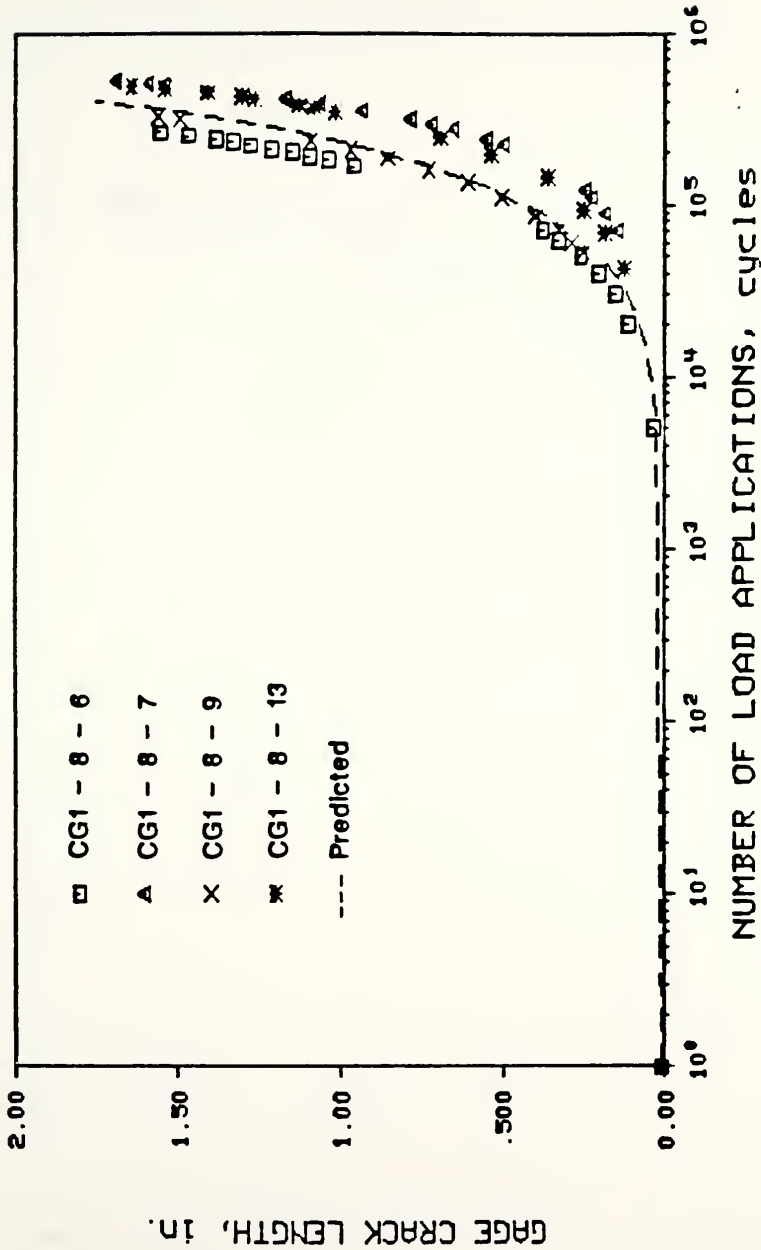


Figure 4.26 Observed and Predicted Crack Growth for Gages CG1-8-6, CG1-8-7, CG1-8-9, and CG1-8-13

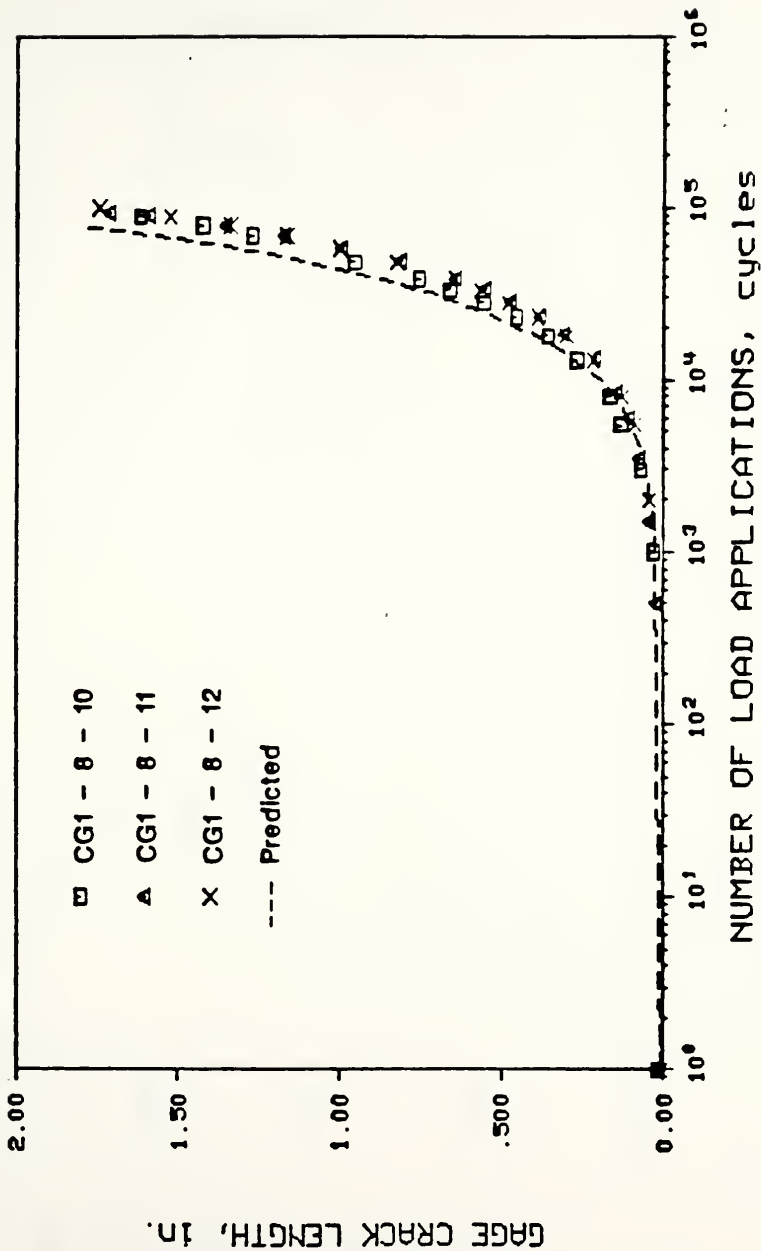


Figure 4.27 Observed and Predicted Crack Growth for Gages CG1-8-10, CG1-8-11 and CG1-8-12



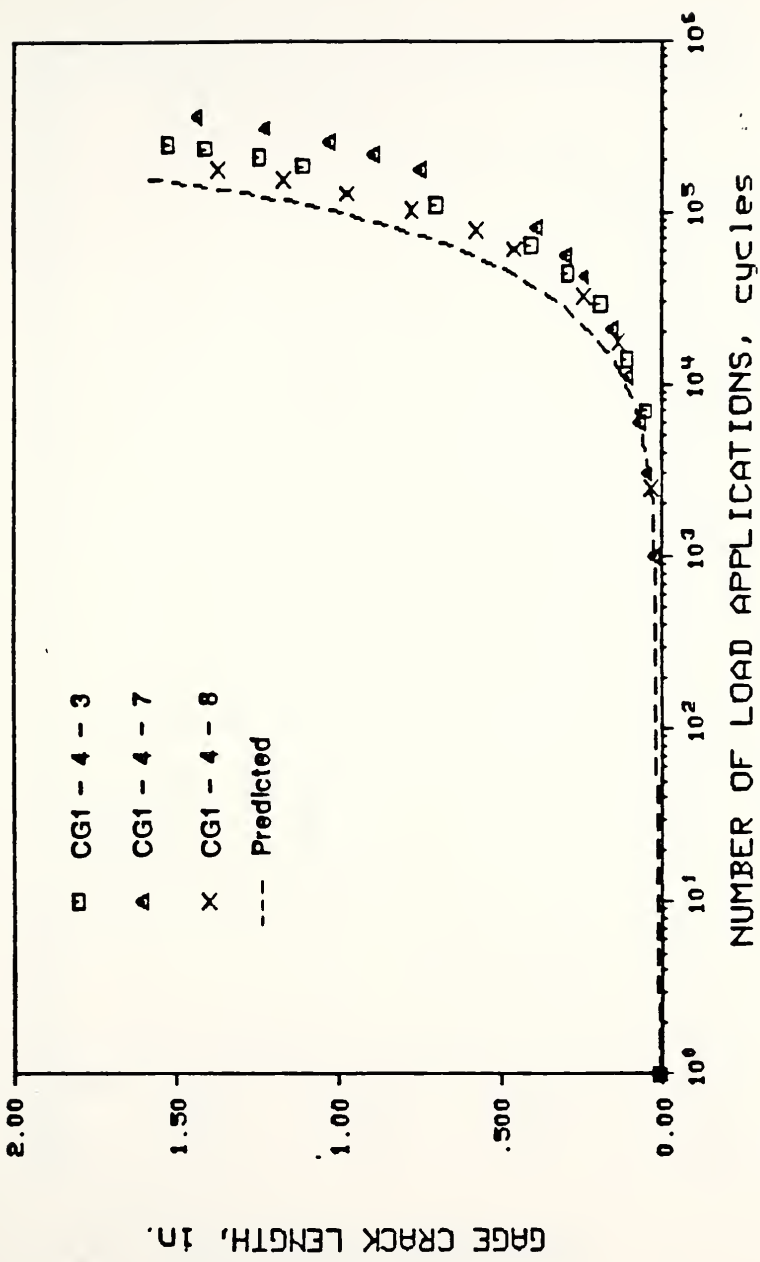


Figure 4.28 Observed and Predicted Crack Growth for Gages CG1-4-3, CG1-4-7 and CG1-4-8

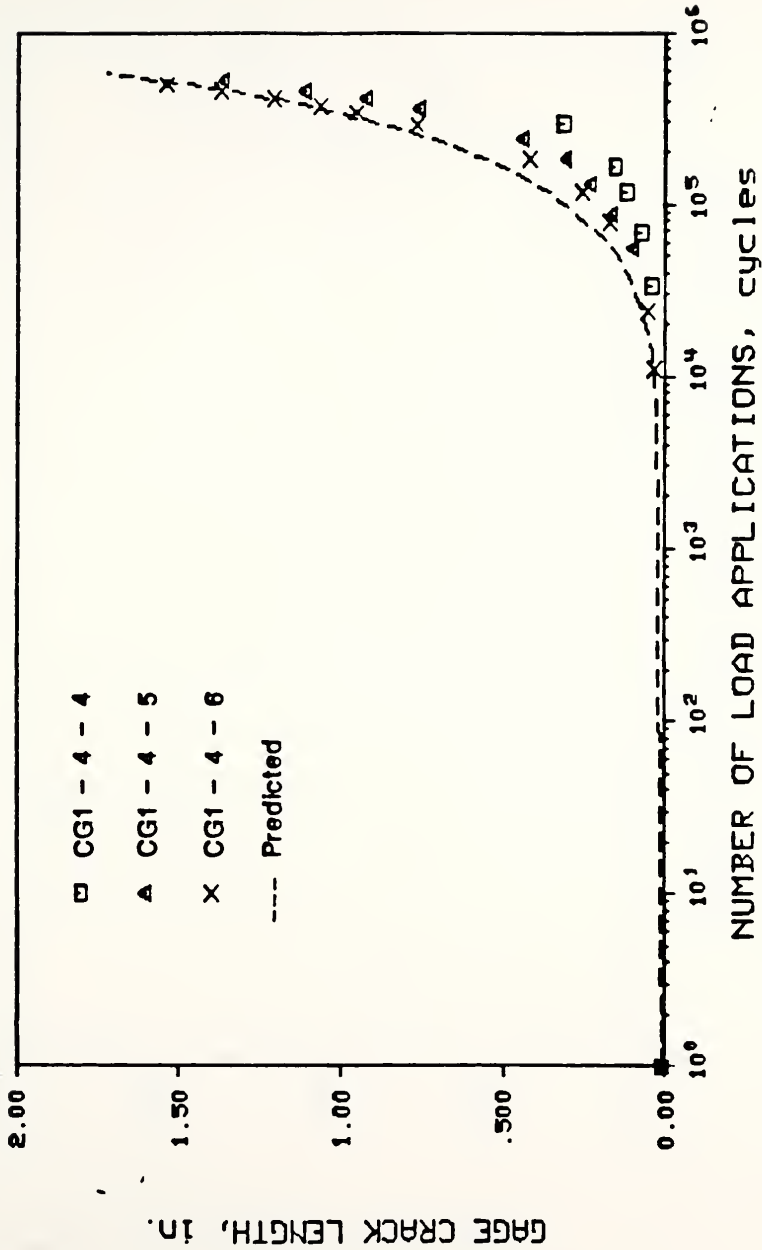


Figure 4.29 Observed and Predicted Crack Growth for Gages CG1-4-4, CG1-4-5 and CG1-4-6

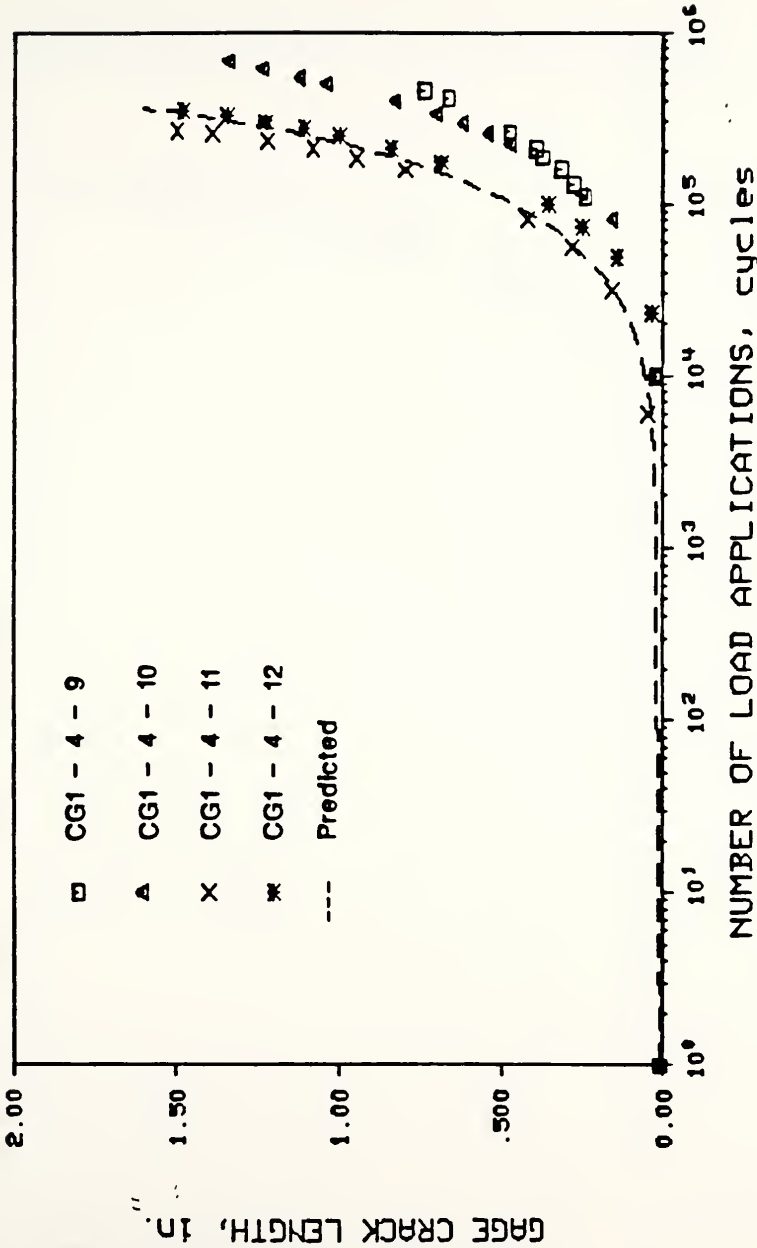


Figure 4.30 Observed and Predicted Crack Growth for Gages CG1-4-9, CG1-4-10, CG1-4-11, and CG1-4-12

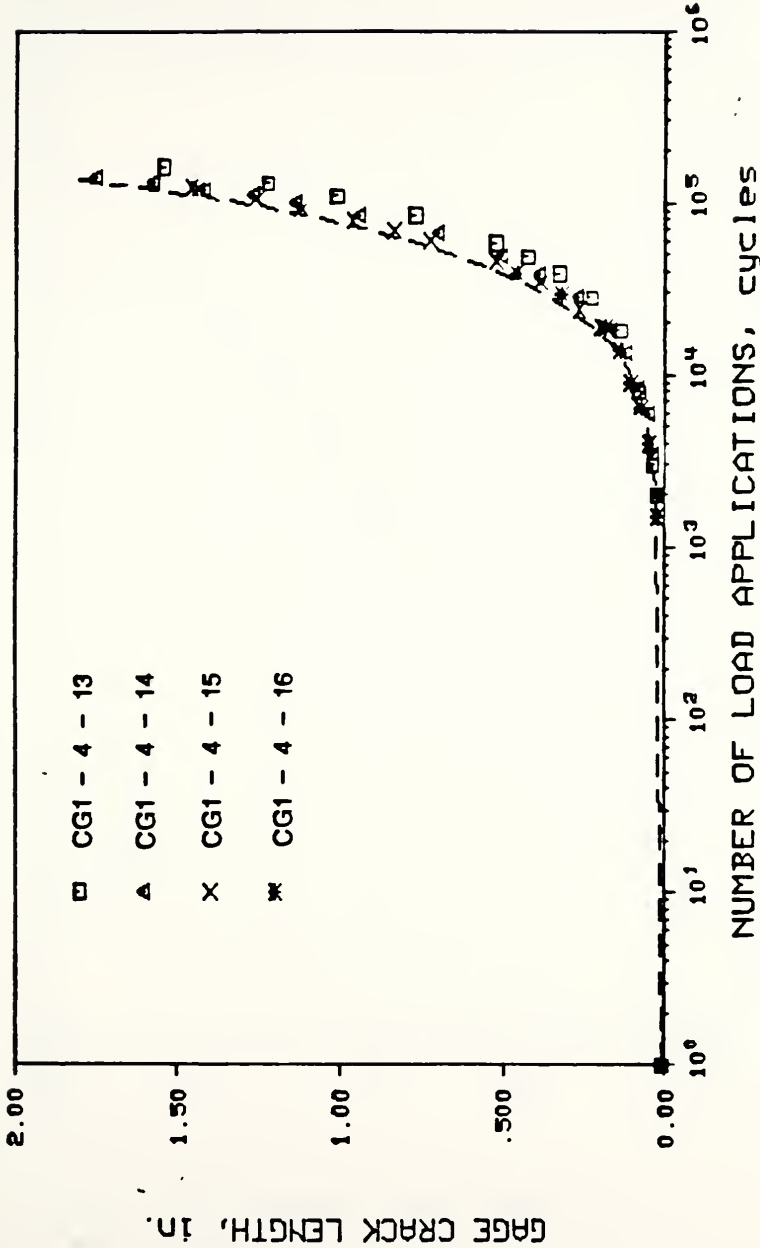


Figure 4.31 Observed and Predicted Crack Growth for Gages CG1-4-13, CG1-4-14, CG1-4-15, and CG1-4-16

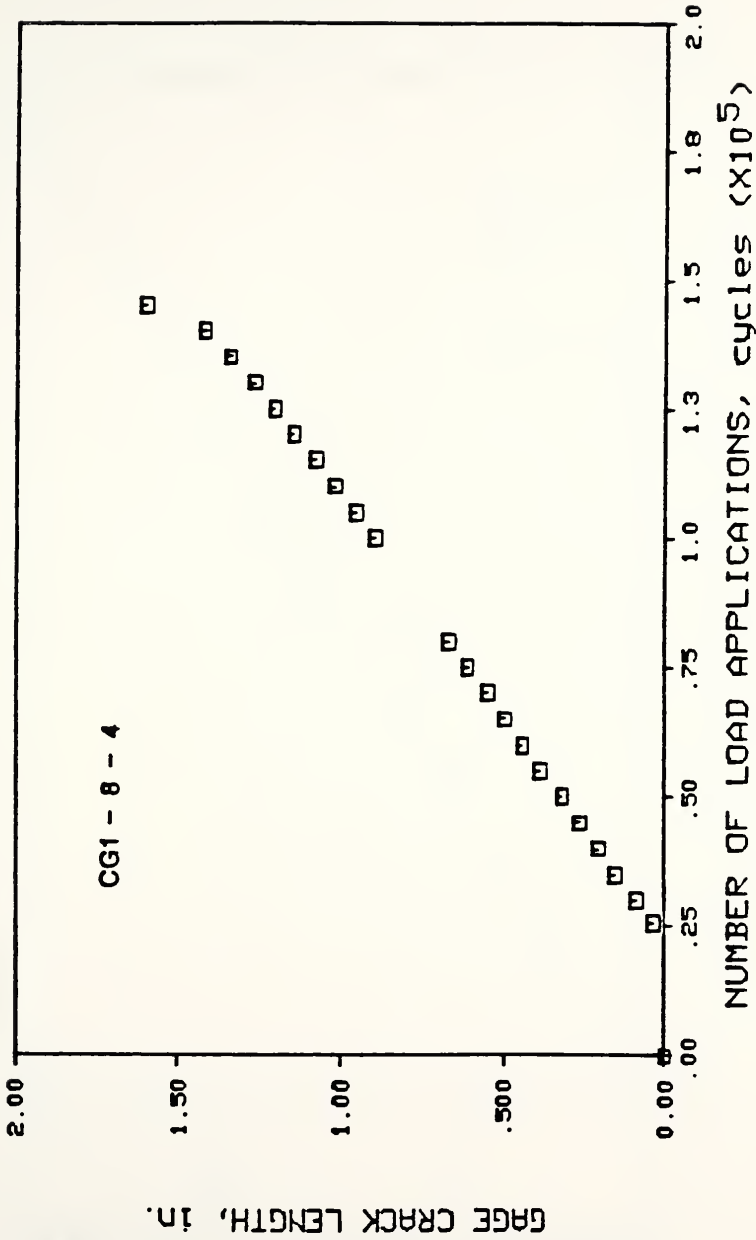


Figure 4.32 Typical Linear Crack Growth Relationship

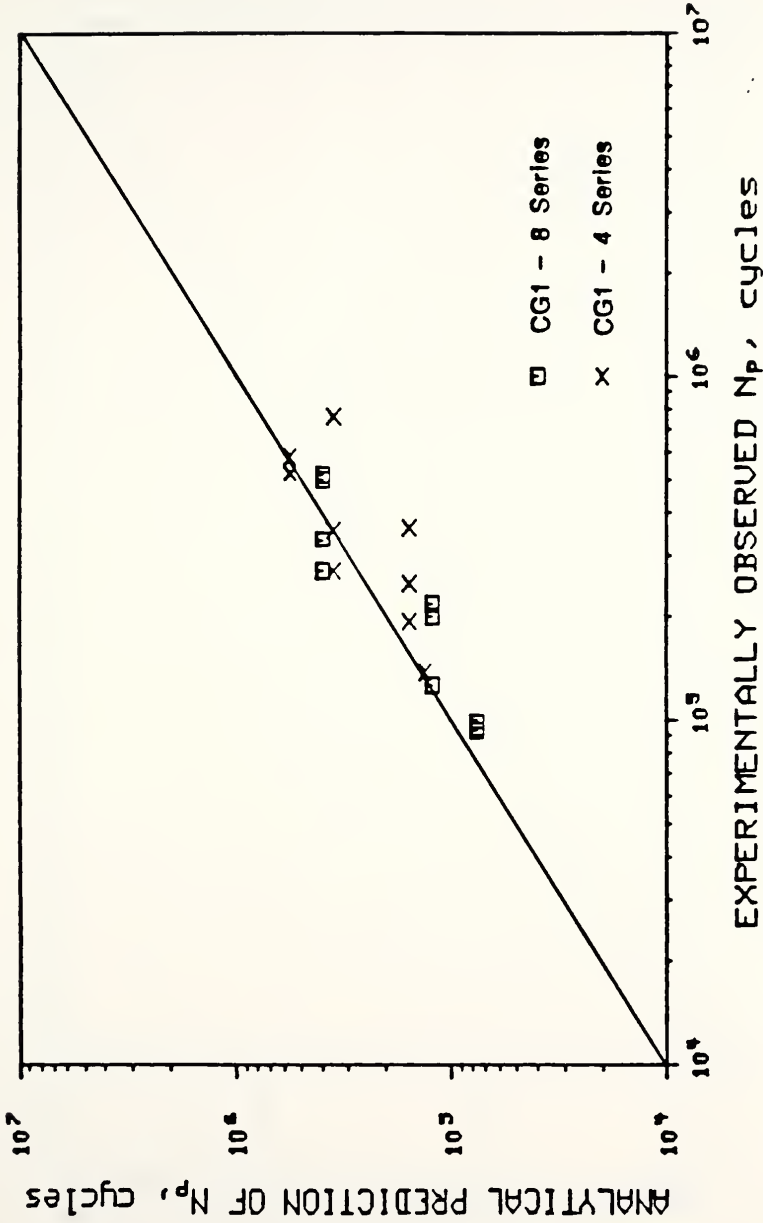


Figure 4.33 Comparison between Analytically Predicted and Experimentally Observed Propagation Life

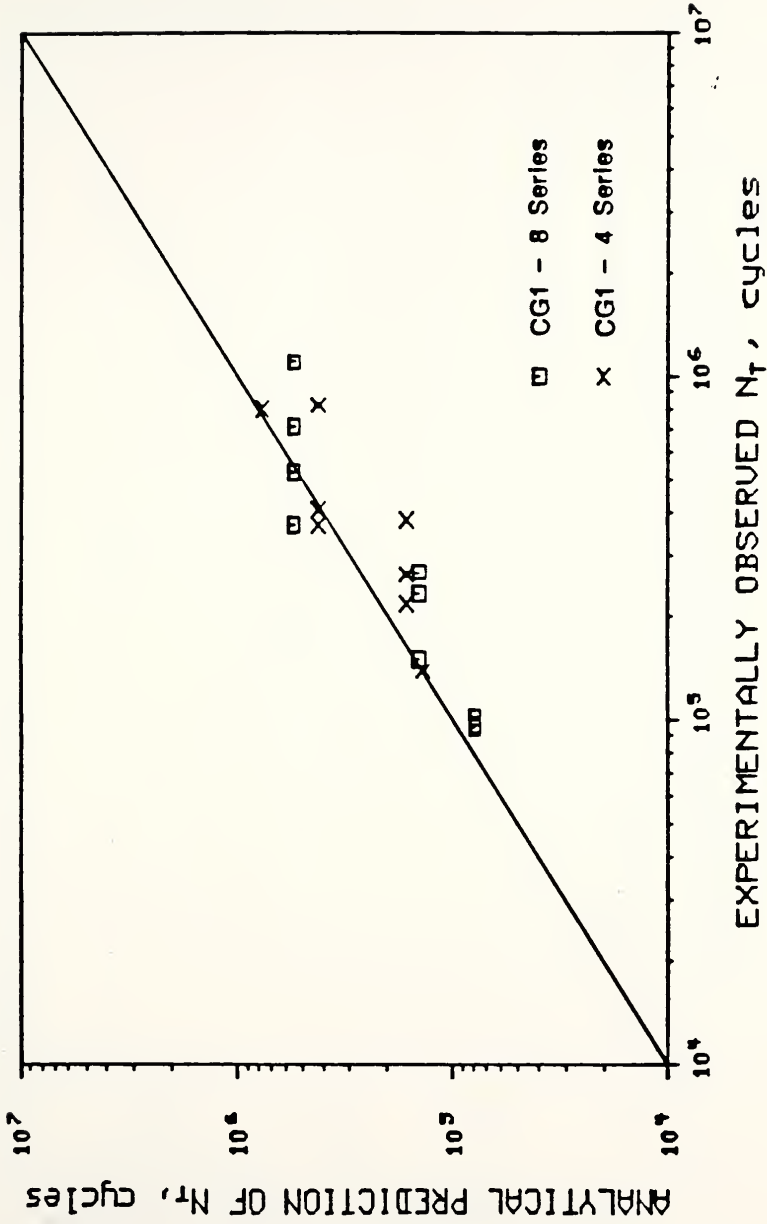


Figure 4.34 Comparison between Analytically Predicted and Experimentally Observed Total Fatigue Life

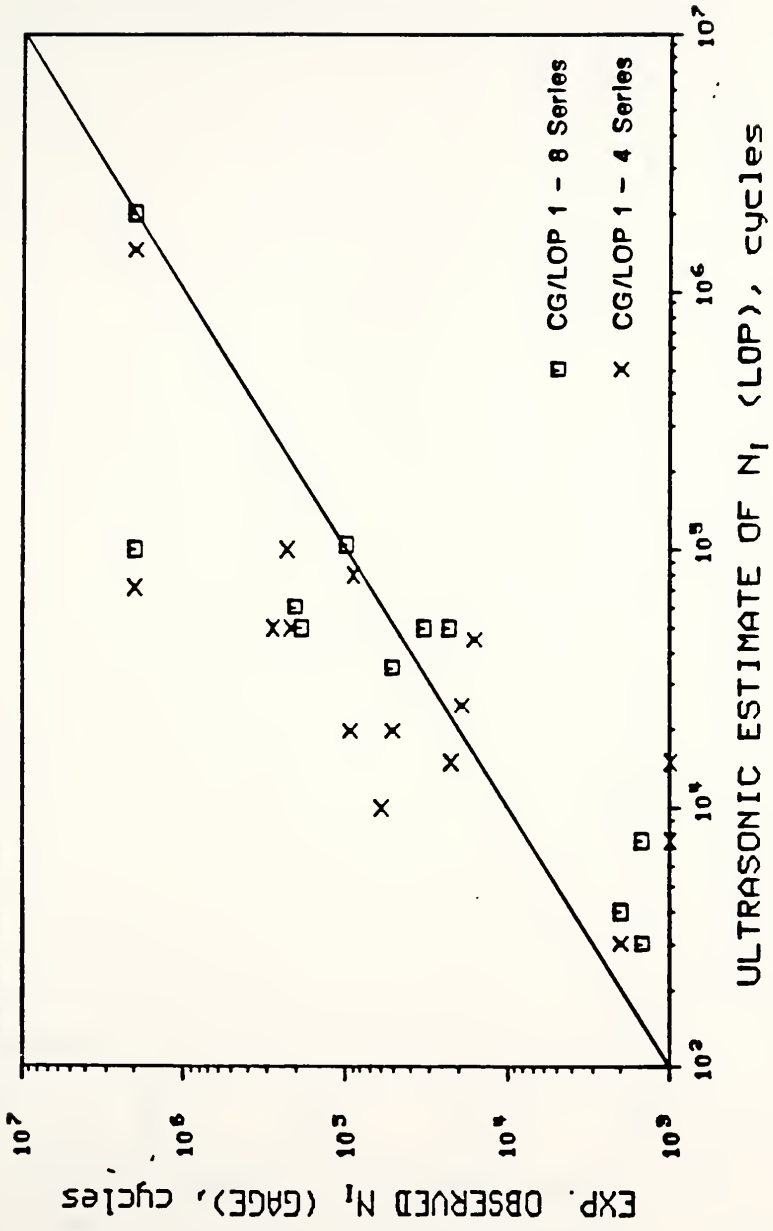


Figure 4.35 Comparison between Experimentally Estimated Gage Initiation Life and Ultrasonic Estimate of LOP Initiation Life



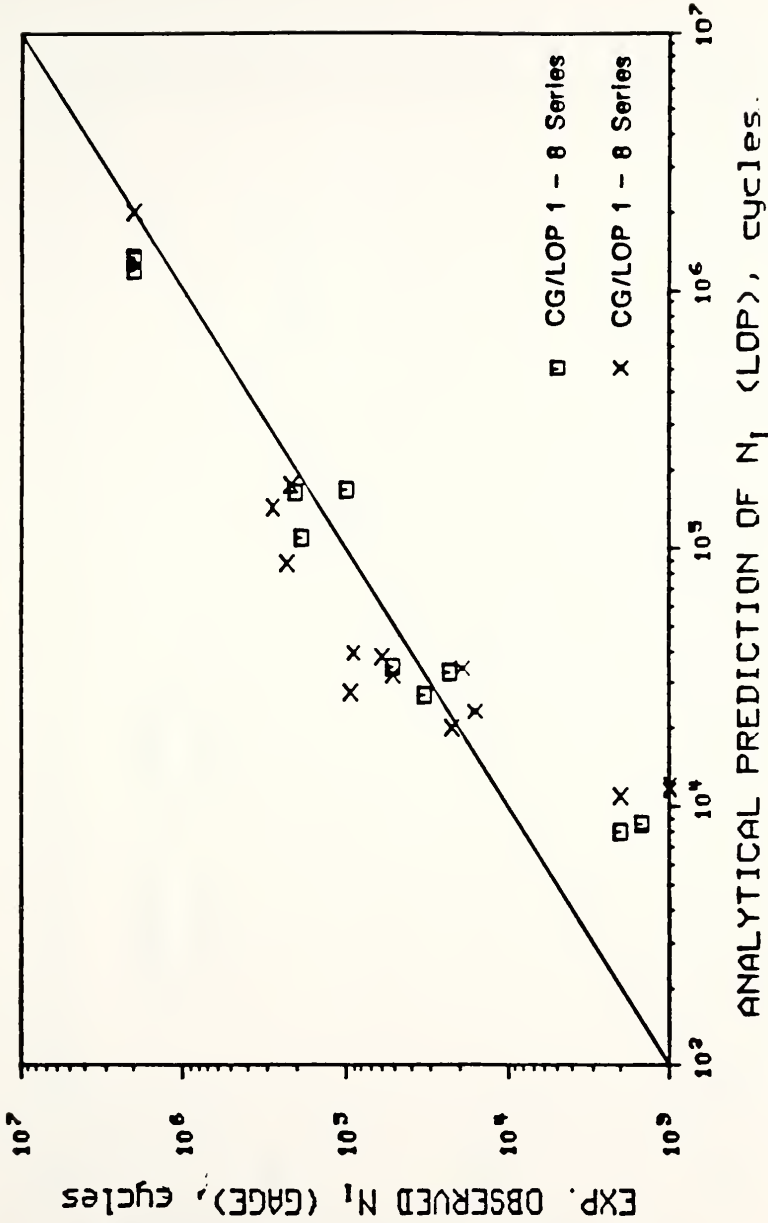


Figure 4.36 Comparison between Experimentally Estimated Gage Initiation Life and Analytically Predicted LOP Initiation Life

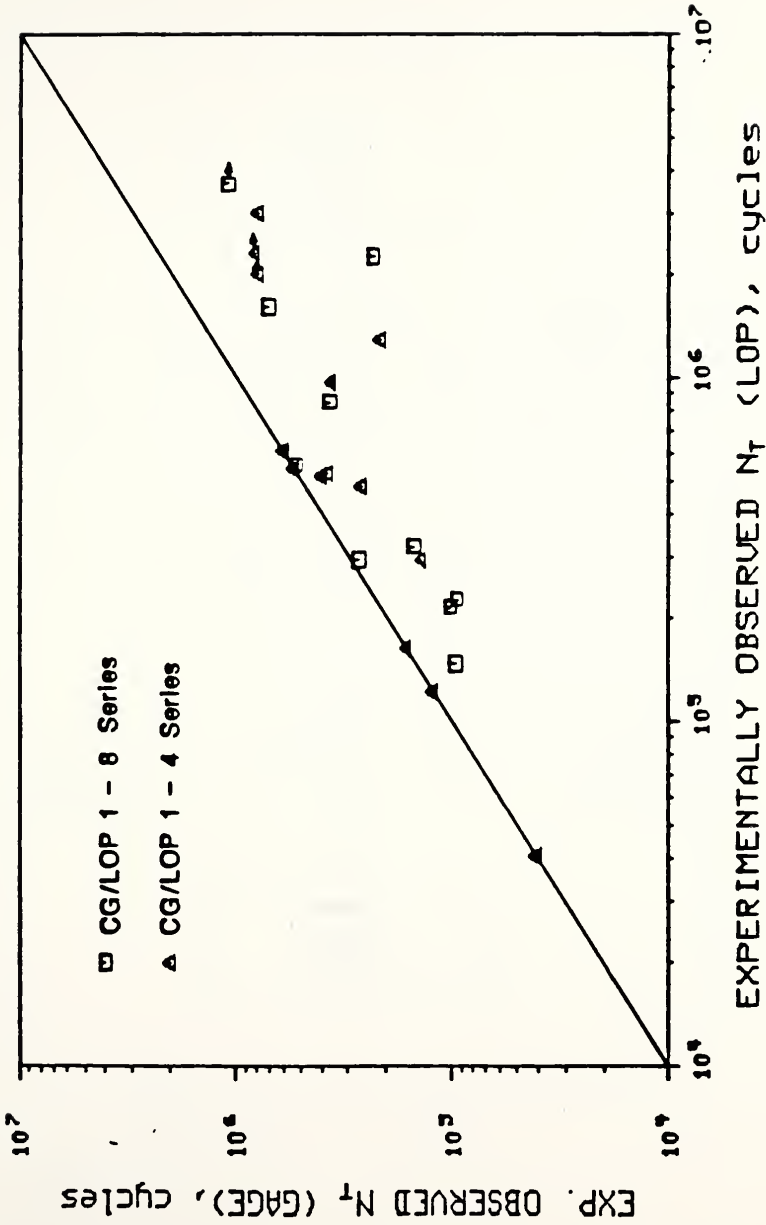


Figure 4.37 Comparison between Experimentally Observed Total Gage Life and Total LOP Fatigue Life

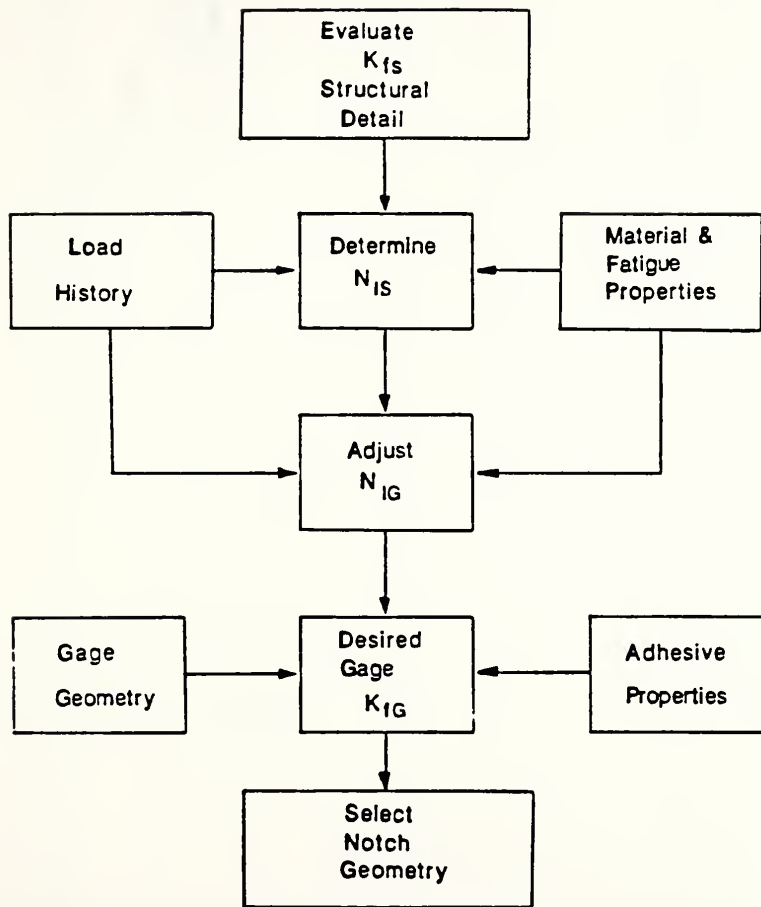
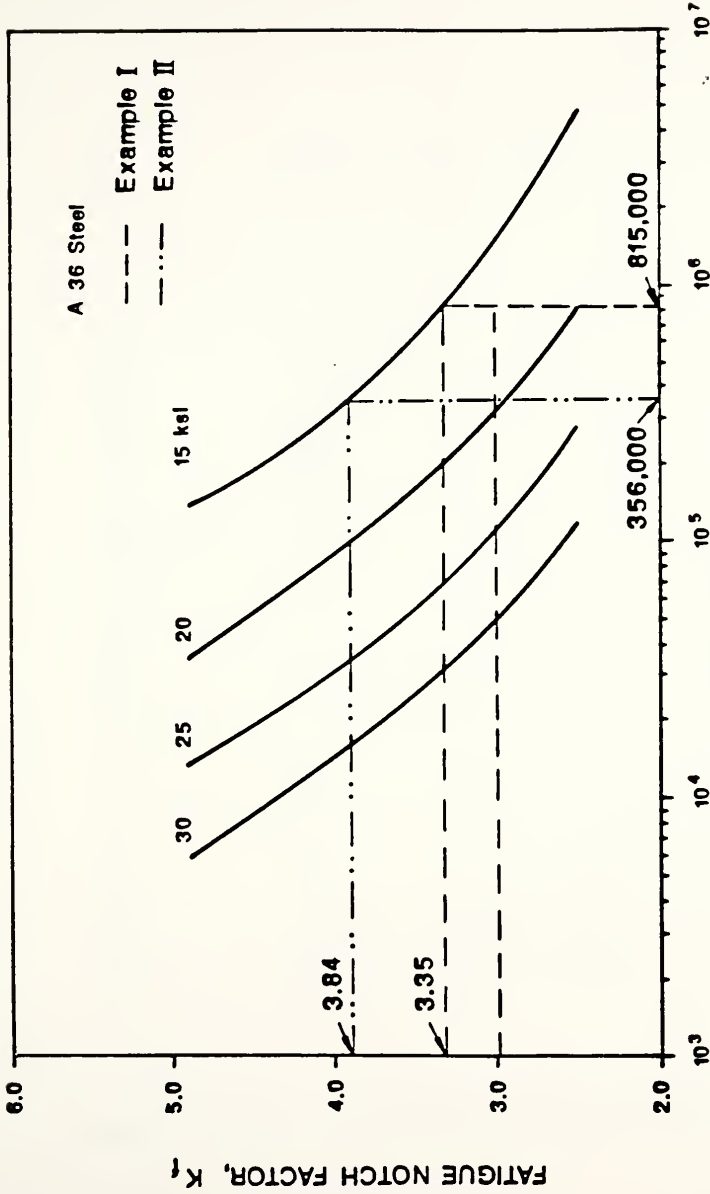


Figure 5.1 Crack Gage Selection Procedure



CRACK INITIATION LIFE,  $N_f$ , Cycles

Figure 5.2 Relation between Fatigue Notch Factor and Crack Initiation Life for A36 Steel

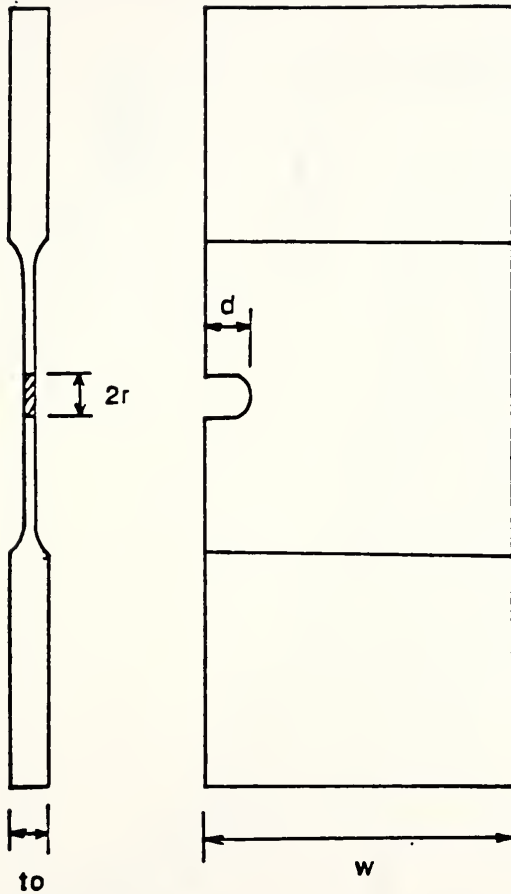


Figure 5.3 General Dimensions of a Crack Gage Notch

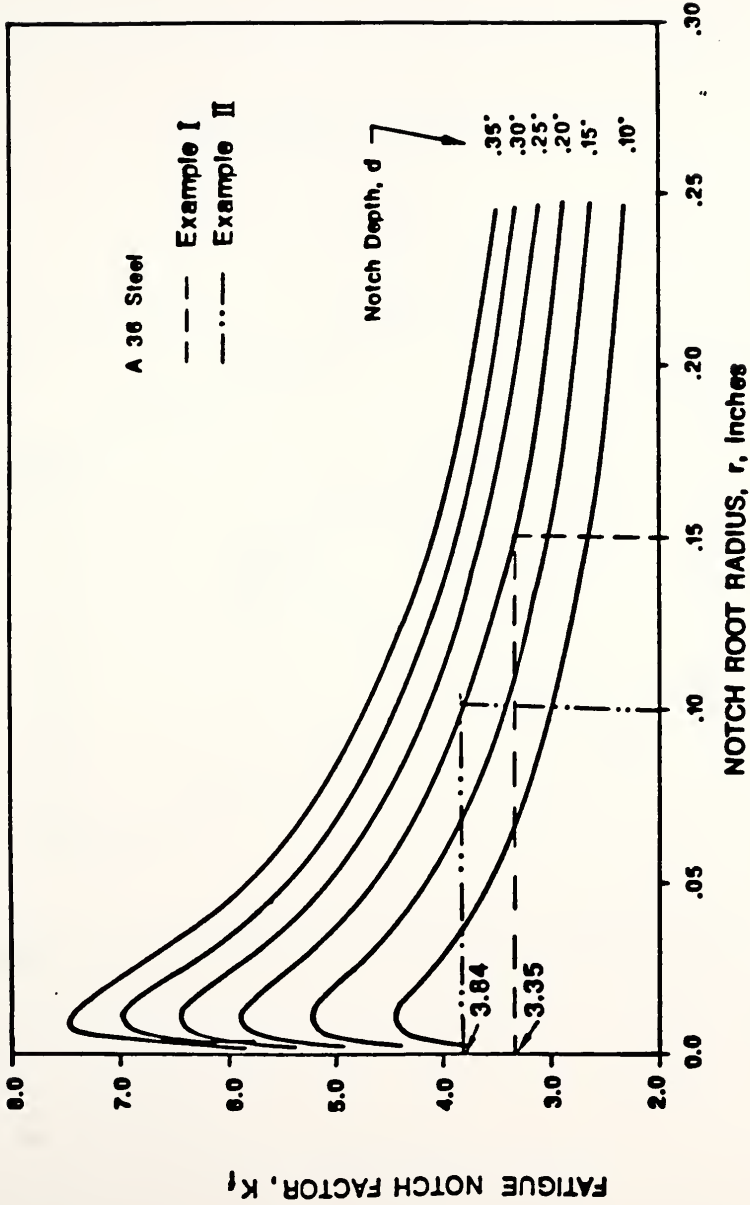


Figure 5.4 Relation between Fatigue Notch Factor and Notch Dimensions

### Fillet Welded Tee Joint

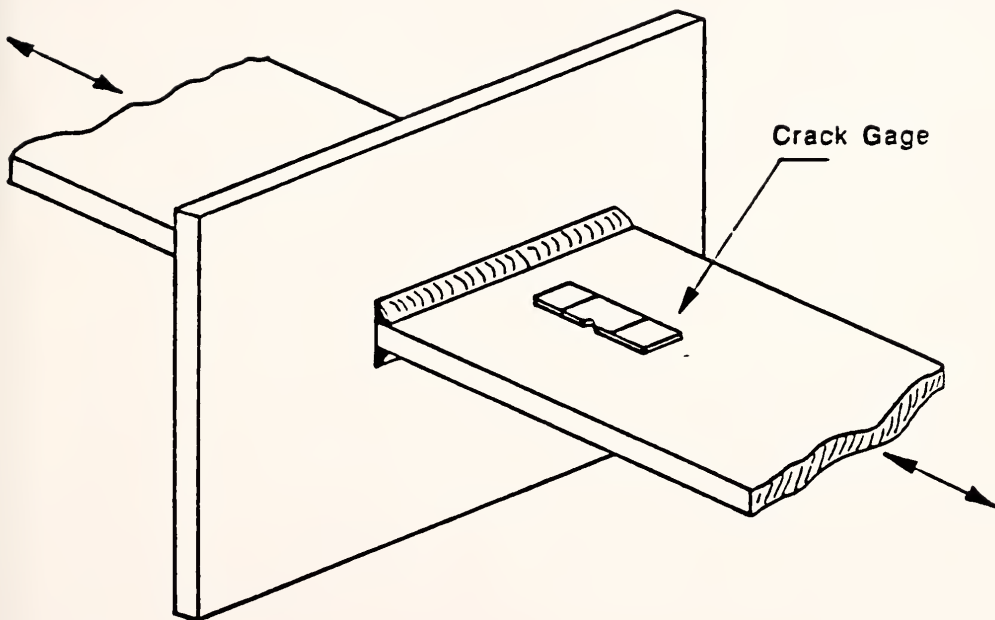


Figure 5.5 Crack Gage Placement on Fillet Welded Tee Joint

## LIST OF REFERENCES

1. "Aircraft Structural Integrity Programs, Airplane Requirements," Military Standards MIL STD-1530A, Air Force Aeronautical Systems Division, (USAF), Dec. 11, 1975.
2. Ashbaugh, N.E., and Grandt, A.F. Jr., "Evaluation of a Crack-Growth Gage for Monitoring Possible Structural Fatigue-Crack Growth," Service Fatigue Loads Monitoring, Simulation, and Analysis, ASTM STP 671, American Society for Testing and Materials, 1979, pp. 94-117.
3. Basquin, O.H., "The Exponential Law of Endurance Tests," Proceedings of the American Society for Testing and Materials, Vol. 10, Part II, 1910, pp. 625-630.
4. Burk, J.D., and Lawrence, F.V., "The Effect of Residual Stresses on Weld Fatigue Life," Fracture Control Program, Report No. 29, College of Engineering, University of Illinois, Urbana-Champaign, Jan. 1978, 126 pp.
5. Crews, J.H., "Crack Initiation at Stress Concentrations as Influenced by Prior Local Plasticity," Achievements of High Fatigue Resistance in Metals and Alloys, ASTM STP 467, American Society for Testing and Materials, 1970, pp. 37-52.
6. Crews, J.H., and Hardrath, H.F., "A Study of Cyclic Plastic Stresses at a Notch Root," Experimental Mechanics, Vol. 6, No. 6, June 1966, pp. 313-320.
7. Dowling, N.E., "Fatigue Failure Predictions for Complicated Stress-Strain Histories," Journal of Materials, Vol. 7, No. 1, March 1972, pp. 71-87.



8. Dumanis-Modan, A., "Evaluation of the Crack Gage as an Advanced Individual Aircraft Tracking Concept," Thesis submitted to the School of Aeronautics and Astronautics in Partial Fulfillment of the Requirements for the Ph.D Degree, Purdue University, West Lafayette, Indiana, Dec. 1982, 326 pp.
9. Ekstrom, D.H., and Munse, W.H., "The Effect of Internal Weld Defects on the Fatigue Behavior of Welded Connections," Civil Engineering Studies, Structural Research Series No. 395, University of Illinois, Urbana-Champaign, Feb. 1973, 89 pp.
10. Fisher, J.W., Pense, A.W., Hausamann, H., and Irwin, G.R., "Quinnipiac River Bridge Cracking," Journal of the Structural Division, ASCE, Vol. 106, No. ST 4, April 1980, pp. 773-789.
11. Fisher, J.W., Pense, A.W., and Roberts, R., "Evaluations of Fracture of Lafayette Street Bridge," Journal of the Structural Division, ASCE, Vol. 103, No. ST 7, July 1977, pp. 1339-1357.
12. Forayth, P.J.E., The Physical Basis of Metal Fatigue, American Elsevier, New York, 1969, 200 pp.
13. Gallagher, J.P., Grandt, A.F. Jr., and Crane, R.L., "Tracking Potential Crack Growth Damage in U.S. Air Force Aircraft," Journal of Aircraft, Vol. 15, No. 7, July 1978, pp. 435-442.
14. Gowda, C.V.B., and Topper, T.H., "Crack Propagation in Notched Mild Steel Plates Subjected to Cyclic Inelastic Strains," Cyclic Stress-Strain Behavior - Analysis, Experimentation and Failure Prediction, ASTM STP 519, American Society of Testing and Materials, 1971, pp. 170-184.
15. Grandt, A.F. Jr., Crane, R.L., and Gallagher, J.P., "A Crack Growth Gage for Assessing Flaw Growth Potential in Structural Components," Fracture, Proceedings of the Fourth International Conference on Fracture, Vol. 3, University of Waterloo Press, Waterloo, Canada, 1977, pp. 39-45.

16. Gray, T.D., and Grandt, A.F., "An Evaluation of the Crack Gage Technique for Individual Aircraft Tracking," Case Studies on Structural Integrity and Reliability, Proceedings of the Army Symposium on Solid Mechanics, AMMKC MS 78-3, Army Materials and Mechanics Research Center, Sept. 1978, pp. 63-82.
17. Gurney, T.R., "Finite Element Analyses of Some Joints with the Welds Transverse to the Direction of Stress," Welding Research Abroad, Vol. 22, No. 10, Dec. 1976, pp. 3-27.
18. Guyot, F., Martelee, J., and Soete, W., "Fatigue Tests on Transverse Butt Welds Characterised by an Incomplete Root Penetration," Welding Research Abroad, Vol. 14, No. 5, May 1968, pp. 2-22.
19. Handel, W., and Munsee, W.H., "Investigation of an Interstate-57 Bridge Beam Brittle Fracture," Civil Engineering Studies, Structural Research Series No. 477, University of Illinois, Urbana-Champaign, March 1980.
20. Halford, G.R., and Morrow, J., "Low Cycle Fatigue in Torsion," Proceedings of the American Society for Testing and Materials, Vol. 62, 1962, pp. 695-707.
21. Harting, D.R., "The S/N Fatigue-Life Gage: A Direct Means of Measuring Cumulative Fatigue Damage," Experimental Mechanics, Vol. 6, No. 2, Feb. 1966, pp. 19A-24A.
22. Higashida, Y., and Lawrence, F.V., "Strain Controlled Fatigue Behavior of Weld Metal and Heat-Affected Base Metal in A36 and A514 Steel Welds," Fracture Control Program, Report No. 22, College of Engineering, University of Illinois, Urbana, Illinois, Aug. 1976, 151 pp.
23. Impellizzeri, L.F., "Cumulative Damage Analysis in Structural Fatigue," Effect of Environment and Complex Load History on Fatigue Life, ASTM STP 462, American Society for Testing and Materials, 1970, pp. 40-68.

24. Jhansale, H.R., and Topper, T.H., "Engineering Analysis of the Inelastic Stress Response of a Structural Metal Under Variable Cyclic Strains," Cyclic Stress-Strain Behavior - Analysis, Experimentation, and Fatigue Predictions, ASTM STP 519, American Society for Testing and Materials, 1973, pp. 246-270.
25. Johnson, W.S., and Paquette, W.J., "Design and Evaluation of a Cracked Gage Concept for Monitoring Potential Crack Growth in Fleet Aircraft," Research Report No. EER-FW-1831, General Dynamics, Fort Worth Division, Texas, July 1977, 41 pp.
26. Koibuchi, K., and Kotani, S., "The Role of Cyclic Stress-Strain Behavior on Fatigue Damage Under Varying Loads," Cyclic Stress-Strain Behavior - Analysis, Experimentation, and Failure Prediction, ASTM STP 519, American Society for Testing and Materials, 1973, pp. 229-245.
27. Kuguel, R., "The Highly Stressed Volume of Material as a Fundamental Parameter in the Fatigue Strength of Metal Members," TAM Report No. 169, Department of Theoretical and Applied Mechanics, University of Illinois, Urbana-Champaign, June 1960.
28. Landgraf, R.W., "The Resistance of Metals to Cyclic Deformation," Achievements of High Fatigue Resistance in Metals and Alloys, ASTM STP 467, American Society for Testing and Materials, June 1969, pp. 3-36.
29. Landgraf, R.W., "Cumulative Fatigue Damage Under Complex Strain Histories," Cyclic Stress-Strain Behavior - Analysis, Experimentation, and Failure Prediction, ASTM STP 519, American Society for Testing and Materials, 1973, pp. 213-228.
30. Landgraf, R.W., Morrow, J., and Endo, T., "Determination of the Cyclic Stress-Strain Curve," Journal of Materials, Vol. 4, No. 1, March 1969, pp. 176-188.
31. Lawrence, F.V., and Munse, W.H., "Fatigue Crack Propagation in Butt Welds Containing Joint Defects," Welding Journal, Vol. 52, No. 5, May 1973, pp. 221s-225s, 232s.

32. Manson, S.S., "Interpretive Report on Cumulative Fatigue Damage in the Low Cycle Range," Welding Research Supplement, Aug. 1964, pp. 344s.
33. Manson, S.S., and Hirschberg, M.H., "Low Cycle Fatigue of Notched Specimens by Consideration of Crack Initiation and Propagation," National Aeronautics and Space Administration, NASA TN D-3146, 1965.
34. Manson, S.S., Freche, J.C., and Ensign, C.R., "Application of a Double Linear Damage Rule to Cumulative Fatigue," Fatigue Crack Propagation, ASTM STP 415, American Society for Testing and Materials, 1967, pp. 384-412.
35. Manual for Maintenance Inspection of Bridges, American Association of State Highway and Transportation Officials, 1983, 50 pp.
36. Manual of Steel Construction, Eighth Edition, American Institute of Steel Construction, Inc., 1980, 807 pp.
37. Martin, J.F., "Fatigue Damage Analysis for Irregular Shaped Structures Subjected to Representative Loads," Fracture Control Program, Report No. 10, College of Engineering, University of Illinois, Urbana-Champaign, Dec. 1973, 137 pp.
38. Martin, J.F., Topper, T.H., and Sinclair, G.M., "Computer Based Simulation of Cyclic Stress-Strain Behavior with Applications to Fatigue," Materials Research and Standards, Vol. 11, No. 2, Feb. 1971, pp. 23-28, 50.
39. Massing, G., "Eigenspannungen und Verfestigung beim Messing," Proceedings of the 2<sup>nd</sup> International Congress of Applied Mechanics, Zurich, 1926, pp. 332.
40. Mattos, R.J., and Lawrence, F.V., "Estimation of the Fatigue Crack Initiation Life in Welds using Low Cycle Fatigue Concepts," Fracture Control Program, Report No. 19, College of Engineering, University of Illinois, Urbana-Champaign, Oct. 1975, 189 pp.
41. Miner, M.A., "Cumulative Damage in Fatigue," Journal of Applied Mechanics, ASME, Vol. 67, Sept. 1945, pp. A159-A164.
42. Morrow, J., "Cyclic Plastic Strain Energy and Fatigue of Metals," Internal Friction, Damping and Cyclic Plasticity, ASTM STP 378, American Society for Testing and Materials, 1965, pp. 45-87.

43. Morrow, J., Fatigue Design Handbook, Section 3.2, Society of Automotive Engineers, New York, 1968, 132 pp.
44. Morrow, J., Wetzel, R.M., and Topper, T.H., "Laboratory Simulation of Structural Fatigue Behavior," Effect of Environment and Complex Load History on Fatigue Life, ASTM STP 462, American Society for Testing and Materials, 1970, pp. 74-91.
45. Newman, R.P., and Dawes, M.G., "Exploratory Fatigue Tests on Transverse Butt Welds Containing Lack of Penetration," British Welding Journal, Vol. 12, No. 3, March 1965, pp. 117-120.
46. Neuber, H., "Theory of Stress Concentration for Shear Strained Prismatical Bodies with Arbitrary Non Linear Stress-Strain Law," Journal of Applied Mechanics, Vol. 28, No. 4, Dec. 1961, pp. 544-550.
47. Neuber, H., Theory of Notch Stresses - Principles for Exact Stress Calculation, 1937, (Translation by Edwards, J.), Ann Harbor, Michigan, 1946.
48. Ori, J.A., and Grandt, A.F. Jr., "Single-Edge-Cracked Growth Gage," Fracture Mechanics, ASTM STP 677, American Society for Testing and Materials, 1979, pp. 533-549.
49. Paris, P.C., and Erdogan, F., "A Critical Analysis of Crack Propagation Law," Journal of Basic Engineering, ASME, Vol. 85, No. 4, 1963, pp. 528-534.
50. Paris, P.C., Gomez, M.P., and Anderson, W.E., "A Rational Analytic Theory of Fatigue," The Trend in Engineering, Vol. 13, No. 1, University of Washington, Jan. 1961, pp. 9-14.
51. Peterson, R.E., "Notch Sensitivity," Metal Fatigue, Sines and Waisman, (editors), McGraw-Hill Book Co., Inc., 1959, 415 pp.
52. Peterson, R.E., "Fatigue of Metals-Engineering and Design Aspects," Materials Research and Standards, Vol. 3, No. 2, Feb. 1963, pp. 122-139.
53. Plummer, F.B. Jr., "Cyclic Plasticity and Structural Energy Dissipation," Thesis submitted to the Department of Theoretical and Applied Mechanics in Partial Fulfillment of the Requirements for the Ph.D Degree, University of Illinois, Urbana-Champaign, 1973.

54. Radzinski, J.B., Srinivasan, R., Moore, D., Thrasher, C., and Munse, W.H., "Fatigue Data Bank and Data Analysis Investigation," Civil Engineering Studies, Structural Research Series No. 405, University of Illinois, Urbana-Champaign, June 1973, 152 pp.
55. Rolfe, S.T., and Barsom, J.M., Fracture and Fatigue Control in Structures, Prentice-Hall, Englewood Cliffs, N.J., 1977, 562 pp.
56. Smith, H.W., Fatigue Damage Indicator, U.S. Patent No. 3,979,949, assigned to the Boeing Company, Seattle, Wash., Sept. 14, 1976.
57. Spanner, J.C. and McElroy, E., "Monitoring Structural Integrity by Acoustic Emission," ASTM STP 571, American Society for Testing and Materials, 1975.
58. Stowell, E.Z., "Stress and Strain Concentration at a Circular Hole in an Infinite Plate," National Advisory Committee for Aeronautics, Technical Note 2073, April 1950.
59. Thang, B.Q., Dubuc, J., Bazergui, A., and Biron, A., "Cumulative Fatigue Damage Under Strain Controlled Conditions," Journal of Materials, Vol. 6, No. 3, Sept. 1971, pp. 718-737.
60. Tobe, Y., and Lawrence, F.V., "Effect of Inadequate Joint Penetration on Fatigue Resistance of High Strength Structural Steel Welds," Welding Journal, Vol. 56, No. 9, Sept. 1977, pp. 259s-266s.
61. Topper, T.H., and Morrow, J., "Simulation of the Fatigue Behavior at the Notch Root in Spectrum Loaded Members (U)," TAM Report No. 333, Department of Theoretical and Applied Mechanics, University of Illinois, Urbana-Champaign, Jan. 1970.

62. Topper, T.H., Wetzel, R.M., and Morrow, J., "Neuber's Rule Applied to Fatigue of Notched Specimens," Journal of Materials, Vol. 4, No. 1, March 1969, pp. 200-209.
63. Torvik, P.J., "On the Determination of Stresses, Displacements, and Stress-Intensity Factors in Edge-Cracked Sheets with Mixed Boundary Conditions," Journal of Applied Mechanics, Vol. 46, Sept. 1979, pp. 611-617.
64. Walker, W.H., "Loading Histories," Specialty Conference on Metal Bridges, ASCE, Nov. 1974, pp. 305-332.
65. Warren, W.G., "Fatigue Tests on Defective Butt Welds," Welding Research, Vol. 6, No. 6, Dec. 1952, pp. 112r-117r.
66. Wetzel, R.M., "Smooth Specimen Simulation of Fatigue Behavior of Notches," Journal of Materials, Vol. 3, NO. 3, Sept. 1968, pp. 646-657.
67. Wetzel, R.M., "A Method of Fatigue Damage Analysis," Metallurgy Department, Technical Report No. SR 71-107, Scientific Research Staff, Ford Motor Co., Sept. 1974.
68. Whitford, D.H. and Dominic, R.J., "B-58 Fleet Life Monitoring and Usage Evaluation by Cumulative Fatigue Damage Method," AFFL DL-TK-70-144; Proceedings, Air Force Conference on Fatigue and Fracture of Aircraft Structures and Materials, H. A. Wood et. al., eds., Air Force Flight Dynamics Laboratory, Wright-Patterson Air Force Base, Ohio, 1970, pp. 847-864.
69. Wilson, W.M., Munse, W.H., and Snyder, I.S., "Fatigue Strength of Various Types of Butt Welds Connecting Steel Plates," Engineering Experiment Station Bulletin Series No. 384, University of Illinois, Urbana-Champaign, March 1950, 60 pp.

**Appendix A Measured LOP Depths**

The lack of penetration (LOP) depths were measured after fracture of each specimen at five different locations as illustrated in Fig. A.1. The LOP depths were measured with the aid of the tele-microscope and digital readout assembly which was used to measure the crack lengths in the crack gages (Sec. 3.5.2). The measured LOP depths are presented in Table A.1.



Table A.1 Measured Lack of Penetration (LOP) Depths

Specimen Number	Lack of Penetration (LOP) Depth, 2a, (in.)					
	1	2	3	4	5	Average
LOP1-8-1	.163	.157	.173	.180	.165	.168
LOP1-8-2	.160	.178	.174	.186	.162	.172
LOP1-8-3	.134	.150	.154	.170	.225	.167
LOP1-8-4	.152	.180	.189	.186	.180	.177
LOP1-8-5	.194	.148	.175	.159	.190	.173
LOP1-8-6	.161	.130	.161	.156	.182	.158
LOP1-8-7	.139	.138	.103	.128	.156	.133
LOP1-8-8	.172	-	-	-	.219	.196
LOP1-8-9	.186	.189	.182	.200	.180	.187
LOP1-8-10	.211	.230	.195	.222	.249	.221
LOP1-8-11	.201	.240	.227	.207	.239	.223
LOP1-8-12	.232	.256	.222	.226	.219	.231
LOP1-8-13	.156	.174	.146	.157	.163	.159
LOP1-4-1	.233	.232	.207	.234	.250	.231
LOP1-4-2	.232	.303	.237	.257	.271	.260
LOP1-4-3	.267	.285	.275	.283	.268	.276
LOP1-4-4	.308	.317	.286	.276	.267	.291
LOP1-4-5	.222	.170	.204	.242	.261	.220
LOP1-4-6	.262	.233	.234	.241	.224	.239
LOP1-4-7	.226	.213	.243	.234	.235	.230
LOP1-4-8	.256	.261	.318	.317	.328	.296
LOP1-4-9	.309	.275	.302	.292	.280	.292
LOP1-4-10	.329	.296	.346	.256	.251	.296
LOP1-4-11	.343	.330	.347	.346	.343	.342
LOP1-4-12	.324	.321	.306	.310	.333	.319
LOP1-4-13	.352	.324	.278	.293	.298	.309
LOP1-4-14	.349	.246	.265	.250	.305	.283
LOP1-4-15	.256	.285	.328	.291	.321	.296
LOP1-4-16	.254	.285	.300	.320	.340	.300

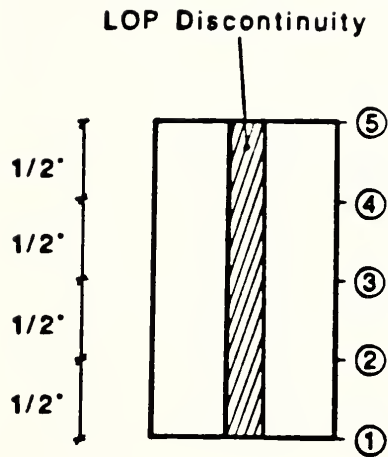
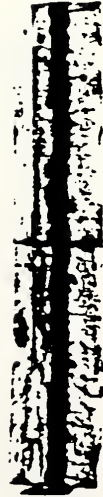


Figure A.1 LOP Depth Measurement Locations

**Appendix B Photographs of Fracture Surfaces**

After each Crack Gage/LOP test the ends of the fractured LOP specimen were machined off approximately one inch from the LOP discontinuity. The two fracture surfaces were then placed side by side and photographed. In Fig. B.1 the photographed fracture surfaces are presented for all the LOP specimens.



(a) LOP1 - 8 - 1  
Stress Range - 15 ksi  
Life - 2,000,000 cycles  
(runout)



(b) LOP1 - 8 - 2  
Stress Range - 15 ksi  
Life - 2,000,000 cycles  
(runout)



(c) LOP1 - 8 - 3  
Stress Range - 15 ksi  
Life - 2,000,000 cycles  
(runout)



(d) LOP1 - 8 - 4  
Stress Range - 25 ksi  
Life - 324,000 cycles

Figure B.1 Photographs of LOP1-8 Weld Specimen Fracture Surfaces



(e) LOP1 - 8 - 5  
Stress Range - 25 ksi  
Life - 296,000 cycles



(f) LOP1 - 8 - 6  
Stress Range - 20 ksi  
Life - 847,400 cycles



(g) LOP1 - 8 - 7  
Stress Range - 20 ksi  
Life - 3,640,000 cycles  
(runout)



(h) LOP1 - 8 - 8  
Stress Range - 25 ksi  
Life - 2,250,000 cycles

Figure B.1 (continued)



(j) LOP1 - 8 - 10  
Stress Range - 30 ksi  
Life - 227,100 cycles



(i) LOP1 - 8 - 12  
Stress Range - 30 ksi  
Life - 215,800 cycles



(k) LOP1 - 8 - 9  
Stress Range - 20 ksi  
Life - 556,400 cycles



(l) LOP1 - 8 - 11  
Stress Range - 30 ksi  
Life - 146,900 cycles

Figure B.1 (continued)



(m) LOP1 - 8 - 13  
Stress Range - 20 ksi  
Life - 1,598,000 cycles

Figure B.1 (continued)



(a) LOP1 - 4 - 1  
 Stress Range - 12 ksi  
 Life - 2,000,000 cycles  
 (runout)



(b) LOP1 - 4 - 2  
 Stress Range - 12 ksi  
 Life - 2,000,000 cycles  
 (runout)



(c) LOP1 - 4 - 3  
 Stress Range - 22.5 ksi  
 Life - 484,800 cycles



(d) LOP1 - 4 - 4  
 Stress Range - 17.5 ksi  
 Life - 539,000 cycles

Figure B.2 Photographs of LOP1-4 Weld Specimen Fracture Surfaces





(e) LOP1 - 4 - 5

Stress Range - 17.5 ksi  
Life - 2,000,000 cycles  
(runout)



(f) LOP1 - 4 - 6

Stress Range - 17.5 ksi  
Life - 2,991,600 cycles



(g) LOP1 - 4 - 7

Stress Range - 22.5 ksi  
Life - 524,100 cycles



(h) LOP1 - 4 - 8

Stress Range - 22.5 ksi  
Life - 1,288,100 cycles

Figure B.2 (continued)



(j) LOP1 - 4 - 10  
Stress Range - 20 ksi  
Life - 2,272,000 cycles  
(runout)



(i) LOP1 - 4 - 12  
Stress Range - 20 ksi  
Life - 516,000 cycles



(l) LOP1 - 4 - 9  
Stress Range - 20 ksi  
Life - 607,900 cycles



(k) LOP1 - 4 - 11  
Stress Range - 20 ksi  
Life - 959,500 cycles

Figure B.2 (continued)



(n) LOP1 - 4 - 14  
Stress Range - 25 ksi  
Life - 295,300 cycles



(p) LOP1 - 4 - 16  
Stress Range - 25 ksi  
Life - 41,100 cycles



(m) LOP1 - 4 - 13  
Stress Range - 25 ksi  
Life - 163,300 cycles



(o) LOP1 - 4 - 15  
Stress Range - 25 ksi  
Life - 122,300 cycles

Figure B.2 (continued)



COVER DESIGN BY ALDO GIORGINI